

https://dspace.org/

Flow injection analysis in analytical chemistry

Jones, Elaine Anne

2015-04-21
http://hdl.handle.net/10539/17471

Downloaded from a DSpace repository. https://dspace.org/

FLOW INJECTION ANALYSIS IN ANALYTICAL CHEMISTRY

Elaine Anne Jones

A Dissertation Submitted to the Faculty of Science,
University of the Witwatersrand, Johannesburg,
for the Degree of Master of Science.

Johannesburg, 1985

ABSTRACT

A flow-injection procedure has been developed for the direct determination of uranium(VI) using a spectrophotometric measurement at 578 nm of the complex formed by the reaction of the uranyl ion (UO_2^{2+}) with the azo dye 2-(5-bromo-2-pyridylazo)-5-diethyl-aminophenol (bromo-PADAP) at a pH value of 8.6.

The physical parameters of the manifold have been optimized by both univariate and simplex methods. These parameters include the length of tubing between the injection and detection points, the flowrate of the reactants and the sample size. The chemical parameters for the reaction of bromo-PADAP with the uranyl ion and the composition of the buffer solution have been optimized by a univariate method.

The effects of many commonly occurring elements and mineral acids have been studied. The interference and tolerance levels have been established under optimum conditions. The relative standard deviation obtained on a synthetic leach solution containing 10 $mg.l^{-1}$ of uranium(VI) was 0.019. The calibration curve was linear over the range 0.2 to 20 $mg.l^{-1}$ uranium(VI). The procedure is simple, rapid and convenient and up to 40 samples can be analysed per hour.

DECLARATION

I declare that this dissertation is my own work.
It is being submitted for the degree of Master of Science
in the University of the Witwatersrand, Johannesburg.
It has not been submitted before for any degree or
examination in any other University.

E.A.Jones

E.A.Jones

To Alex and my mother

ACKNOWLEDGEMENTS

This study was undertaken in the Analytical Science Division of the Council for Mineral Technology (MINTEK).

I would like to thank:

The management of MINTEK for permission to undertake the project;

Professor R.A. Hasty for his guidance and assistance during the course of this research;

My colleagues for their helpful discussions, advice and patience;

Janice Haines and Alex Watson for their moral support;

Renee Bergman for answering all my queries.

CONTENTS

CHAPTER

1. INTRODUCTION..... 1
1.1 CHEMISTRY OF URANIUM..... 1
1.1.1 Inorganic Compounds of Uranium..... 2
1.1.2 Organic Compounds of Uranium..... 3
1.1.3 Analytical Chemistry of Uranium..... 3
(a) Gravimetric Methods..... 4
(b) Titrimetric Methods..... 4
(c) Colorimetric and Spectrophotometric Methods..... 4
(d) Fluorimetric Methods..... 4
(e) X-Ray Methods..... 5
1.2 PROCESS CONTROL OF URANIUM..... 5
1.2.1 Continuous Flow Analysis..... 6
1.2.2 Flow Injection analysis..... 6
1.3 DETERMINATION OF URANIUM BY FIA..... 7
1.4 AIMS OF THIS INVESTIGATION..... 8

2. THEORY..... 9
2.1 COLORIMETRIC AND SPECTROPHOTOMETRIC METHODS OF ANALYSIS..... 9
2.1.1 Absorption of Radiant Energy..... 10
2.1.2 Beer's Law..... 10
2.2 PYRIDYLAZO COMPOUNDS AS METALLOCHROMIC INDICATORS.... 11
2.2.1 Azo Compounds of the Pyridine Series..... 11
(a) Preparation of Reagents..... 12
(b) Acid-base Equilibria..... 12
2.2.2 Bromo-PADAP Complexes of Uranium..... 17
(a) Effect of pH on Complex Formation..... 19
(b) Effect of Fluoride on Complex Formation.... 19
(c) Nature of bromo-PADAP Uranium Complexes.... 22
(d) Stability Constants..... 23
(e) Spectral Data..... 23

2.3 OPTIMIZATION OF FIA METHODS..... 24
2.3.1 Optimization Procedures..... 25
(a) Univariate Method of Optimization..... 25
(b) Simplex Method of Optimization..... 27
(i) Basic rules of the simplex method..... 29
(ii) Fixed size simplex..... 32
(iii) Variable size simplex..... 32
2.4 FLOW INJECTION ANALYSIS..... 40
2.4.1 Dispersion In FIA..... 44
(a) Dispersion Patterns..... 46
(i) Limited dispersion..... 51
(ii) Medium dispersion..... 51
(iii) Large dispersion..... 51
(b) Dispersion Number and Variance..... 52
(c) Dispersion Models..... 53
(i) Taylor's Model..... 53
(ii) Tanks-in-series Model..... 55
(iii) Comparison of dispersion models..... 57
(d) Reactor Geometry and Dispersion..... 57
(i) Dispersion due to radial diffusion..... 57
(ii) Coiled tubes..... 59
(iii) Packed-bed reactor..... 62
(e) Chemical Effect on Dispersion..... 62
2.4.2 Detectors..... 63

3. FIA OPTIMIZATION OF URANIUM(VI) DETERMINATION..... 65
3.1 APPARATUS AND REAGENTS..... 66
3.2 CALIBRATION OF THE SAMPLE INJECTOR..... 67
3.3 EXPERIMENTAL PROCEDURE..... 67
3.4 EFFECT OF ETHANOL IN THE BUFFER-COMPLEX SOLUTION..... 70
3.5 UNIVARIATE METHOD OF OPTIMIZATION..... 70
3.5.1 Results and Discussion..... 71
(a) Effect of Sample Size..... 71
(b) Effect of Reaction Coil Length..... 77
(c) Effect of Flowrate..... 80
(d) Sampling Frequency..... 85

(e) Effect of bromo-PADAP Concentration..... 85
(f) Effect of Buffer Concentration..... 92
3.6 MODIFIED SIMPLEX METHOD OF OPTIMIZATION 92
3.6.1 Results and Discussion..... 93
(a) Two-Variable Simplex Optimization..... 93
(b) Three-Variable Simplex Optimization..... 99
3.7 COMPARISON OF THE OPTIMIZATION PROCEDURES..... 102

4. INTERFERENCE STUDIES..... 105
4.1 INTERFERENCES IN THE FIA DETERMINATION OF URANIUM(VI) 109

4.1.1 Apparatus and Reagents..... 109
4.1.2 Procedure..... 109
4.1.3 Results and Discussion..... 109
(a) Effect of Acids..... 109
(b) Effect of elements..... 112
4.2 ANALYSIS OF A SYNTHETIC LEACH SOLUTION..... 120

5. CONCLUSION..... 124

REFERENCES..... 126

APPENDIX I..... 135

APPENDIX II..... 141

LIST OF TABLES

TABLE

2.1 Azo compounds of the pyridine series..... 13
2.2 Acid dissociation constants..... 18
2.3 Absorption maxima of reagents and molar absorptivities. 18
2.4 Stability constants..... 23
2.5 Spectral data for uranyl complexes of PADAP derivatives..... 24
2.6 Progress of simplex showing rejected and new vertices and responses..... 31
2.7 A general comparison of limited, medium and large dispersion..... 50
2.8 Comparison of turbulent flow, curved channel and packed column with respect to straight tubing in a laminar flow..... 58

3.1 Optimization factors, with chosen levels or ranges.... 71
3.2 Opt_mization using a Modified Simplex approach with two variables..... 94
3.3 Optimization using a Modified Simplex approach with two variables 95
3.4 Optimization using a Modified Simplex apnroach with two variables..... 96
3.5 Optimization using a Modified Simplex approach with three variables..... 100

4.1 Spectral data of metal-bromo-PADAP complexes..... 106
4.2 Comparative spectral data for complexes of bromo-PADAP PAR and o-PAP..... 108
4.3 Elemental interferences..... 118
4.4 Tolerance limits of interfering elements in bromo-PADAP method..... 119

LIST OF FIGURES

FIGURE

2.1 Wavelength absorbance curves..... 20
2.2 pH absorbance curves..... 20
2.3 Effect of fluoride on complex formation..... 21
2.4 Single variable-at-a-time method..... 26
2.5 Failure of a single variable on a ridge..... 28
2.6 Progress of a fixed size simplex, superimposed on a hypothetical response surface..... 30
2.7 Flow chart summarizing rules for the acceptance or rejection of a vertex, either fixed or variable size simplex..... 34
2.8 Two dimensional simplex indicating possible vertex locations in the modified simplex method..... 35
2.9 Possible locations for the new vertex after a boundary violation in the simplex method..... 37
2.10 Progress of the variable size simplex..... 38
2.11 Progress of the fixed size simplex..... 39
2.12 Schematic of the basic flow injection manifold..... 41
2.13 The dispersion number δ as a function of the Reynold's number R_e for aqueous solutions in the laminar, transient and turbulent regions of flow..... 43
2.14 Diagrammatic effects of convection and radial diffusion on the concentration profiles of injected samples monitored downstream from injection..... 45
2.15 Influence of flow geometry on the shape of the residence time distribution curves..... 47
2.16 Parameters for defining dispersion in FIA..... 49
2.17 Comparison of tanks-in-series model and dispersion signals in a FIA system..... 56
2.18 Peaks obtained with straight and coiled tubing under experimental conditions..... 60

3.1 Schematic flow diagram for the determination of uranium(VI)..... 68
3.2 Calibration plot for the injection valve..... 69
3.3 Effect of sample size on peak height..... 73
3.4 Influence of injection geometry on $S_{1/2}$ 74
3.5 Influence of coil length on $S_{1/2}$ 76
3.6 Effect of coil length of reaction coil..... 78
3.7 Effect of coil length and sample size on peak height.. 79
3.8 Relationship between peak height, extrapolated peak height and residence time for varying sample sizes.... 81
3.9 Influence of sample size on the D_f value..... 82
3.10 Effect of flowrate..... 83
3.11 Relationship between peak height, extrapolated peak height and residence time for varying flowrates..... 84
3.12 Influence of flowrate on the D_f value..... 86
3.13 Sampling rate..... 87
3.14 Recorder trace for sampling rate..... 88
3.15 Effect of varying bromo-PADAP concentration..... 90
3.16 Effect of concentration of buffer solution..... 91
3.17 Optimization using a Modified Simplex approach with two variables..... 97
3.18 Optimization using a Modified Simplex approach with two variables 97
3.19 Optimization using a Modified Simplex approach with two variables..... 98
3.20 Optimization using a Modified Simplex approach with three variables..... 98
3.21 Scatter diagrams of peak heights vs. variable values for the Modified Simplex optimizations..... 104

4.1 Spectra of bromo-PADAP complexes of zinc, copper and cobalt..... 107
4.2 Interference from inorganic acids..... 110
4.3 Response vs log H_3PO_4 concentration..... 111
4.4 Effect of bromo-PADAP on iron interference..... 113
4.5 Interferences in direct bromo-PADAP method..... 114

4.6 Recorder output for RSD of uranium(VI)..... 121
4.7 Calibration curves for U_3O_8..... 122

I-1 The apparatus..... 140

LIST OF SYMBOLS

C	concentration ($mol.l^{-1}$)
C_o^o	concentration of the injected sample ($mol.l^{-1}$)
C^{max}	concentration of the element of fluid at peak maximum (at t = T)($mol.l^{-1}$)
C_o^{max}	concentration of the element of fluid at peak maximum extrapolated to t = 0 ($mol.l^{-1}$)
C-curve	C = E = dF/dt
D	dispersion (dimensionless)
D_a	axial dispersion coefficient ($cm^2.sec^{-1}$)
D_c	molecular diffusion coefficient ($cm^2.sec^{-1}$)
D_i	dispersion in the injector
D_f	dispersion from flow
Dn	Dean number (dimensionless)
D_t	dispersion from injector, flow, detector etc.
E-curve	E = C = dF/dt
F-curve	time record of exit concentration from a reactor, measured as C/C_o^o
F	mean linear flow velocity ($mm.sec^{-1}$)
H	peak height/plate height at t = T (mm)
H_c	peak height of coiled tube
H^{max}	signal height at peak maximum
H_c^o	peak height recorded with flow cell filled with solution of concentration C_o^o(mm)
H_o	peak height extrapolated to t = 0 (mm)
L	total length of line (mm)
L_i	length of a mixing stage (mm)
L_s	length of sample zone (mm)
$L_{1/2}$	sample zone length corresponding to $S_{1/2}$(mm)
M_i	mass of injected sample (mol.)
N	number of mixing stages
Q	pumping rate ($ml.min^{-1}$)
R_e	Reynold's number ($R_e = 21.2Q/d$)(dimensionless)
r	tube radius (mm)
Sc	Schimdt number (dimensionless)

S^{max}	maximum sampling frequency (samples.h^{-1})
S	sample size (μl)
$S_{½}$	sample volume necessary to reach 50% of C_o^o at C^{max} (μl)
T	mean residence time (sec)
t_i	mean residence time in one tank (sec)
t_s	sample zone length in time units (sec)
u	mean velocity of flow in axial direction (cm.sec^{-1})
V_d	dead volume of sample injector (μl)
W	reduced peak width (at t = T)(mm)
W_b	peak width at peak base (mm)
W_o	reduced peak width extrapolated to t = 0 (mm)
η	dynamic viscosity (poise)
ν	kinematic viscosity, $\nu = (\eta/\rho)$(cm^2.sec^{-1})
ρ	density (g.ml^{-1})
σ^2	variance/standard deviation (dimensionless)
σ_t^2	variance in time units (sec)
σ_v^2	variance in volume units (ml)
τ	reduced time, $\tau = (tD)/a^2$ (dimensionless
τ_m	reduced mean residence time, $\tau_m = (t_{r}$ $/a^2$ (dimensionless)
δ	dispersion number (dimensionless)
ξ	decrease in sample dispersion by coiling a straight tube
a	proportionality constant
A	absorbance/optical density
β'	stability constant
ϵ	molar absorptivity (l.mol^{-1}.cm^{-1})
$[H^+]$	hydrogen ion concentration
nm	nanometer
P	transmitted radiant energy
P_o	incident radiant energy
pKa	acidity constant
μ	ionic strength
λ	wavelength (nm)

α	optimization coefficient
β	contraction coefficient
γ	expansion coefficient

CHAPTER 1

INTRODUCTION

Uranium is widely distributed in the earth's crust and hydrosphere. The crust contains about 0.0004 per cent which is equivalent to the combined contents of gold, silver and mercury, and about equal to that of tin. It is found together with other elements such as niobium, vanadium, thorium, zirconium and the rare earths elements. The level of uranium concentration varies with the type of rock. Pegmatites, (high silica igneous rocks) contain 25 $\mu g.g^{-1}$ whereas low silica basic rocks, e.g. basalts, are low in uranium content with only about 0.2 $\mu g.g^{-1}$. The important uranium ores are[1,2];

uraninite [UO_2],
brannerite [$(U,Ca,Fe,Th,Y)_3Ti_5O_{16}$)],
kasolite [$PbO.UO_3.SiO_2.H_2O$],
carnotite [$K_2(UO_2)_2(VO_4)_2.nH_2O$],
autunite [$Ca(UO_2)_2(PO_4)_2.nH_2O$], and
uranophone [$CaO.2UO_2.2SiO_2.6H_2O$].

The concentration of uranium in sea water is approximately 1 $\mu g.l^{-1}$. Naturally occurring uranium is a mixture of three isotopes ^{234}U, ^{235}U, and ^{238}U, with ^{238}U being the most abundant isotope[1-4].

1.1 Chemistry of Uranium

Uranium is a member of the actinide group of the Periodic Table, the series of elements from 89 through to 103. The 5f electron shell is filled in this series and is analogous to the lanthanide or rare earth series in which the 4f electron shell is filled.

The electronic configuration of the atom of uranium is $5f^3$ $6d$ $7s^2$ for the shell above the radon core. The 5f electrons are, with few exceptions, involved in chemical bonding and in the formation of aqueous ions.

The accepted coordination number for uranium is eight. There

are very few available data for the configuration of uranium coordination compounds. The tendency for uranium-containing molecules to polymerize is attributed to the extra stability afforded by filling the coordination requirements.

1.1.1 Inorganic Compounds of Uranium

Uranium has several oxidation states viz., (0), (III), (IV), (V), (VI), the latter because of its high charge is unstable in aqueous solution but is stabilized by the formation of the uranyl ion UO_2^{2+} which exists not only in aqueous solution but also in solids such as uranyl nitrate, uranates, and the hexavalent oxide. Solutions of UO^{3+} are rose-purple, those of U^{4+} are deep green and those of the uranyl ion UO_2^{2+} bright yellow. Absorption spectra can be used to identify the oxidation states of the uranium in solution. The uranyl ion (UO_2^{2+}) is the only stable state in solutions in contact with air. U^{3+} rapidly oxidizes to U^{4+} and UO_2^{+} easily disproportionates to a mixture of UO_2^{2+} and U^{4+}. U^{4+} is present in acid solutions possibly as $U(H_2O)_n^{4+}$ where n = 6 or 8. The oxidation of U^{4+} solutions to UO_2^{2+} is slow but the rate can be increased by the addition of small amounts of copper(II) and iron(III).

Uranium is chemically characterized by a high reactivity in the metallic state. The redox potential of the

$$U(III) + 3e^- \rightleftharpoons U(0) \qquad (1.1)$$

system is -1.80V, placing the metal close to aluminium and beryllium, but well below magnesium in the electrochemical series. Uranium(III) slowly evolves hydrogen from aqueous solution, but otherwise is similar to the trivalent rare earths. Fluoride and oxalate precipitate uranium(III) from acid solution; whereas sulphide, sulphate, chloride, bromide, iodide, nitrate and perchlorate do not. Uranium(IV) is chemically similar to cerium(IV); fluoride, iodate, substituted arsenates and cupferron precipitate it even from rather strong acid solution. The familiar test for the presence of sodium, (i.e., precipitation of sodium uranyl acetate), is useful also for qualitative identification of the uranyl (UO_2^{2+}) ion. Hydrogen peroxide precipitates

uranium(VI) and also oxidises and precipitates uranium(IV) from moderately acid solution.

The absorption and fluorescence spectra of uranium solutions and compounds are analytically useful. The sharp absorption and fluorescence bands in many media reflect the importance of the 5f electrons. The order of stability for anionic complexes is:

$$U^{4+} > UO_2^{2+} > U^{3+} > UO_2^{+}$$

The order is the same for hydrolytic reaction. The formation of stronger complexes with the uranyl ion than with the trivalent species is attributed to the higher charge on the uranium atom in the uranyl ion. The order of stability of anionic complexes is:

fluoride > nitrate > chloride >
bromide >iodide > perchlorate:
carbonate > oxalate > sulphate

1.1.2 Organic Compounds of Uranium

Numerous organic compounds are formed especially with uranium(VI). Aqueous soluble chelates form with citrate, tartrate, arsenazo and ethylenediaminetetraacetic acid(EDTA). Uranyl chloride, nitrate, and, to a lesser extent, sulphate and phosphate, extract into organic solvents. Solvents with a dielectric constant of about 10 are among the best extractants. Complexes of uranium(IV) extract to a lesser extent than those of uranium(VI). Complexes of uranium(III) are similar to those of the trivalent rare earths and only extract to a very small extent. Uranium(IV) chelates of cupferron and thenoyltrifluoroacetone are readily extractable into solvents with a low dielectric constant, as are those of the uranium(VI) chelates with such species as oxine, dibenzoylmethane, acetylacetone, diethyldithiocarbamate and pyridylazonaphthol.

1.1.3 Analytical Chemistry of Uranium

The primary use of uranium is the generation of atomic energy which creates a need for careful monitoring of uranium processing

plants and atomic stations. The measurement of uranium can be done by any one of a number of techniques.

(a) Gravimetric Methods

Common precipitants include ammonia, peroxide, oxalate, cupferron and 8-hydroxyquinoline. There is no highly selective precipitant for uranium in any of its oxidation states. Gravimeteric methods are therefore limited unless preliminary separation is employed. The usual weighing form is U_3O_8 obtained as the end product upon ignition of most organic compounds or mixtures and of most inorganic salts.

(b) Titrimetric Methods

A titrimetric method is usually chosen when a high-precision assay is required. With high-radiation-level samples the analytical method must be simple in technique, rapid, use maintenance-free apparatus and involve a minimum of manipulation. For remote titrimetry the controlled-potential coulometric method offers the advantages of a minimum amount of manipulation and a relatively high tolerance to diverse ions.

(c) Colorimeteric and Spectropnotometric Methods

Colorimetric and spectrophotometric methods for the determination of uranium are very numerous and are used over a wide range of uranium concentrations from a few $\mu g.g^{-1}$ to 10 per cent or more. Uranium is usually detected by its colour reactions with inorganic and organic reagents.

(d) Fluorimetric Methods

The determination of uranium by the measurement of its fluorescence, particularly in fused fluxes containing sodium fluoride, has probably received more study than any other technique. Two reasons for this are the extreme sensitivity, a detection limit of about $10^{-10} g.g^{-1}$, and the dependence of the fluorescence intensity on a large number of variables.

The two general approaches are measurement in liquid media and measurement after fusion in a flux containing sodium fluoride. The

former allows the use of simple fluorimeters and avoids high-temperature fusions. Fusion methods, however, are more popular for reasons of greater sensitivity, specificity and freedom from quenching.

(e) X-Ray Methods

X-ray techniques are especially applicable for the determination of uranium due to its high molecular weight relative to the common alloying metals and various elements present in samples. X-ray techniques that have been apolied include absorption, fluorescence, absorption edge and Raleigh scattering.

1.2 Process Control of Uranium

In most classical assay systems, the reagents and samples are placed in a reaction vessel, allowed to react for a certain time and then transferred to a measuring system. These batch operations have been used for making either kinetic or equilibrium analytical measurements. Theoretical considerations are based on uniform distribution. The ever increasing demand for analytical methods for many different types of plant control has led to the development of a large number of instruments for automated analysis. Developments in this field have been further stimulated by the additional advantages of automation which result in an increase in the precision of the analysis, the reliability of the equipment and a decrease in the cost of an individual assay.

Conventionally, continuous flow analyzers refer to any proce in which the concentration of the analyte is measured without interruption in a stream of liquid or gas. Successive discrete samples pass through a tube in the analyzer and reagents are added at strategic points. Mixing, reaction and extraction,etc., take place while the sample solution is on its way towards a flow cell where the signal is continuously monitored and recorded. Two classes of continuous flow analyzers are in use today, continuous flow and flow injection.

1.2.1 Continuous Flow Analysis

In 1957, Skeggs[5] introduced continuous flow analysis (CFA), an automated technique for the analysis of discrete samples by use of segmented continuously flowing streams. The samples were aspirated from their cups by a peristaltic pump into the tubing of the system. The sample volume was determined by the diameter of the pump tubing and the speed of the pump. At the end of the sampling period, the probe was moved to a wash vessel to prevent cross-contamination of the samples. The reagents and the air were continuously fed into the system by a peristaltic pump. The flowrates were determined by the diameter of the pump tubings and the speed of the pump. The proportion of sample to reagent was fixed by the initial concentrations of the analyte and reagent and by the ratio of their two flowrates.

Air-bubbles were used to segment the reaction stream so as to prevent excessive dispersion of the sample by the dispersive forces inherent in the laminar flow of the system. The air-bubbles prevented excessive dilution of the sample, minimized the overlap between samples boluses and assisted in the mixing of the reagent and sample. Before the sample reached the detector, the air-bubbles were removed from the stream and the resulting non-segmented stream passed through the flow-cell of the detector. This very successful method is the basis for the bulk of the mechanised colorimetric analyzers in use today.

The usefulness of CFA is limited by the inherent compressibility of air which causes the stream to pulsate and therefore neither the tube length nor its diameter can be decreased below certain values. The air also prevents miniaturization of the system. Other limitations include (a) the necessity for removing the air bubbles before measurement, (b) irregularities in the bubble pattern and (c) restricted dispersion of the analyte and carrier stream in the liquid bubbles.

1.2.2 Flow Injection Analysis

The introduction of Flow Injection Analysis (FIA) in 1974 by Ruzicka and Hansen in Denmark[6], and Stewart and co-workers in the U.S.A.[7,8], was an important breakthrough in automated chemical

analysis. FIA is based on the injection of a liquid sample via a valve or syringe into a moving, non-segmented continuous carrier stream of a suitable liquid. The injected sample forms a zone which is transported by the carrier stream towards a detector that continuously measures the absorbance, electrical potential or other physical parameter as it continuously changes by the passage of the sample zone through the detector flowcell. Following injection, the sample aliquot may be delivered directly to the detector or dispersed in the carrier stream to facilitate sample conditioning prior to measurement. The dispersion of the injected sample in the carrier stream is induced by the flow process alone and does not require any mechanical assistance. As the amount of sample injected and its residence time in the system are reproducible, the conventional concept of "steady-state signal" can be abandoned, the sampling frequency increased and the sample consumption reduced.

The use of narrow bore tubing as the reaction conduit is the key to significant dispersion of the sample in the carrier stream. In fact, by varying the operating parameter values of a FIA system, including sample size, flowrate, tube length and tube diameter, a wide range of dispersion conditions can be established to attain optimum conditions for a particular analytical technique. It is this controlled dispersion that allows FIA to operate in diverse situations[9-14].

1.3 Determination of uranium by FIA

Lynch et al [40] have described a flow injection method in which the uranium in the injected sample is extracted with a solution of tributyl phosphate in hexane and the organic phase is separated. The extract is reacted with an ethanolic solution of bromo-PADAP and the resulting complex is measured spectrophotometrically. Silfwerbrand-Lindh et al [41] have described a flow injection method in which tightly coiled teflon tubing and packed bed mixers were used to ensure proper mixing of the aqueous and ethanolic streams.

1.4 Aims of the Investigation

The aims of this investigation were:

(a) the application of FIA to the direct spectrophotometric determination of uranium(VI) using the azo dye of the pyridine series, bromo-PADAP,

(b) the study of the interference of selected elements and mineral acids in the determination of uranium(VI) and

(c) the optimization of the physical parameters of the FIA manifold and the chemical parameters of the reagents by univariate and simplex methods.

CHAPTER 2

THEORY

FIA is a suitable system for automation of an on-line control of process streams as it is precise, economical with respect to sample and reagent consumption, does not rely on reaction completion and the sampling rate can be varied from a few samples to several hundred per hour. A sensitive and practical method for the measurement of uranium in a FIA system is based on the use of an azo dye of the pyridine series and a spectrophotometric measurement. The optimum physical and chemical parameters can be determined by univariate and simplex methods of optimization.

2.1 Colorimetric and Spectrophotometric Methods of Analysis

Colorimetric and spectrophotometric procedures are among the most frequently used methods of quantitative analysis. They are based on the absorption of visible light or other radiant energy by the solution. The amount of radiant energy absorbed is proportional to the concentration of absorbing material in solution and by measuring this absorption it is possible to determine quantitatively the amount of substance present[15].

Colorimetric analysis refers to the quantitative determination of a coloured substance from its ability to absorb light. Visual colorimetric methods rely on the comparison of a coloured solution of unknown concentration with one or more solutions of known concentration.

Spectrophotometric methods are not limited to the use of visible light but include those that employ radiant energy in other regions of the electromagnetic spectrum, such as the ultraviolet or the infred.

Ions or molecules that have little or no colour can be determined spectrophotometrically after reaction with a suitable reagent that converts them to a highly coloured product. Most inorganic substances are determined this way. For example, uranium

which can be used for its determination.

2.1.1 Absorption of Radiant Energy

Light is absorbed by a substance only when the energy of the light corresponds to the energy needed to cause some change in the chemical molecule. Thus, light of certain energies or wavelengths is absorbed, whereas light of other wavelengths is not. The changes in the molecule caused by the absorption of radiation may be electronic (change in energy of the electrons distributed about the atoms in the molecule), vibrational (change in the average separation of the nuclei of two or more atoms), or rotational (rotation of a chemical dipole). Radiation of higher energy is necessary to effect electronic transitions (changes) than is necessary to effect rotational or vibrational transitions. Electronic transitions, therefore, are caused by the absorption of visible light and ultraviolet radiation, whereas rotational and vibrational transitions are caused by absorption of infrared and longer wavelength radiation.

It is useful to know which wavelengths of radiant energy are most strongly absorbed in a particular solution and by measuring the amount of absorption as the wavelength of an incident beam through a solution varies, an absorption spectrum can be plotted. An important use of absorption spectra is in the selection of a wavelength suitable for quantitative analysis.

2.1.2 Beer's Law

This fundamental law of colorimetric and spectrophotometric methods states that the amount of radiant energy in the spectrum between the ultraviolet and the infrared that is absorbed or transmitted by a solution is an exponential function of the concentration of the absorbing substance present and of the sample path length.

$$\log \frac{P_o}{P} = -abc = A \qquad (2.1)$$

where P_o = incident radiant energy

P = transmitted radiant energy

a = a proportionality constant (absorptivity)

b = internal cell length, cm

c = concentration of the solution

A = absorbance

The value of the absorptivity "a" depends on the units used for expressing the concentration of the absorbing solution. If the concentration is expressed in molarity (moles.l^{-1}), the molar absorptivity ϵ is written in place of absorptivity a. Thus Beer's Law becomes

$$A = \epsilon bc \qquad (2.2)$$

2.2 Pyridylazo Compounds as Metallochromic Indicators

2.2.1 Azo Compounds of the Pyridine series

Pyridine azo compounds with the hydroxy group in the ortho-position with respect to the azo group are very valuable analytical reagents. They have been widely used in complexometric and extraction-photometric methods for determining different cations[16-27]. Those more frequently used are 1-(2-pyridylazo)-2-naphthol (PAN) and the water-soluble and more sensitive reagent 4-(2-pyridylazo)rescorcinol (PAR)[16,17].

In the search for new and sensitive reagents, thorough studies have been made of some azo compounds containing 5-substituted pyridine. Highly sensitive reagents for metals have been obtained by introducing the dimethylamino or the diethylamino groups which are strongly electron donating groups (Table 2.1). Shibata et al.[28] synthesized fifteen dyes containing the m-methylaminophenol group and studied their analytical potential for the spectrophotometric determination of metals. Florence et al.[29,30] synthesized the diethylaminophenol analog of PAR, 2-(2-pyridylazo)-5-diethyl-aminophenol (PADAP), and established that this reagent was twice as sensitive towards uranium(VI) as PAR with a molar absorptivity of 6.59×10^4 at a pH value of 8.2 and a wavelength of 564 nm

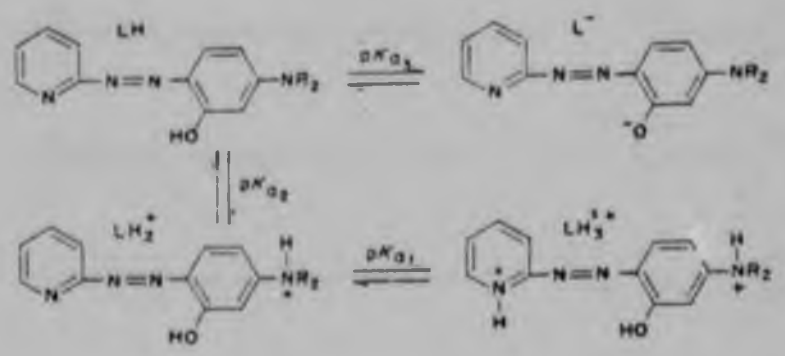
Introduction of an electronegative substituent such as chlorine, bromine and iodine ions, lowers the basic properties of the pyridine ring, shifts the absorption spectrum of the reagent by approximately 10 nm towards the longer wavelength region and slows down the reaction rate with uranium(VI)[31,32].

(a) Preparation of Reagents

The reagents are prepared by coupling the appropriate methyl- or ethyl-aminophenols with the substituted 2-pyridyldiazote and then recrystallizing from ethanolic solution (Appendix I). Table 2.1 lists the 2-pyridylazo compounds and includes their formulae and common names.

(b) Acid-base Equilibria

All the 3-alkylaminophenol derivatives are sparingly soluble in water but are soluble in various organic solvents, including methanol, ethanol, methylisobutylketone, benzene and chloroform. They are yellow in weakly acidic and neutral solutions and orange-red in alkaline solution. Four acid-base reactions are involved in the equilibria where R is the methyl radical.

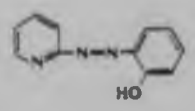
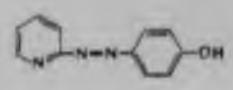
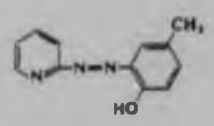
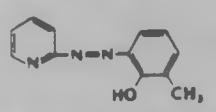
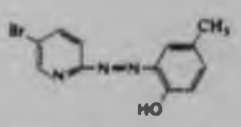
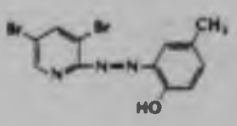
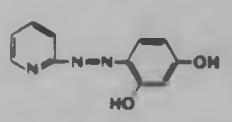
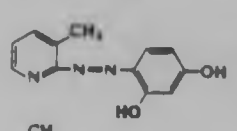
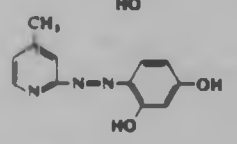
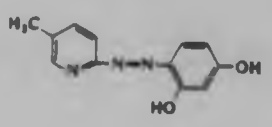
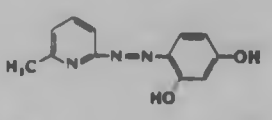
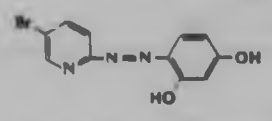
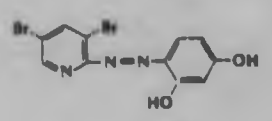
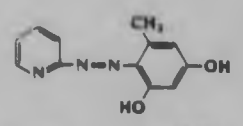
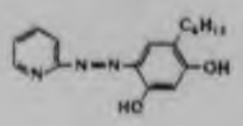


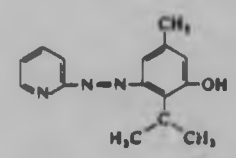
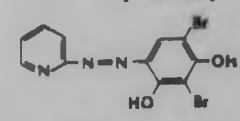
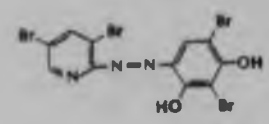
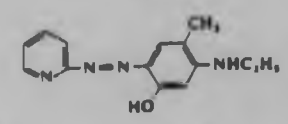
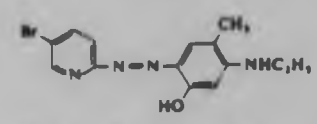
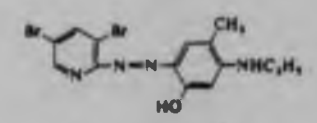
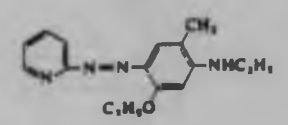
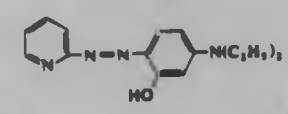
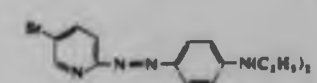
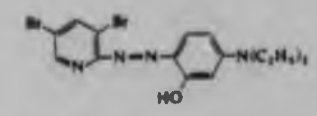
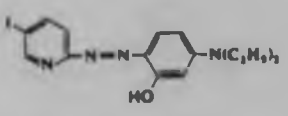
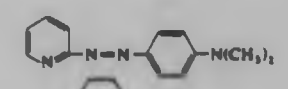
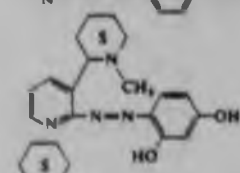
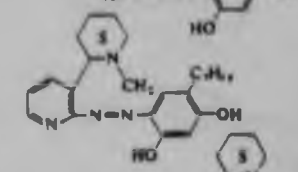
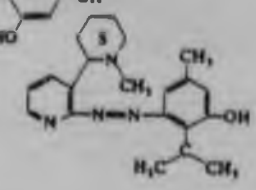
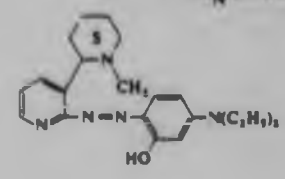
The acid-base equilibria of DMPAP may be formulated as follows:

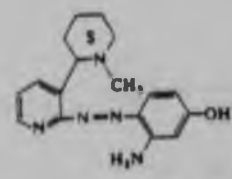
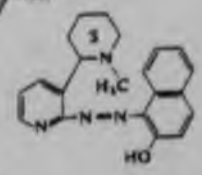
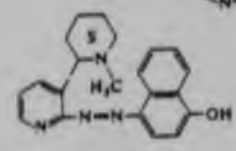
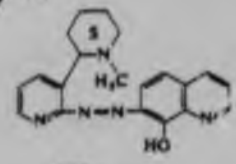
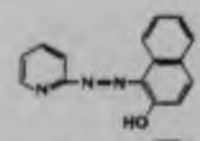
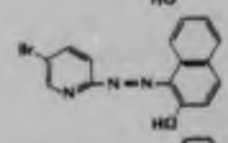
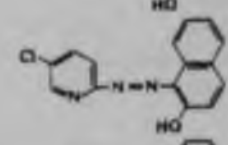
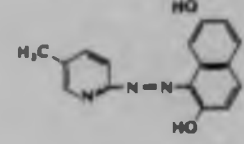
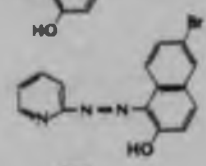
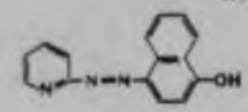
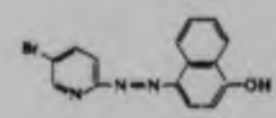
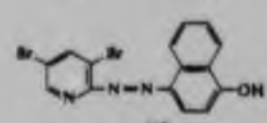
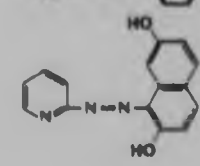
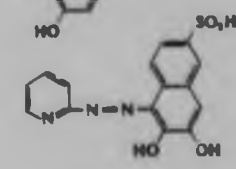
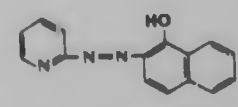
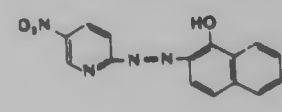
$$LH_3^{2+} \overset{pKa_1}{\rightleftharpoons} LH_2^{+} + H^{+} \qquad (2.3)$$

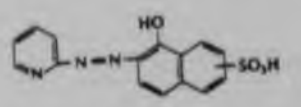
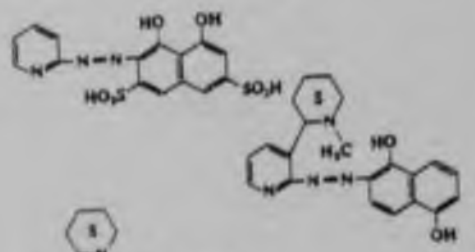
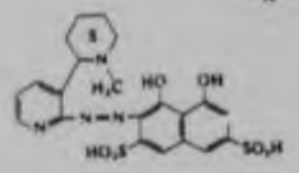
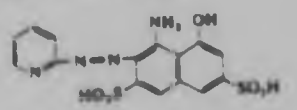
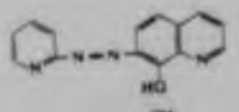
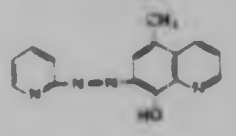
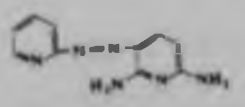
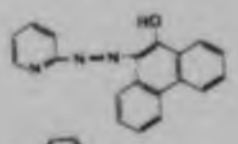
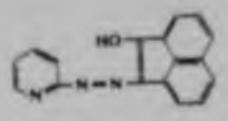
$$LH_2^{+} \overset{pKa_2}{\rightleftharpoons} LH + H^{+} \qquad (2.4)$$

Table 2.1 Azo compounds of the pyridine series

o-PAP	o-(2-pyridylazo)phenol	
p-PAP	p-(2-pyridylazo)phenol	
PAC	2-(2-pyridylazo)-p-cresol	
o-PAC	6-(2-pyridylazo)-o-cresol	
5-bromo-PAC	2-[(5-bromo-2-pyridyl)azo]-p-cresol	
3,3-dibromo-PAC	2-[(3,5-dibromo-2-pyridyl)azo]-p-cresol	
PAR	4-(2-pyridylazo)resorcinol	
3-methyl-PAR	4-[(3-methyl-2-pyridyl)azo]resorcinol	
4-methyl-PAR	4-[(4-methyl-2-pyridyl)azo]resorcinol	
5-methyl-PAR	4-[(5-methyl-2-pyridyl)azo]resorcinol	
6-methyl-PAR	4-[(6-methyl-2-pyridyl)azo]resorcinol	
5-bromo-PAR	4-[(5-bromo-2-pyridyl)azo]resorcinol	
3,5-dibromo-PAR	4-[(3,5-dibromo-2-pyridyl)azo]resorcinol	
PAO	4-(2-pyridylazo)orcinol; 5-methyl-4-(2-pyridylazo)	
PAR-4-hexyl	4-hexyl-6-(2-pyridylazo)resorcinol	

PAT	5-(2-pyridylazo)thymol	
PAR-2,6-dibromo	2,6-dibromo-4-(2-pyridylazo)resorcinol	
tetrabromo-PAR	2,6-dibromo-4-[(3,5-dibromo-2-pyridyl)azo]-resorcinol	
PAAC	5-(ethylamino)-2-(2-pyridyl)-p-cresol	
5-bromo-PAAC	2-[(5-bromo-2-pyridyl)azo]-5-(ethylamino)-p-cresol	
3,5-dibromo-PAAC	2-[(3,5-dibromo-2-pyridyl)azo]-5-(ethylamino)-p-cresol	
EMPAP	N-ethyl-6-methyl-4-(2-pyridylazo)-m-phenetidine	
PADAP	5-(diethylamino)-2-(2-pyridylazo)phenol	
5-bromo-PADAP	2-[(5-bromo-2-pyridyl)azo]-5-(diethylamino)phenol	
3,5-dibromo-PADAP	2-[(3,5-dibromo-2-pyridyl)azo]-5-(diethylamino)-phenol	
5-iodo-PADAP	5-(diethylamino)-2- (5-iodo-2-pyridyl)azo phenol	
Pada; PAA	N,N-dimethyl-p-(2-pyridylazo)aniline	
MAAR	4-[[3-(1-methyl-2-piperidyl)-2-pyridyl]azo]resorcinol	
MPPAR-4-heptyl	4-heptyl-6-[[3-(1-methyl-2-piperidyl)-2-pyridyl]azo]-resorcinol	
MPPAT	5-[[3-(1methyl-2-piperidyl)-2-pyridyl]azo]thymol	
DMPPP	5-(diethylamino)-2-[[3-1-methyl-1-2-piperidyl)-2-pyridyl]azo]phenol	

AMPPAP	3-amino-4-[3-(1-methyl-2-piperidyl)-2-pyridyl]-azo]phenol	
MAAN	1-[[3-(1-methyl-2-piperidyl)-2-pyridyl]azo]-2-naphthol	
p-MAAN	4-[[3-(1-methyl-2-piperidyl)-2-pyridyl]azo]-1-naphthol	
MAAOx	7-[[3-(1-methyl-2-piperidyl)-2-pyridyl]azo]-8-quinolinol	
PAN	1-(2-pyridylazo)-2-naphthol	
5-bromo-PAN	1-[(5-bromo-2-pyridyl)azo]-2-naphthol	
5-chloro-PAN	1-[(5-chloro-2-pyridyl)azo]-2-naphthol	
5-methyl-PAN	1-[(5-methyl-2-pyridyl)azo]-2-naphthol	
PAN-6-bromo	6-bromo-1-(2-pyridylazo)-2-naphthol	
p-PAN	4-(2-pyridylazo)-1-naphthol	
5-bromo-p-PAN	4-[(5-bromo-2-pyridyl)azo]-1-naphthol	
3,5-dibromo-p-PAN	4-[(3,5-dibromo-2-pyridyl)azo]-1-naphthol	
2,7-PADN; 2,7-PAN	1-(2-pyridylazo)-2,7-naphthalenediol	
PADNS	6,7-dihydroxy-5-(2-pyridylazo)-2-naphthalene-sulfonic acid	
α-PAN	2-(2-pyridylazo)-1-naphthol	
5-nitro-α-PAN	2-[(5-nitro-2-pyridyl)azo]-1-naphthol	

α-PAN-x-S	2-(2-pyridylazo)-1-naphthol-x-sulfonic acid (x=4,5,6,7 or 8)	
PACh	4,5-dihydroxy-3-(2-pyridylazo)-2,7-naphthalenedisulfonic acid; (2-pyridylazo)chromotropic acid	
MP-1,5-PADN	2-[[3-(1-methyl-2-piperidyl)-2-pyridyl]azo]-1,5-naphthalenediol	
MPPACh	4,5-dihydroxy-3-[[3-(1-methyl-2-piperidyl)-2-pyridyl]azo]-2,7-naphthalenedisulfonic acid	
PA-H; PAH	4-amino-5-hydroxy-3-(2-pyridylazo)-2,7-naphthalenedisulfonic acid; (2-pyridylazo)-H-acid	
PAOx	7-(2-pyridylazo)-8-quinolinol	
PAOx-5-methyl	5-methyl-7-(2-pyridyl)-8-quinolinol	
DAPAPy	2,6-diamino-3-(pyridylazo)pyridine	
PAPh; PAPhen	10-(2-pyridylazo)-9-phenanthrol	
PAAC; PAAcn	2-(pyridylazo)-1-acenaphthylenol	

$$LH \overset{pKa_3}{\rightleftharpoons} L^- + H^+ \qquad (2.5)$$

The three acidity constants are then:

$$pKa_1 = \frac{[LH_2^+][H^+]}{[LH_3^{2+}]} \qquad (2.6)$$

$$pKa_2 = \frac{[LH][H^+]}{[LH_2^+]} \qquad (2.7)$$

$$pKa_3 = \frac{[L^-][H^+]}{[LH]} \qquad (2.8)$$

Johnson and Florence determined the pKa_1 values by a graphical method and the constants are reported in Table 2.2. The pKa_2 values which are due to the dimethylamino group increase in the order[28]:

DMTAP < DMQAP < 5-chloro-DMPAP ≡ 5-bromo-DMPAP < DMPAP

whereas the pKa_3 values increase in the order:

DMTAP < 5-chloro-DMPAP ≡ 5-bromo-DMPAP < DMPAP < DMQAP

The wavelengths of absorbance maxima and molar absorptivity of each species are shown in Table 2.3. The shift of maximum wavelength from neutral to basic species increase in the order:

DMQAP < DMTAP < DMPAP < 5-chloro-DMPAP < 5-bromo-DMPAP

2.2.2 Bromo-PADAP Complexes of Uranium

Bromo-PADAP has found wide application as a very sensitive reagent for the determination of uranium by spectrophotometry and has been studied by Johnson and Florence[31-41].

Table 2.2 Acid dissociation constants

Reagents	pKa_1	pKa_2		pKa_3	
DMTAP	<1	2.8		9.9	
DMQAP	<1	3.1		13.1	
DMPAP	<1	3.6		12.1	
5-chloro-DMPAP	<1	3.4	2.1	11.6	11.4
5-bromo-DMPAP	<1	3.4	2.2	11.6	11.2
bromo-PADAP	<1	2.2		11.3	
PAR	3.1	5.6		11.9	

Table 2.3 Absorption maxima of reagents and molar absorptivities
(Aqueous 40% v/v methanol solution)

Reagents	pH 1		pH 6		NaOH 0.1M	
	λ_{max}	ϵ	λ_{max}	ϵ	λ_{max}	ϵ
DMQAP	504	4.6	478	4.5	490	2.6
DMTAP	540	6.1	502	4.6	524	4.1
DMPAP	524	2.2	435	3.0	494	3.0
5-chloro-DMPAP	465	4.7	440	4.6	508	4.6
5-bromo-DMPAP	466	4.7	444	4.7	510	4.7

λ_{max} is given in nm. All molar absorptivities are given as $10^4 l.mol^{-1}.cm^{-1}$.

(a) Effect of pH on Complex Formation

Complex formation was studied over a range of pH values between 3 to 8 with bromo-PADAP and uranyl ion concentrations of 1.00 x 10^{-5}M and 1.00 x 10^{-3}M respectively. After two hours, the measured spectra indicated the formation of a single complex with two maxima, one at 554 and the other at 586 nm (Figure 2.1). The complex was stable for several days. The pH-absorbance curves (Figure 2.2) show pH-dependence with maxima at a pH value of 4.1.

Johnson and Florence[33] noted an unstable complex at a pH value of 7.6 which forms initially but rapidly decays with maxima at 546 and 580 nm. A metal to ligand ratio of 1:1 was established by these investigators. The complex almost completely disappeared after standing for another 30 minutes.

Using Job's method of continuous variation[27,34] and the mole ratio method, the composition of the complex at a pH value of 4.1 was determined as having an uranyl ion to ligand ratio of 1:1. Using a 100-fold excess of uranyl ions, the molar absorptivity was 4.65 x 10^4 l.mol^{-1}.cm^{-1} at 554 nm and 5.53 x 10^4 l.mol^{-1}.cm^{-1} at 586 nm.

(b) Effect of Fluoride on Complex Formation

The presence of fluoride in a solution of bromo-PADAP and uranyl ion buffered to a pH value of 7.6 results in a slow increase in the pink colour in the presence of excess bromo-PADAP. The colour of the complex formed under similar conditions at a pH value of 4.1 is mauve. A quantitative study of the effect of varying the fluoride ion showed that above a mole ratio of 2000 (fluoride : uranyl ion) the complex formation becomes independent of fluoride concentration (Figure 2.3). The spectrum of the complex shows two maxima, at 542 and 578 nm with molar absorptivities of 5.51 x 10^4 and 7.32 x 10^4 l.mol^{-1}.cm^{-1}., respectively.

The pH-absorbance curves in the presence of fluoride show a maximum at a pH value of 7.3. Using Job's method and the mole ratio method, the composition of the complex at a pH value of 7.3 was determined as 1:1 (uranyl ion : fluoride).

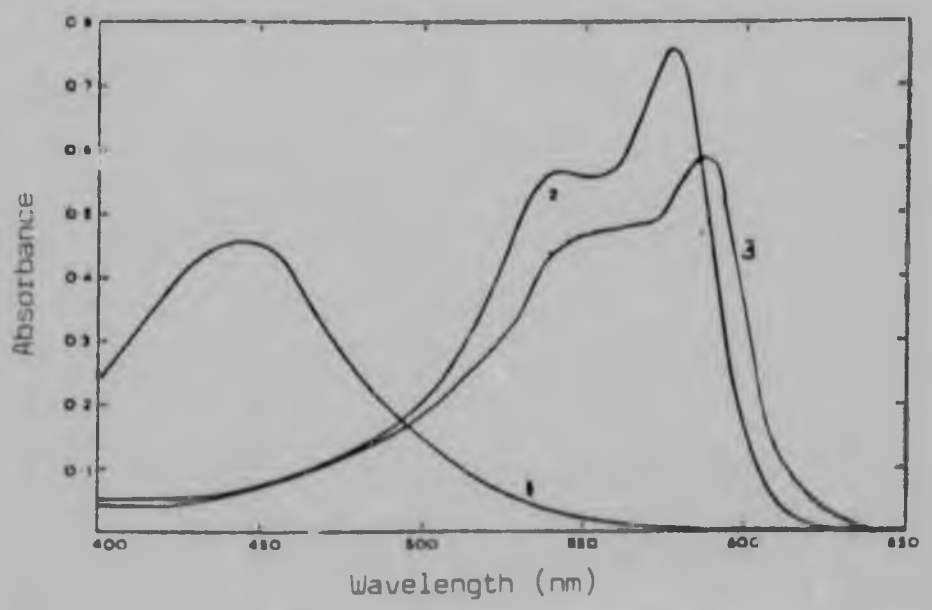


Figure 2.1 **Wavelength absorbance curves**

1 Free bromo-PADAP (1.0×10^{-5}M UO_2^{2+} vs blank: pH 8)

2 Uranyl bromo-PADAP complex (1.0×10^{-3}M vs blank : pH 7.3)

3 Uranyl bromo-PADAP complex (1.0×10^{-3}M vs blank : pH 4.1)

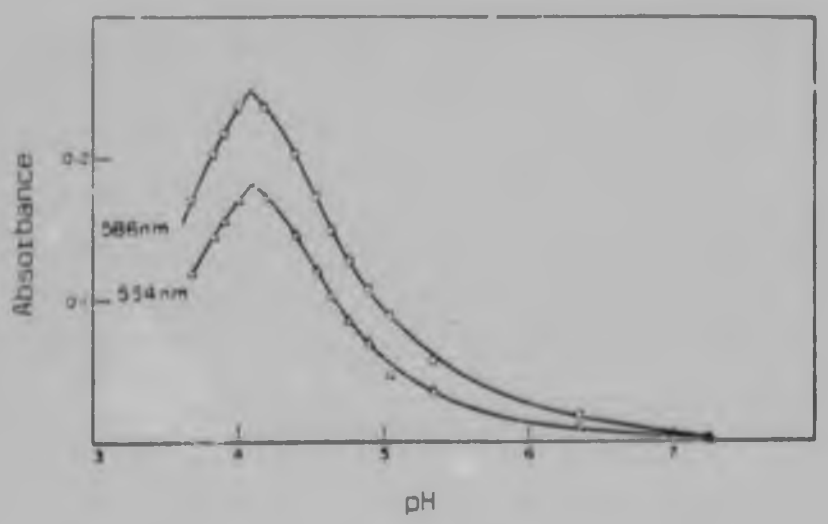


Figure 2.2 **pH absorbance curves**

Conditions: Bromo-PADAP = UO_2^{2+} = 1.0×10^{-5}M

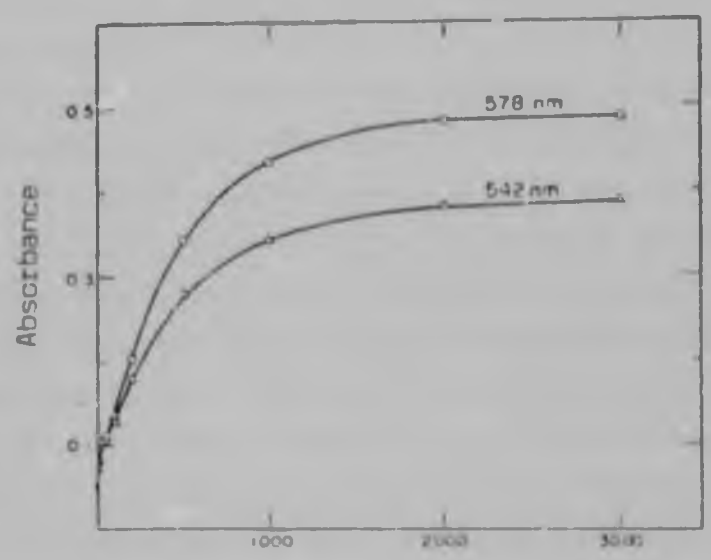
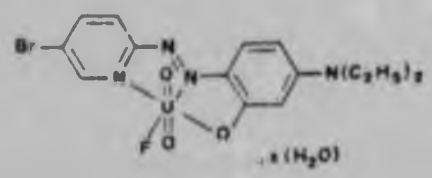


Figure 2.3 Effect of fluoride on complex formation

Conditions: Bromo-PADAP = UO_2^{2+} = 1.0×10^{-5}M;
pH, 7.6

(c) Nature of bromo-PADAP Uranium Complexes

The uranyl complexes, each having double maxima and each extractable into a wide range of polar and many less polar solvents, remain extractable in the presence of excess anions such as nitrate, chloride, perchlorate, sulphite and chromate, showing that the complexes are not ion association complexes. Johnson and Florence[34] examined the bromo-PADAP molecule and found that the dye, when complexed, exhibited a single negative charge by the loss of the hydroxyl proton. The uranyl ion has two positive charges. The neutral 1:1 complex therefore requires an additional single negatively charged ligand. The addition of fluoride results in the formation of a different stable complex at a pH value of 7.3 in the solution in which the original complex has decayed and Johnson and Florence deduced that the fluoride entered as an auxiliary ligand. They decomposed the complex by shaking a chloroform extract of the dye with distilled water. Equimolar concentrations of uranyl ion and fluoride were produced corresponding to the formula UO_2(bromo-PADAP$^-$)F. Two water molecules are probably associated with the complex to give the usual coordination number of six for the uranyl ion complex. A possible structure is shown below assuming that bromo-PADAP coordinates through the same atoms as does PAR.



In the absence of fluoride, the 1:1 complex that forms and decays rapidly is the hydroxy-analog of the fluoro-complex UO_2(bromo-PADAP$^-$)OH. When uranium(VI) reacts with the dye at a pH value of 7.3, the reaction rate of the dye with the small amount of UO_2OH^+ is faster than the polymerization of UO_2OH^+. The formation of the more stable hydroxy-uranyl polymer eventually eliminates UO_2OH^+ from the complex.

Johnson and Florence established that other anionic ligands such as bromide, cyanide and thiocyanate did not enter into the complex

formation as did the fluoride and that the complex formed in each case had an identical spectrum to the postul UO_2(bromo-PADAP$^-$)OH complex. This complex decomposed as did the UO_2(bromo-PADAP$^-$)OH complex.

(d) Stability Constants

Stability constants for the two stable complexes are given in Table 2.4. The ratio of the heights of the two peaks for the complex, when corrected for blank absorbance, is the same at all pH values. The stability constants for each complex determined at the two wavelengths of the double peaks are the same at all pH values.

Table 2.4 Stability constants

Complex	pH	λ	β'
UO_2(bromo-PADAP$^-$)OH	4.1	554	1.32×10^5
	4.6	586	3.30×10^5
UO_2(bromo-PADAP$^-$)F	7.3	542	4.51×10^5
	7.3	578	4.42×10^5

λ = wavelength, nm
β' = stability constant
UO_2^+ = bromo-PADAP = 1.0×10^{-5}M
μ = ionic strength = 0.1

(e) Spectral Data

The spectral data for uranyl complexes of PADAP derivatives (Table 2.5) show that with the exception of 5-bromo-DMPAP, the molar absorptivities are all $(7.3 \pm 0.3) \times 10^4 l.mol^{-1}.cm^{-1}$.,

regardless of whether the substituent is electron-withdrawing or electron-repelling. The substituent has a more marked effect on the wavelength of the absorption maximum, with halogen substituents causing much larger bathochromic shifts than other substituents.

Table 2.5 Spectral data for uranyl comolexes of PADAP derivatives

Reagent	λ_{max} nm	pH	Molar absorptivity $10^4 l.mol^{-1}.cm^{-1}$	Mole ratio
PAR	530	8.0	3.60	1:1
iodo-PADAP	583	8.0	7.12	1:1
bromo-PADAP	579	7.6	7.32	1:1
chloro-PADAP	576	8.0	7.10	1:1
PADAP	564	8.2	7.60	1:1
5-Me-PADAP	568	8.0	7.20	1:1
5-bromo-DMPAP	576	8.0	6.20	1:1
QUADAP	564	8.0	7.60	1:1
PAAP	540	8.0	3.80	1:1

2.3 Optimization of FIA Methods

Many workers have demonstrated that it is relatively simple to adapt a standard manual spectrophotometric procedure to FIA with little loss of sensitivity. However, an examinaton of the literature shows that for a given procedure conditions used by different workers and described by them as optimum may vary appreciably. This is not surprising since in any flow method, in addition to the normal chemical variables, such as reagent concentration, pH value, etc., the physical variables such as flowrate, length of tubing between points of injection and determination, tube diameter and the sample size must be taken into account. Thus even an experimentally simple single channel FIA

system will have five variables. The conventional optimization procedure of altering one variable at a time while keeping the rest fixed (the univariate method) is therefore time consuming and may be inadequate as a means of reliably de.ermining the best set of experimental conditions. The usefulness of the simplex method of optimizaton is not merely that it will find a specific set of operating conditions giving improved performance, but rather that the impro ements can be achieved in a simple and efficient manner handling several variables at once.

2.3.1 Optimization Procedures

Optimization techniques[43-49] require the definition of a "response" of the system that is to be maximized and of the experimental variables on which it is dependent. In a two variable system, the variables can be represented as the axes of a graph, with each point in the space described corresponding to one set of experimental conditions. Each experiment will have a response and this can be shown as the third dimension. Thus in the simplest case of a two variable system a "response surface" will be created which may be vizualized as a "hill" the crest of which is the maximum response. The picture becomes increasingly complex the greater the number of variables. Optimization procedures are a means of proceeding from a given, or starting set of conditions to those that give a maximum response. An ideal optimization procedure should be capable of finding the highest maximum reliably and rapidly, irrespective of the nature of the surface.

(a) Univariate Method of Optimization

The univariate method involves keeping all but one variable constant, finding the best value for this variable under those conditions and then repeating the procedure for each variable in turn. The conventional univariate approach considers each variable several times, the procedure continuing until no further improvement is obtained.

Figure 2.4[44] shows isoresponse contours as a function of two variables x_1 and x_2 for a hypothetical chemical system. In this example, x_2 is fixed initially and x_1 is varied along

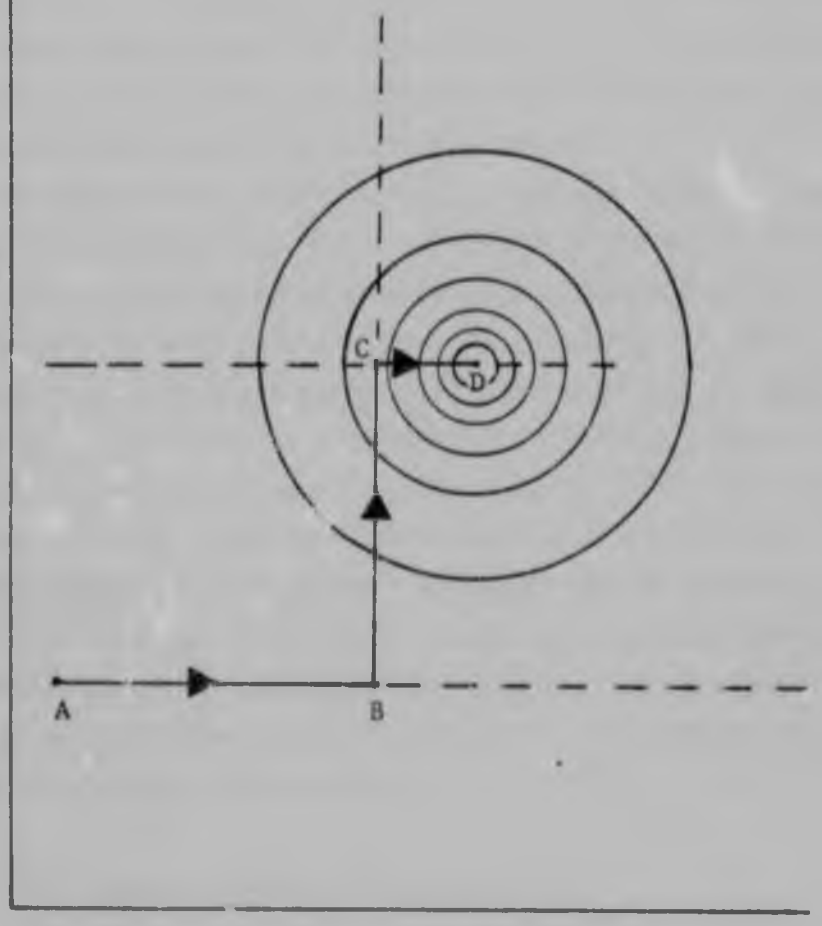


Figure 2.4 Single variable-at-a-time method

the line segment AB and its extensions. An optimum response is obtained at point B. The optimized variable is now kept constant and x_2 is varied along the line segment BC and its extensions until a new optimum response in obtained at point C. In general, one cycle of altering the variables is not sufficient precisely to define the optimum. In Figure 2.4, the first search in the second cycle would take place along the line segment CD and its extensions and stop at a point D which is closer to the true optimum than either of the optima obtained in the previous cycle.

The sequential single-variable approach does not guarantee that the optimum will be located. When the response surface contains a ridge, the single variable procedure is unsatisfactory. Holding x_2 constant (Figure 2.5) and varying x_1 along the line segment AB and its extensions will find a single variable optimum at B. However, additional experiments varying x_2 while holding x_1 constant will indicate that the optimum value for x_2 is also at B. The presence of the ridge will not be detected by this strategy and B will be falsely accepted as the optimum. Ridges of this kind can occur frequently in chemical systems and result from a non-independence of the chosen variables. Indications of ridges are helpful because they indicate regions of the response surface that can be profitable or convenient.

(b) Simplex Method of Optimization

The simplex method of optimization[47] is better suited to systems where variables interact because these variables can be changed simultaneously in what is essentially a "hill climbing" approach to the problem. The objective of pattern search-methods such as simplex is to "home-in" on the optimum region of the response surface from a given subregion by forcing the movement in the direction of the steepest ascent as estimated by the response measurements. The optimum obtained will in general be a local optimum. Assurance that it is a "global" (overall) optimum can be increased if the search is repeated but starting from different initial points. If more than one local optimum is found, the best can be taken as the global optimum.

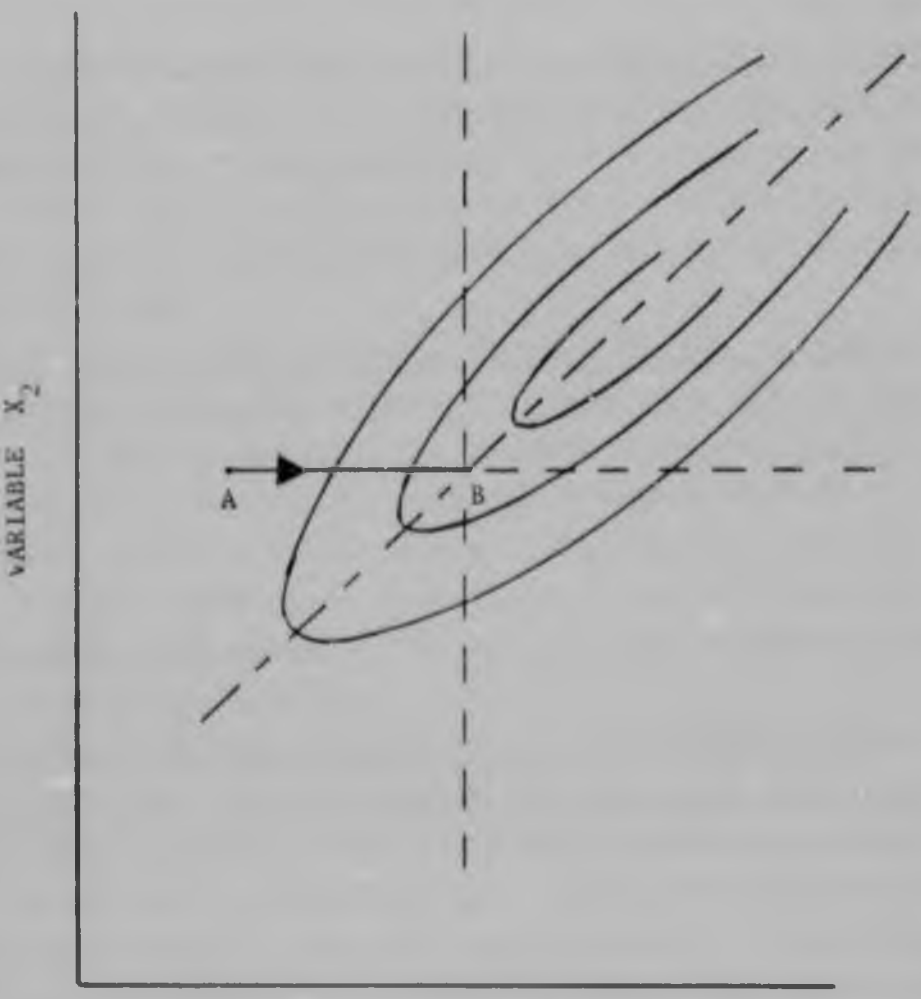


Figure 2.5 Failure of a single variable on a ridge

(i) Basic rules of the simplex method [48]

(a) A move towards the optimum response is made after each observation of the response . This move is made after ranking the responses. For situations involving more than two factors, the ranking is performed as best, next to best, ..., and worst.

(b) A move is made such that the vertex having the worst response is rejected and replaced by a new vertex generated by reflection through the midpoint of the remaining hyperface . The progress from the initial simplex ABC to the final simplex JKO may be seen in Figure 2.6. The ranking, rejection and generation of each new simplex is shown in Table 2.6.

(c) If, on ranking the vertices of the next simplex, the newly created vertex is the worst vertex, then reject the next-to-worst vertex . If this procedure is not adopted, the worst simplex generated will be identical to the previous simplex and the optimization process will terminate abruptly, hence the ranking order. For any n-dimensional problem, B, N and W are the only vertices being investigated. This rule has been invoked for runs 10, 13, 14 and 1[illegible] in Table 2.6.

(d) If a vertex has been retained for n+1 moves where n is the number of vertices, then the response for that vertex is re-evaluated This procedure prevents the simplex becoming stranded on one point whose response may be erroneously high. Vertex H is retained five times before a vertex K, having a higher response, is found (Figure 2.6). For a two dimensional simplex, the optimum is reached when the figures closed pack to form a hexagon. This can be seen in Figure 2.6 and Table 2.6 where the vertex K has the highest response. This phenomenon does not occur when dealing with systems of higher dimensions.

(e) Boundary constraint violations are accorded a suitably bad response If one or more of the new vertex levels are found to be outside the boundary constraints of each variable imposed by the usable range of the variable, that particular experiment is not performed. However, the reponse is assigned a suitably low (bad) value and included in the next round of calculations. Application of Rules (b) and (c) will force the simplex back into its boundaries and it will continue to seek the optimum response.

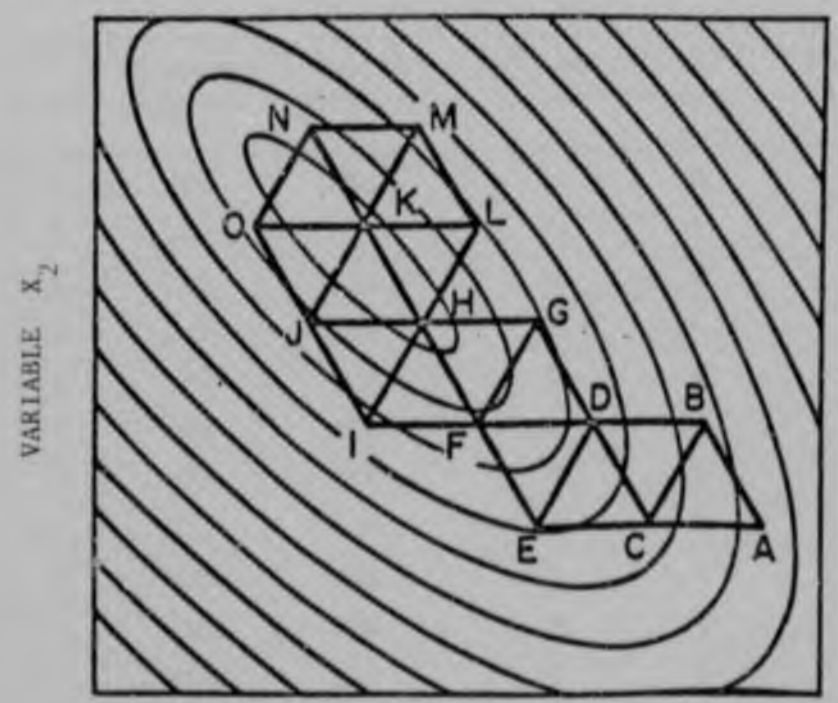


Figure 2.6 Progress of a fixed size simplex, superimposed on a hypothetical response surface

Table 2.6 Progress of simplex showing rejected and new vertices and responses

Move	Current Simplex	Ranked+ Vertices	Rejected Vertex	New Vertex	Response for New Vertex
4	ABC	ABC*	A	D	65
5	BCD	BCD	B	E	60
6	CDE	CDE	C	F	76
7	DEF	EDF	E	G	71
8	DFG	DGF	D	H	91
9	FGH	GFH	G	I	66
10	FHI	IFH	F	J	77
11	HIJ	ILH	I	K	95
12	HJK	JHK	J	L	72
13	HKL	LHK	H	M	66
14	KLM	MLK	L	N	85
15	KMN	MNK	M	O	83
16	KNO	ONK	N	P(=J)	77

+ Ranked in order worst, next-to-worst, best.

* Response for the initial simplex are A=37, B=45, C=53.

(ii) Fixed size simplex

Three limitations are apparent when using the fixed size simplex (Figure 2.6):

(a) the optimum is never located except by chance,

(b) a false optimum may be located, and

(c) the progress towards an optimum can only proceed at a fixed rate.

None of these limitations are severe and in fact may, in certain circumstances, prove to be beneficial. To obtain a precise location of an optimum, a small vertex can be started in the region of the optimum located by the larger simplex. On the other hand, if only an improvement in the response is desired, then the fixed size simplex would prove to be entirely adequate.

The location of a local rather than a global optimum is a problem not only restricted to this type of search procedure. Restarting the process from a different point in the factor space will, in all probability, establish whether the first optimum was local or not.

Nelder and Mead[47] recognised that the fixed size simplex cannot accelerate its progress in accordance with the response surface. However, the fixed size simplex provides a valuable tool for the localization and tracing of a moving optimum. For example, instrumentation that is prone to drift may be continually monitored and held at its peak performance by employing a small fixed size simplex and interfacing the equipment to a microcomputer.

(iii) Variable size simplex

There are several methods of optimization using a variable size simplex, that employed in the present work being the Modified Simplex Method (MSM) of Nelder and Mead. In this method, they describe the precise location of the optimum including an acceleration of the simplex and the incorporation of the expansion and contraction of the system. Together these operations provide the means by which the simplex figure may expand and accelerate towards the region of the optimum and then reduce its search region until the optimum is located with the desired precision. The MSM is better suited to systems in which there are several variables that

are inter-dependent and changing simultaneously in what is essentially a "hill climbing" approach to the problem.

The movement of the variable size simplex is governed by the same rules as the fixed size simplex. Additional tests are used to decide the operation to perform in a given situation. These rules are presented as a flow chart in Figure 2.7.

In an n-variable system, n+1 experiments are required for the first simplex. The variables can be thought of as n-orthogonal axes with each experiment represented by one point in this space. The geometric figure whose vertices are the n+1 points is known as the simplex. The simplex takes the form of a triangle in a two-variable system, a tetrahedron in a three-variable system, and so on.

At the conclusion of the first set of experiments, the responses in a two- variable system can be determined as the best (B), the next best (N) and the worst(W). The MSM of Nelder and Mead is a logical algorithm consisting of reflection, expansion, contraction and massive contraction rules that allows the simplex to conform to the topography of the response surface. In the initial simplex BNW (Figure 2.8), $\bar{P}$ is the centroid of the face remaining when the worst vertex, W, is eliminated.

Reflection is accomplished by extending the line segment $W\bar{P}$ beyond $\bar{P}$ to generate a new vertex C_R.

$$C_R = \bar{P} + \alpha(P - W) \qquad (2.9)$$

Initially the point is chosen with $\alpha = 1.0$. Three possibilities exist for the measured response at C_R.

(a) The response at C_R is more favourable than the response at B. The search continues by choosing another point C_E with α greater than 1 (usually 2.0). This is called expansion.

$$C_E = \bar{P} + \gamma(P - W) \qquad (2.10)$$

where γ is the expansion coefficient (γ greater than 1, usually 2.0) which determines how much further than C_R the segment C_E is to be expanded. If the response at C_E is better than the

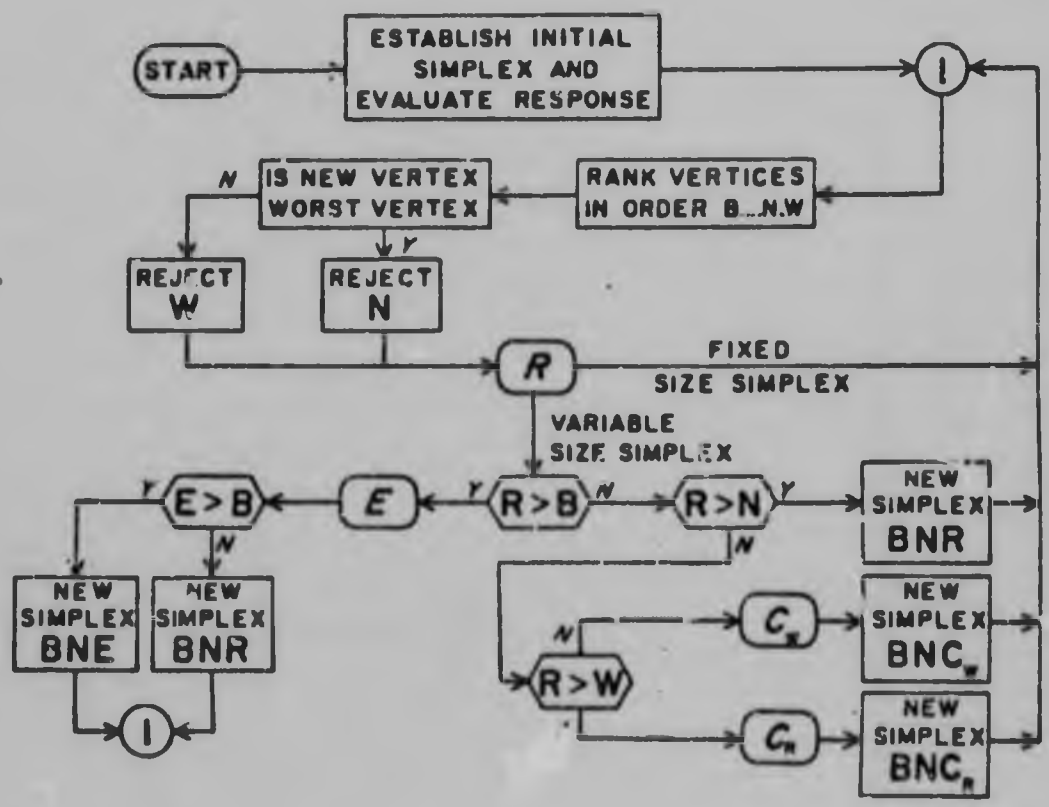


Figure 2.7 Flow chart summarizing rules for the acceptance or rejection of a vertex either fixed or variable size simplex

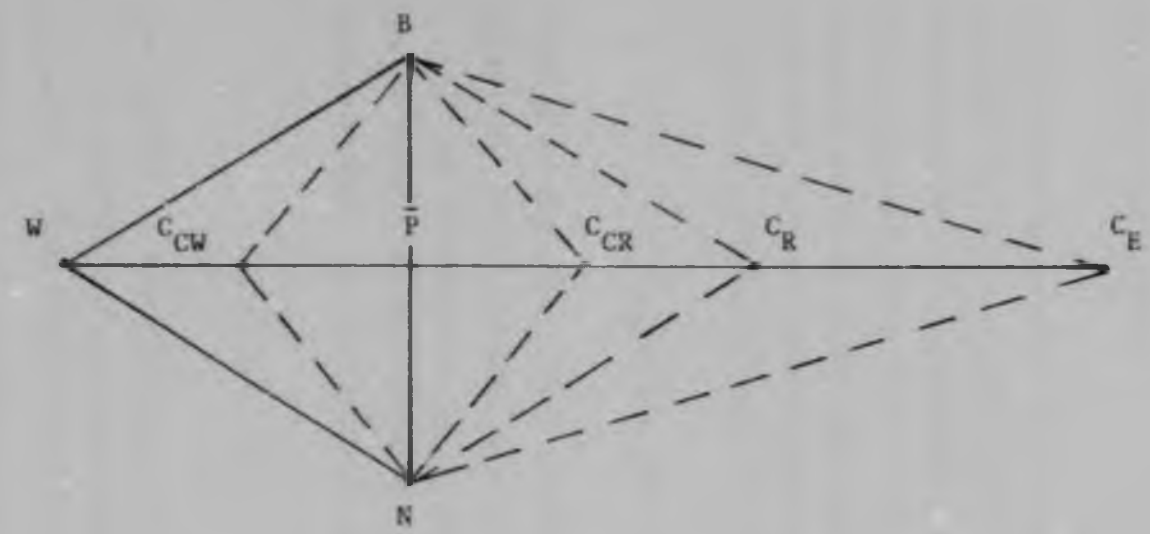


Figure 2.8 Two dimensional simplex indicating possible vertex locations in the modified simplex method.

response at B, it is retained as the new simplex BNC_E and the entire procedure is repeated. If the response at C_E is not better than at B, then the expansion is said to have failed and BNC_R is taken as the new simplex. The algorithm is started using the new simplex.

(b) If the response at C_R is less desirable than the response at N, a step in the wrong direction has been taken and the simplex should be contracted. A contraction may be either positive or negative. The designation stems from the sign of α in equation (2.9). If the response at C_R is worse than the response at N but better than that at W, the new vertex should be closer to C_R than to W giving a positive contraction with $0 < \alpha < 1$.

$$C_{CR} = \bar{P} + \beta (P - W) \qquad (2.11)$$

Where β is the contraction coefficient ($0 < \beta < 1$ usually 0.5). The process is restarted with the new simplex BNC_{CR}.

If the response at C_R is worse than the previous worst vertex W then the new vertex should be closer to W than to C_R, giving a negative contraction with $-1 < \beta < 0$.

$$C_{CW} = \bar{P} - \beta (P - W) \qquad (2.12)$$

The process is restarted with the new simplex BNC_{CW}.

In the MSM, contractions seldom fail to give a more favourable response. When these "failed contractions" occur, Nelder and Mead suggest shrinking the simplex about B by producing a new simplex containing B and new vertices halfway between B and each vertex of the old simplex.

(c) If the response at C_R is between that of B and N, neither expansion nor contraction is recommended and the process is restarted with the new simplex BNC_R. The progress of the simplex is shown in Figure 2.8.

False high results caused by experimental error which might

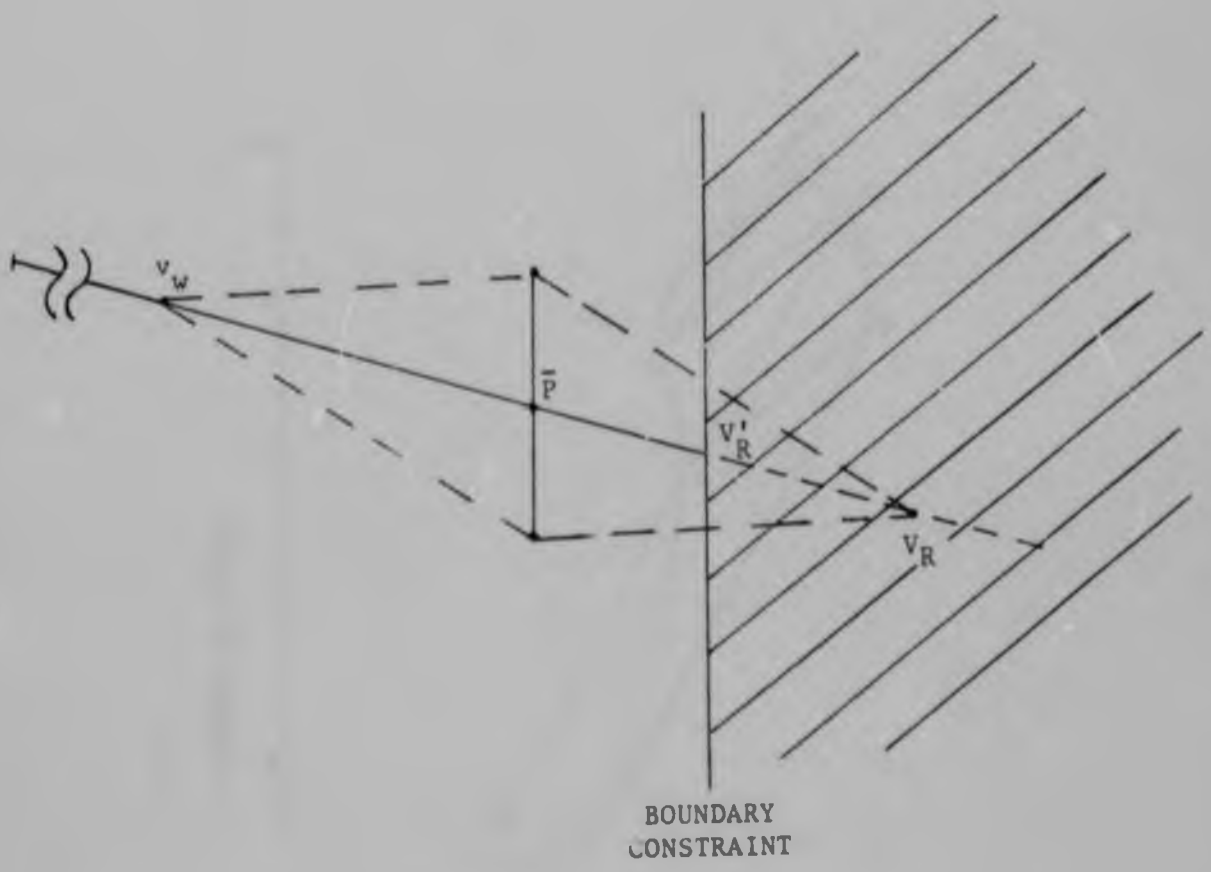


Figure 2.9 Possible locations for the new vertex after a boundary violation in the simplex method.

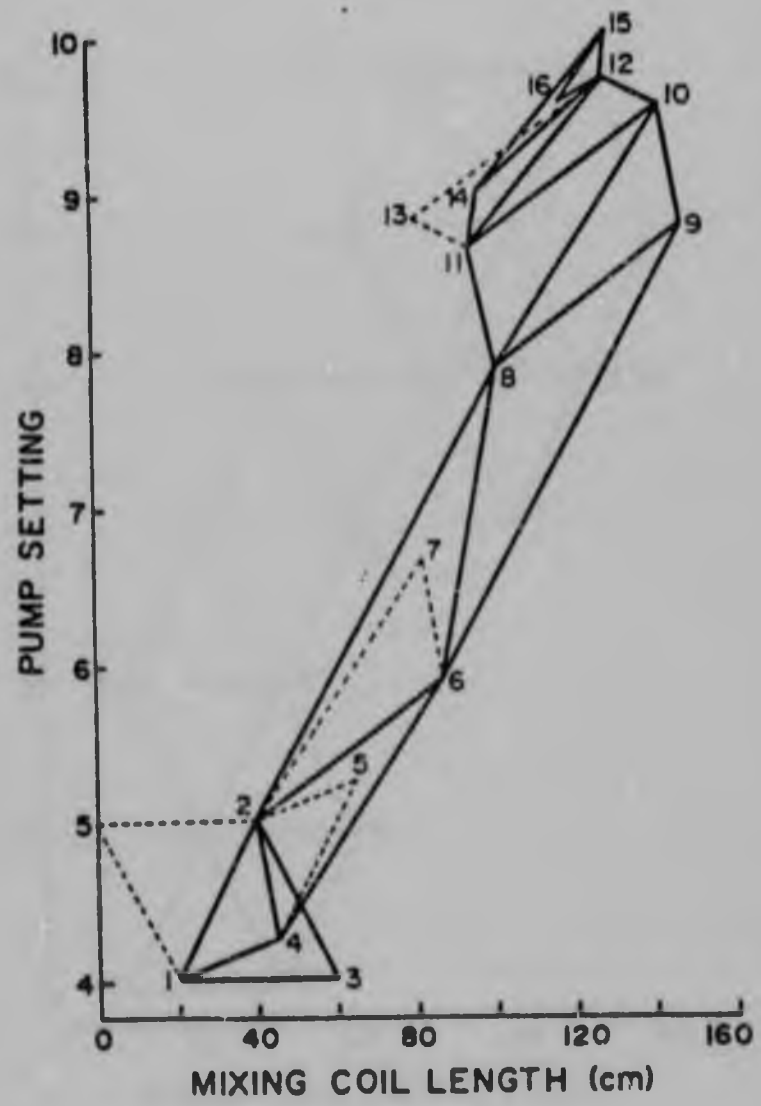


Figure 2.10 Progress of the variable size simplex

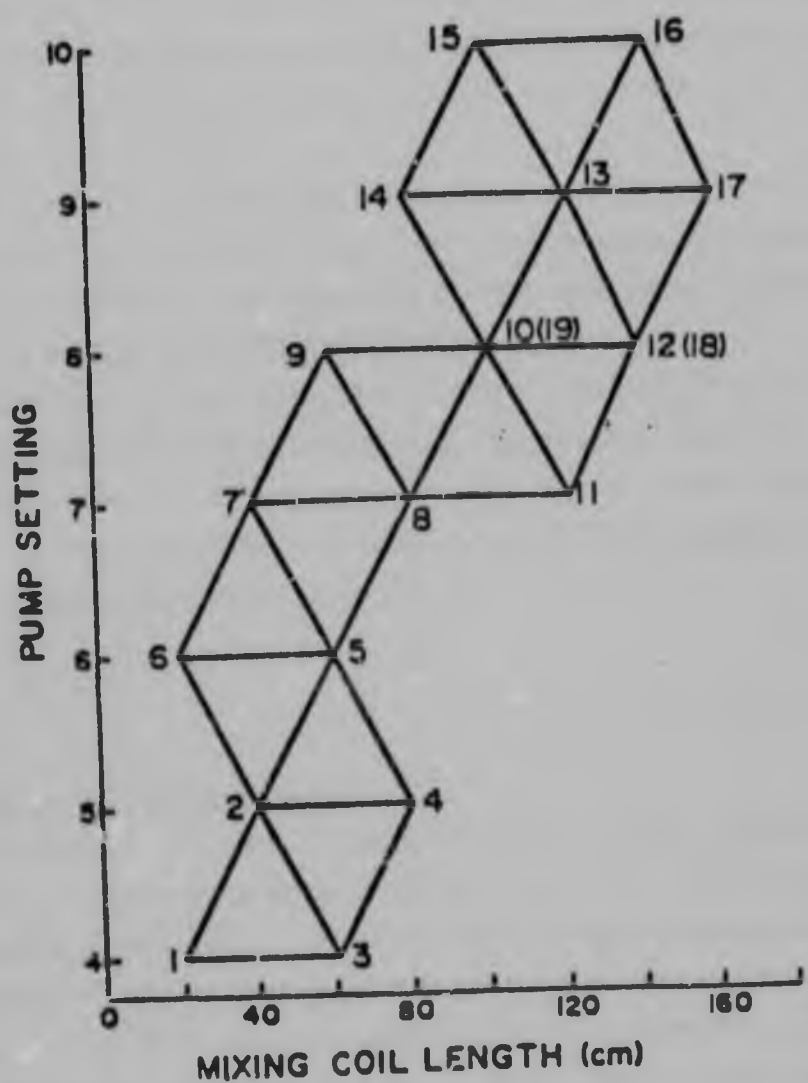


Figure 2.11 Progress of the fixed size simplex

mislead the simplex can be detected and corrected if the response of a new vertex appearing as best in n+1 successive simplices is re-evaluated. The average response can be taken as the response of that vertex from then on.

If one or more of the new vertex levels are found to be outside the boundary constraints, which are arbitrary restrictions initially imposed on the inputs, (Figure 2.9) that particular experiment is not performed.

The simplex is halted when the step size becomes less than some predetermined value (e.g., 1 per cent of the domain of each variable), or when the differences in the responses approach the value of the indeterminate error.

Comparisons of the progress of the fixed simplex and variable size simplex in the MSM are given in Figures 2.10 and 2.11 illustrating the difference in the rates at which they approach the optimum. The expansion and contraction of the variable size simplex is shown in Figure 2.10.

2.4 Flow Injection Analysis

Since its introduction the technique of FIA has proved to be highly versatile and capable of automation in a wide variety of analytical procedures[50]. A simple FIA system typically consists of a length of small bore (<1 mm) tubing, an injection valve and a detector with a flow cell (Figure 2.12). A number of operations can be performed on the sample as it moves through the reaction tube between the injector and the detector, such as extraction, dialysis, or reaction, but in the simplest case it merely disperses into the carrier stream.

In a typical FIA analysis, the sample travels as a gradually expanding plug and is slowly diluted by the carrier stream. Dispersion is a term frequently used in FIA to describe the degree of dilution a sample undergoes in the reaction tube, the injector and the detector. Dispersion is generally defined as the ratio of the concentration of the sample in the injector before mixing has occurred, to the maximum concentration of the sample at the detector

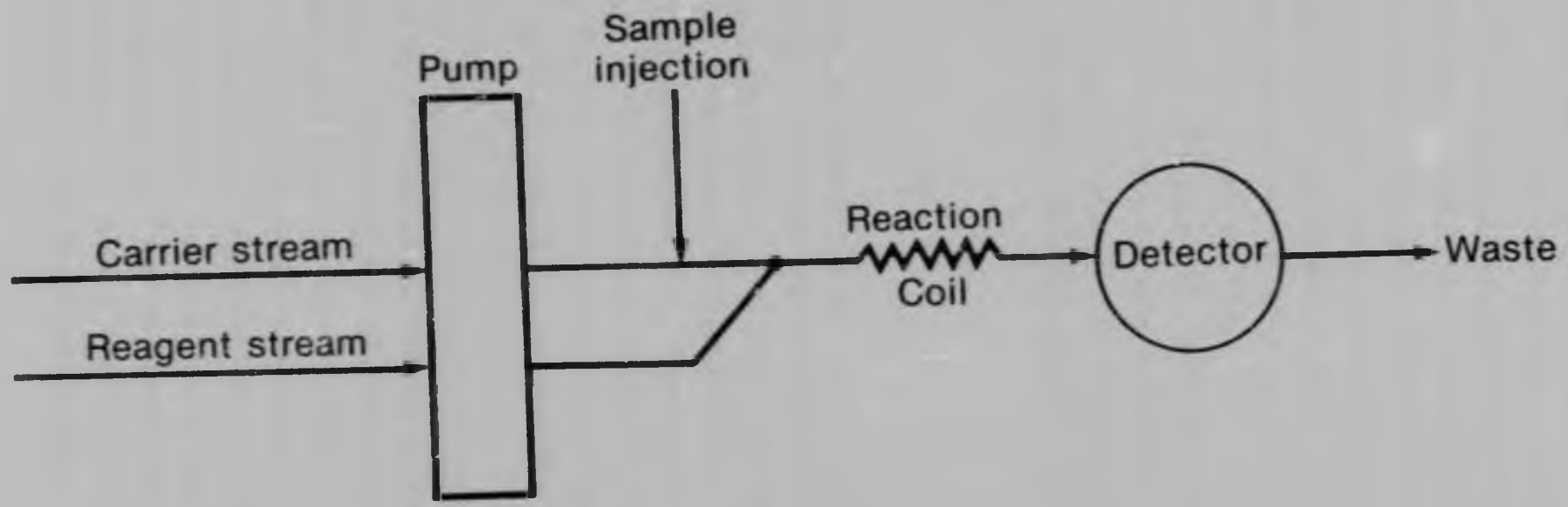


Figure 2.12 Schematic of the basic flow injection manifold

and it must be determined experimentally for each system.[13,50]

Because of differences in physical properties, such as density and viscosity, which determine the inertial and viscous forces for a flowing stream,[13,51] the flowing fluid can exhibit either turbulent or laminar characteristics. Laminar flow fixes the fluid elements in well-defined streamlines. That is, the elements at the centre axis of the tubing move at twice the average flow velocity whereas the elements at the walls move slowly. On the other hand, when fluid elements are randomly fluctuating in the form of eddies, the flow is said to be a turbulent flow.

The quantity that is frequently used to differentiate the flow as laminar or turbulent is the Reynolds number, R_e, and is commonly recognised as the ratio of the inertial forces to the viscous forces. For very dilute solutions, Ruzicka et al[52] defined the quantity as:

$$R_e = 10.6(F/a) \qquad (2.13)$$

where F is the flowrate ($ml.min^{-1}$) and a is the inner diameter of the tubing (mm). In general when the R_e is less than 1000, the flow is said to be laminar. Turbulent flow has a R_e value greater than 2000, whereas the intermediate values (1000 - 2000) represent an incipient turbulent flow (Figure 2.13)

At large R_e ($> 10^4$), the chaotic movement of the elements of the fluid results in similar dispersion in all directions yielding a flat velocity profile. At very small R_e (= 0.1) the parabolic velocity profile of the laminar flow is averaged by the radial molecular diffusion and dispersion is also prevented. However, Ruzicka et al[52] recognised that the velocity profile is not the only factor influencing the band spreading. Tube length also has a significant effect on peak spreading. Consequently, they realised that turbulent flow is not a necessary condition for achieving the preservation of discrete sample patterns in an unsegmented flowing stream. Laminar flow is preferable not only because it can provide a well-defined sample zone, but because it also has the advantages of reducing reagent consumption and eliminating the need for high pumping pressure.

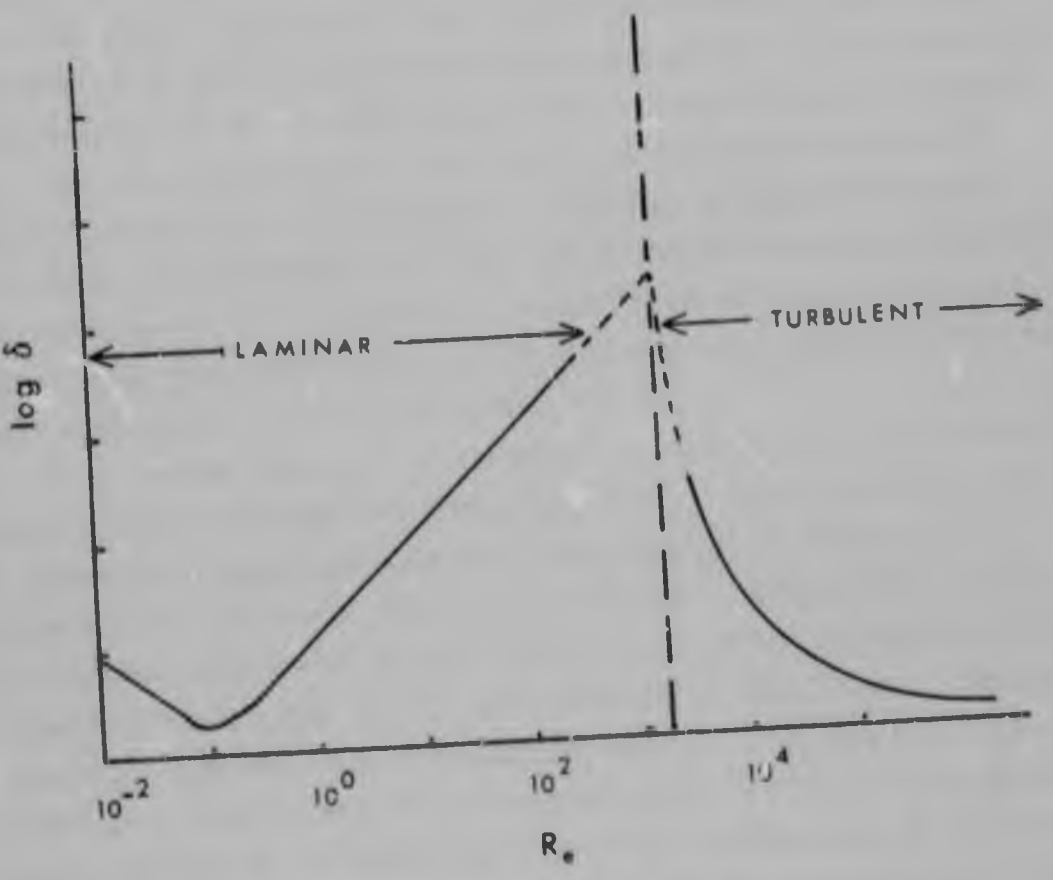


Figure 2.13 The dispersion number δ as a function of the Reynolds number R_e for aqueous solutions in the laminar, transient, and turbulent regions of flow

2.4.1 Dispersion in FIA

Effective dilution of the sample in FIA is dependent on the dispersion processes occurring as the sample travels between the point of injection and the point of detection. Dispersion is the result of diffusion and convection in axial and radial directions. The nature and magnitude of the dispersion depend on the physical parameters of the flow, the mechanical parameters of the manifold and the geometry of the reactor as well as chemical factors involved.

Van den Berg[53] stated that the axial dispersion should be kept as low as possible because it adversely affects the sample integrity, the throughput and the sample dilution thereby decreasing the sensitivity of the method. Ranger[54] stated that the radial rather than the axial dispersion contributes most significantly to sample dispersion in the FIA system.

For laminar flow in a cylindrical tube, the axial dispersion results from diffusion and convection[13,55]. Axial diffusion is a spontaneous molecular movement from a region of higher concentration to one of lower concentration. Convection arises from the parabolic movement of the flowing fluid, thus its magnitude is directly proportional to the mean velocity of the fluid. Radial dispersion results from molecular diffusion. For laminar flow with parabolic profile, transport of solute occurs radially from the slower moving regions at the mean velocity of the sample zone to the faster moving stream at the central axis. The effects of convection and diffusion on the concentration profile of the injected sample are shown in Figure 2.14. Radial dispersion dictates the peak height obtained thus it is intimately related to the analytical sensitivity, whereas axial dispersion determines the spreading or width of the signal or peak and is related to the sample throughput rate. The relative importance of axial and radial diffusion processes depends on the flowrate, the radius of the manifold tubing, residence time in the manifold, the geometric shape of the reactor and the magnitude of the diffusion coefficient.

The shape and size of the reaction vessel influence the type of flow and the dispersion. In a vessel with a stabilised flow, the two extreme flow patterns, plug and mixed flow, are not fully developed

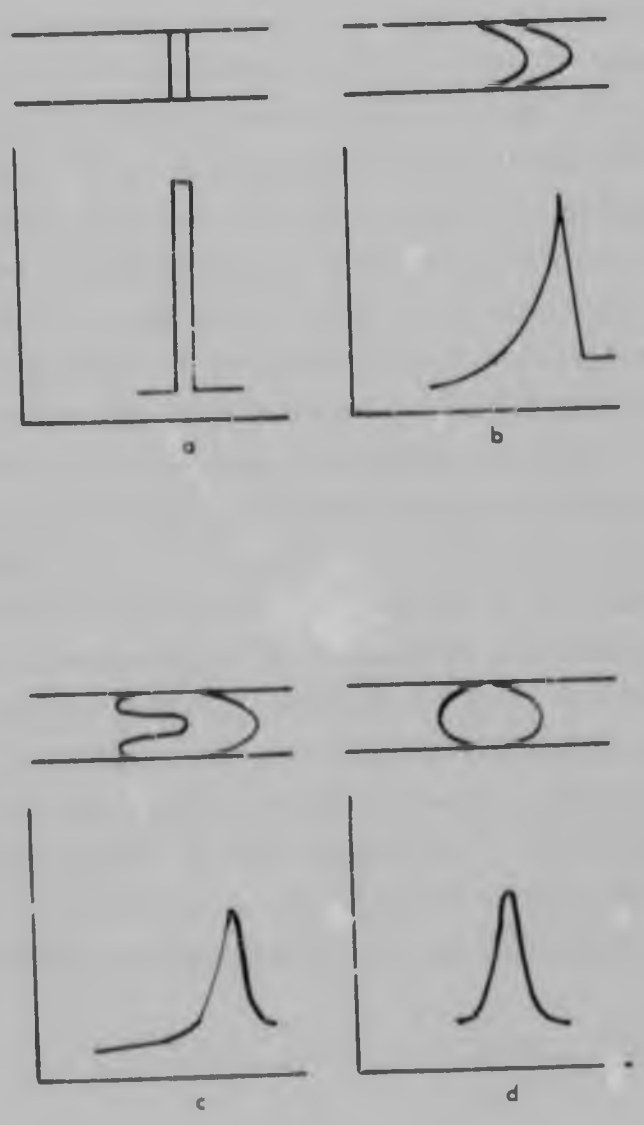


Figure 2.14 Diagrammatic effects of convection and radial diffusion on the concentration profiles of injected samples monitored downstream from injection.

(a) No dispersion
(b) Dispersion predominantly by convection
(c) Dispersion by convection and diffusion
(d) Dispersion predominantly by diffusion

and the resulting arbitrary flow contains in reality contributions from both these ideal types in different proportions. As each element of fluid passes through the reactor at different times, there is a distribution of residence times that can be observed at the exit of the reactor for those elements that entered the vessel simultaneously. When a sample has been introduced into the fluid stream, a gradual increase in concentration is observed by the detector after a certain period of time. If this resulting concentration C is plotted as C/C_o^o versus time (C_o^o being the initial concentration of the sample), an F-curve is obtained[50]. The time-span between the introduction of the sample and the inflection point on the curve is the mean residence time, T. The slope of the ascending part of the curve is inversely proportional to the dispersion.

The C-curve is obtained by normalising the reponse obtained. By measuring C and plotting it versus time, a peaked curve is obtained which is in direct relation to the peaks obtained in FIA. The time span between the injection of the sample and the peak maximum is the mean reactor holding time, T, and the peak width is directly proportional to the dispersion. If the C-curve is normalised by dividing C by the area under the concentration curve the relationships between the E-, F- and C-curves are

$$E = C = dF/dt \quad \text{and} \quad F = \int_o^t E\,dt = \int_o^t C\,dt \qquad (2.14)$$

The influence of the reactor geometry on the residence time distribution (RSD) is shown by the graphical representation of the E-, F- and C-curves (Figure 2.15). As the C-curve is related to the FIA curve, it can be inferred that the plug type of flow is desirable for methods requiring limited dispersion, whereas mixed flow should be used for gradient techniques. Medium dispersion is a mixture of the two types of flow.

(a) Dispersion Patterns

A convenient way to describe the dispersion pattern is to use the concentration gradients formed when a sample plug is flowing in the carrier stream through a narrow open tube. The value of the

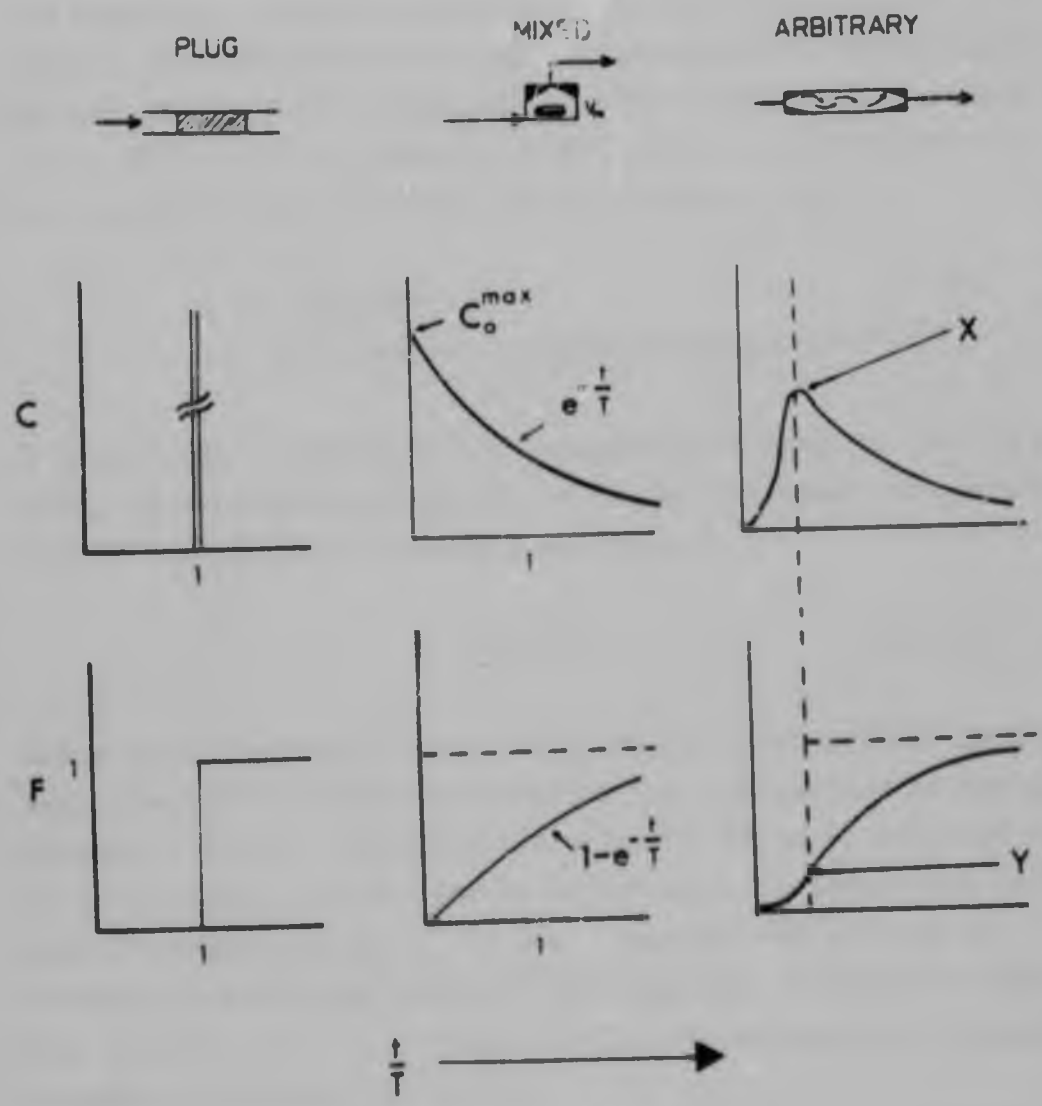


Figure 2.15 Influence of flow geometry on the shape of the residence time distribution curves

X Maximum value

Y Maximum slope

concentration gradient varies over a wide range for all the various flow parameters that can be encountered in FIA. In most FIA methods, the analytical readout is based on the measurement of the peak height, and therefore on the concentration within the imaginary element of fluid that corresponds to the maximum of the recorded curve, C^{max}, which is related to the original concentration of the injected sample solution, C_o^o, by (Figure 2.16);

$$D = C_o^o/C^{max} \qquad (2.15)$$
$$= [(\text{constant } 1)(H_o^o)]/[(\text{constant } 2)(H^{max})]$$

If Beer's Law is obeyed in the concentration range of both C_o^o and C^{max}, and the recorder response is linear throughout the region of H^{max} and H_o^o, then D can be simplified to

$$D = H_o^o/H^{max} \qquad (2.16)$$

where H_o^o is the signal height obtained with undispersed original sample and H^{max} is the signal height that corresponds to the peak maximum. Thus D describes not only the degree of dilution of the original sample but also the ratio in which the sample has been mixed with the carrier stream. It does, however, not provide any information about the shape of the signal nor the time to return to the baseline which is a primary factor for determining the sample frequency and sample carry-over.

Ruzicka et al[56] divided this "practical dispersion" into three regions and called them limited, medium and large dispersion, each corresponding to a range of values for the practical dispersion. Any dispersion has a negative effect on sampling frequency and sensitivity. The appropriate degree of dispersion in a FIA system, however must be a compromise based on consideration of the degree of mixing required, the sampling interval that can be accepted, the degree of completeness to which the reaction has to proceed and, most critically, the type of analytical readout to be used, i.e., peak height or peak width. Based on this understanding, a general comparison among the limited, medium and large dispersions is summarized in Table 2.7[57,58].

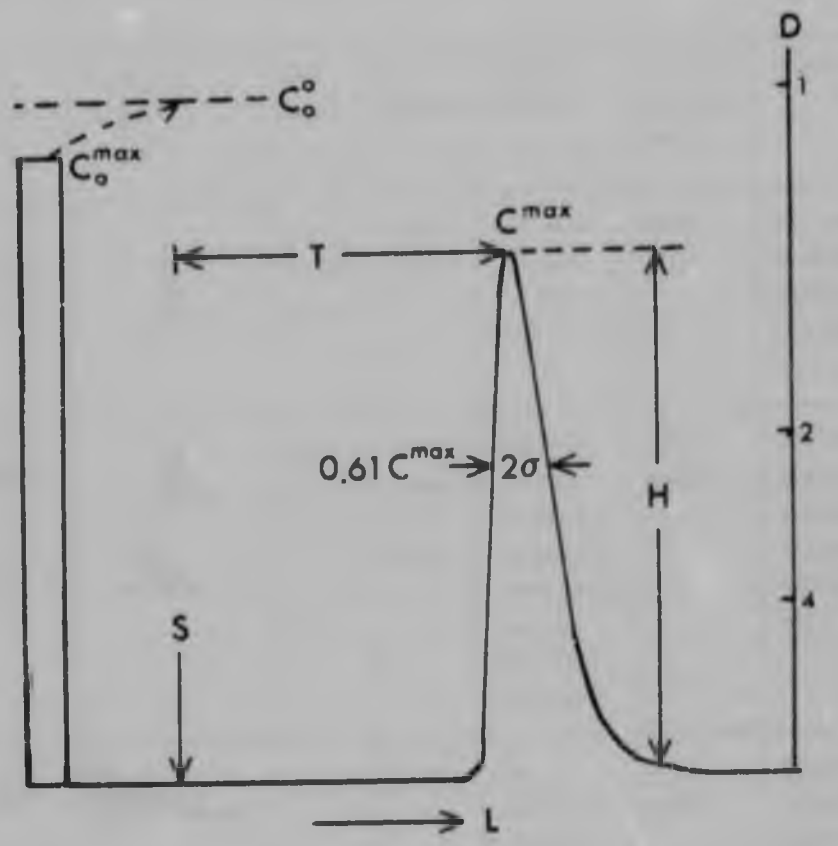
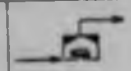


Figure 2.16 Parameters for defining dispersion in FIA

Table 2.7 A general comparison of limited, medium and large dispersion

Dispersion type	D*	Reactor geometry used	Response signal shape	Tube radius	Line length	Mixing device	Analytical readout	Applications
Limited dispersion	1 - 3			Small <0.5mm in i.d.	Short ($L<1_s$)	Not used (mixing is limited)	Peak height	pH, pCa or conductivity measurement of the original sample solution
Medium dispersion	3 - 10	 	 	Small ~ 0.5-1.0 in i.d.	More flexible D=(L)	Depends on the chemistry involved; some degree of mixing is needed.	Peak height	Colour or complex formation; change of pH; adjustment of ionic strength etc.
Large dispersion	≥10			--	--	Use a mixing chamber	Peak width	Titration; kinetic measurement; multicomponent resolution

+ Dispersion, D, is defined as C_o^o/C^{max} where C^{max} is the concentration corresponding to the maximum of the recorded peak.

Sample volume (a) Limited dispersion. ≤ 5 which is the volume of sample whose resulting D value is exactly 2.
(b) Medium dispersion. Depends on the geometry of the manifold.
(c) Large dispersion. Depends on the volume of the mixing chamber.

(i) Limited dispersion

A system with limited dispersion (D = 1 - 3) is used when it is required to measure a characteristic parameter of the sample itself, and mixing with the carrier is to be minimized or avoided. In fact, the FIA system in this instance merely serves as a means of transporting the sample from the point of injection to the point of detection, and hence the tube connecting these two points is short and of small inner diameter (0.3 - 0.5mm) ensuring that the middle of the sample zone is preserved unmixed. An example is the potentiometric determination of pH value where the parameter on the injected sample is available in 5-6 seconds of the introduction of the sample[50].

(ii) Medium dispersion

Systems with medium dispersion (D = 3 - 10) are the most interesting from an analytical viewpoint because they can be applied to a large number of analytical procedures, and in particular to spectrophotometric determinations. In this type of determination an adequate degree of mixing can be achieved by the use of mixing aids such as a mixing coil. A suitable compromise is therefore achieved between the requirements of mixing and reaction time on the one hand and maximum acceptable broadening of the sample zone on the other, as the latter affects carry-over and hence the sampling rate[50].

(iii) Large dispersion

Large dispersion (D > 10) is used for creating a concentration gradient of the sample that extends over a longer period of time, either for the purpose of rapidly diluting a sample that is too concentrated or to exploit the concentration gradient at the interface between the carrier stream and the sample zone. This approach is used for performing titrations where the sample is injected into an inert carrier stream and led to a small mixing chamber, dominating the volume of the FIA system, in which a strictly exponential concentration gradient of the sample is formed. This gradient is then allowed to mix with the titrant stream containing an indicator if necessary, and the mixture is monitored in a detector.

Examples are the spectrophotometric titration of an acid with a base and the potentiometric titration of calcium(II) with EDTA[50]. There are some non-traditional FIA processes derived from the concept of large dispersion. These are finding useful application in dealing with some special FIA problems such as, (a) when samples have too high a concentration but their dilution in advance is inconvenient, (b) when large dispersion is required but the sample volume used is too large to achieve it. These processes include merging-zone, stream-splitting (split sample zone), and zone-sampling processes.

(b) Dispersion Number and Variance

The dispersion of the sample plug in a tubular reactor is the result of redistribution of the fluid similar to molecular diffusion. The symmetrical C-curve would then have the equation

$$C = 1/2(\pi\delta)^{1/2}\exp|-(1 - t/T)^2/4\delta| \qquad (2.17)$$

which is a Gaussian curve. The dispersion number, δ, is the dimensionless group D_a/FL (F is the mean flow velocity, L the reactor length and D_a the axial dispersion). The curve is Gaussian with the variance related to the dispersion number as follows

$$\sigma^2 = 2\delta; \qquad C^{max} = 1/2(\pi\delta)^{1/2}; \qquad (2.18\ a\text{-}b)$$

$$W_{0.6} = 2(2\delta)^{1/2}; \qquad W_B = 4\sigma = 4(2\delta)^{1/2} \qquad (2.18\ c\text{-}d)$$

where W is the peak width, (W_B at peak base, $W_{0.6}$ at 60 per cent peak height). Thus the dispersion can be found by computing the variance σ^2 or by measuring the height C^{max}, the width at $0.6C^{max}$, etc. As the variances are additive, the total residence time is given by

$$T_{total} = T_a + T_b + ...T_n \qquad (2.19)$$

and

$$\sigma_{total} = \sigma_a^2 + \sigma_b^2 + ...\sigma_n^2 \qquad (2.20)$$

In this manner it possible to assess the effect of the addition of a particular reaction coil, a change of flow-through cell and the addition of more reagent streams on the overall dispersion of the system.

The sample throughput is limited by the sample dispersion D which is related to the standard deviation of the peak, σ. The throughput rate is limited to the maximum value S_{max} beyond which excessive carryover will make the estimation of the peak very unreliable. Thus

$$S_{max} = 3600/k\sigma_t = 60Q/k\sigma_v \quad \text{(samples per hour)} \qquad (2.21)$$

where k is a factor depending on acceptable carryover, σ_t^2 and σ_v^2 are the variances expressed in a unit of time or volume respectively and Q is the pumping rate ($ml.min^{-1}$). Overall peak variance is composed of three contributions;

$$\sigma^2_{overall} = \sigma^2_{injection} + \sigma^2_{flow} + \sigma^2_{detector} \qquad (2.22)$$

Using a detector with a small holdup volume and fast response, the overall peak variance becomes

$$\sigma^2_{overall} = \sigma^2_{flow} + \sigma^2_{reactor_1} + \sigma^2_{reactor_2} + \ldots\ldots\ldots \qquad (2.23)$$

showing that the geometry of the flow system influences the dispersion.

(c) Dispersion Models

Two dispersion models have been used. These are the Taylor's model, and the tanks-in-series model.[13,50]

(i) Taylor's Model

This model has the advantage of being the analog of the differential equation which describes a diffusion process in the presence of convection. In the case of large L (reaction coil or tubing length) and small u (mean flow velocity), the solution for the

C-curve is a Gaussian type function, i.e.,

$$C = (M/\pi a^2)(4\pi Dt)^{-1/2} \exp\{-(x - L)^2/4Dt\} \qquad (2.24)$$

where M is the mass of the material injected at point L = 0 at time t = 0. From equations (2.17) and (2.24), the shape of the C-curves is obtained. It also follows from Taylor's work that radial diffusion will start to affect the velocity profiles if the residence time $T = r^2/3.8^2 D_c$, where D_c is the molecular diffusion coefficient.

Ruzicka and Hansen[13] have discussed FIA systems using Taylor's model and experimentally verified that

$$(C_o^o/C^{max}) \propto (T)^{0.5} \qquad (2.25)$$

$$(C_o^o/C^{max}) \propto (L)^{0.5} \qquad (2.26)$$

$$(C_o^o/C^{max}) \propto (a)^2 \qquad (2.27)$$

But Taylor's solution requires that the mean residence time T, should be long in order to stabilise the radial concentration changes, i.e.,

$$T >> (a^2/14.4D) \qquad (2.28)$$

or expressed in the reduced time

$$(\tau_m) >> 0.07 \qquad (2.29)$$

where $$(\tau_m) = (T)D/a^2 \qquad (2.30)$$

Golay et al.[59] indicated that for Taylor's effect to develop T has to be larger than 0.8. For a normal FIA system with $D = 5 \times 10^5 (cm^2.sec^{-1})$ and a radius of 0.025(cm) the mean residence time has to be 100 seconds or more to satisfy this criterion.

(ii) Tanks-in-series model

Betteridge[60] recognised that the tanks-in-series model taken from chemical engineering is analogous to the concept of a height equivalent to a theoretical plate model for chromatography. It postulates that the reactor tube between the points of injection and detection consists of a number of well-stirred imaginary tanks of equal size in series. Thus

$$C/C_o^o = 1/T_t(T/T_i)^{N-1}1/(N-1)!.\exp(-T/T_i) \qquad (2.31)$$

where T_i is the mean residence time in one hypotnetical tank and N is the number of tanks containing the sample material.

The actual size of the imaginary tank is a function of the tube dimensions and the flowrate. A small value for N results in skewed concentration curves whereas a very large value results in near Gaussian shape concentration curves with a variance

$$\sigma^2 = T^2/N \qquad (2.32)$$

as given by van den Berg et al.[53] For $N > 10$, where the shape of the peak can be considered practically symmetrical, it can be shown that by comparing equations (2.18a) and (2.32) the dispersion number is

$$\delta = 1/2(T^2/N) \qquad (2.33)$$

The applicability of this model to a FIA system is best demonstrated by Figure 2.17. The further the sample zone travels the more spread out it becomes, and the more Gaussian in shape the concentration curve becomes resembling the curves of the tanks-in-series model shown in the same figure.

Any practical system will always consist of several sections each of which has individual flow patterns which, through individual contributions, will yield a certain C-curve. As the variances are additive (and related to N), the contribution of a certain part of the manifold (coil, flow,etc.,) can be established from the differences in the variances of the C-curves with and without the

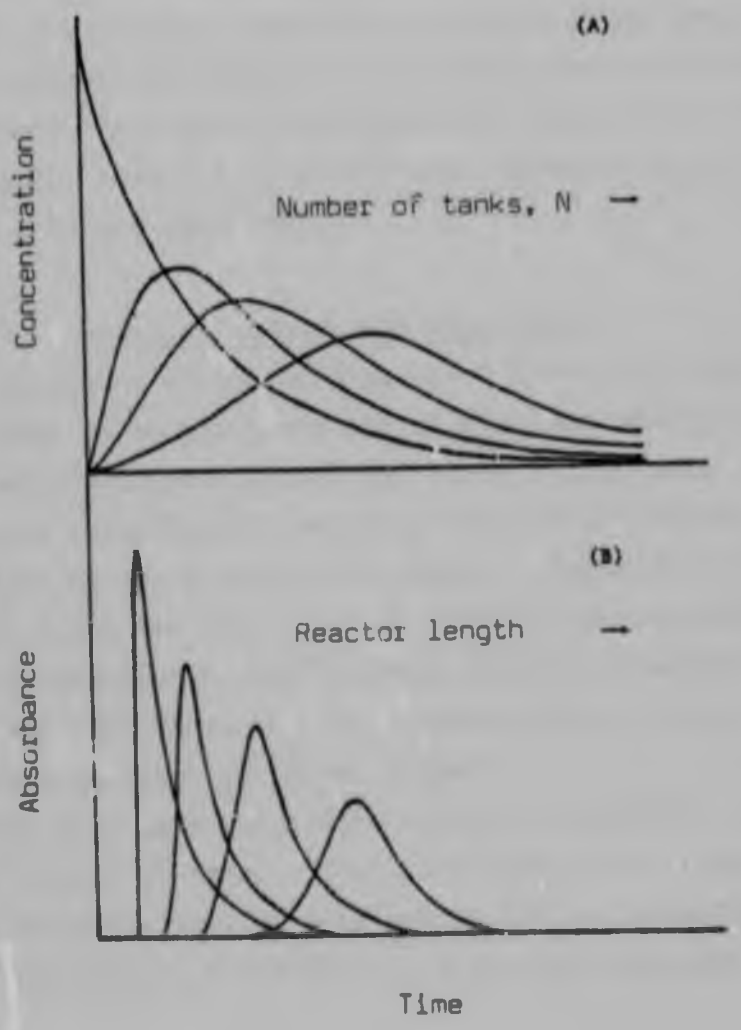


Figure 2.17 Comparison of tanks-in-series model (A) and dispersion signals in a FIA system (B)

particular component included in the tested circuit.

(iii) Comparison of dispersion models

Taylor's dispersion model provides an appropriate approximation for narrow and long reactor tubing and a s.ow flowrate. For other conditions, the tanks-in-series model seems to provide a better theoretical basis for the investigation of dispersion. Furthermore, the tanks-in-series model seems to be the best for use in a reactor vessel with a uniformly repeated pattern of structure such as a single bead reactor.

(d) Reactor Geometry and Dispersion

Since one of the advantages of FIA is its capacity to handle large rates of sampling, the use of straight tubing for the reactor may sometimes become impractical since it can cause peak broadening or provide insufficient residence time for any chemical reaction to take place as required by the method. Reijn et al.[61] state that straight tubes are probably only used for rapid determinations of molecular dispersion coeff.cients; this is, however, understating the use of straight tubes in F.A. Nevertheless, the use of other types of reactor geometry is rather common.

Plug flow sets the limits for both analytical sensitivity and sample throughput rate. Thus, the best way to improve the analytical efficiency of a method in FIA is to increase the plug flow characteristics in the flow. The ways of approaching plug flow are[62];

(i) turbulent flow
(ii) induce secondary flow by coiling the flow path
(iii) disrupt the laminar flow by packing the reactor.

A general comparison of these three approaches with respect to a laminar flow n straight cylindrical tubing is shown in Table 2.8

(i) Dispersion due to radial diffusion

Radial diffusion is the molecular displacement in the radial direction. It counteracts the convective spreading by trying to establish a uniform concentration distribution of the original sample and displacing it over a cross-section. During this displacement, a

Table 2.8 Comparison of turbulent flow, curved channel and packed column with respect to straight tubing in a laminar flow

Comparison / Approaches	Axial dispersion	Radial dispersion	Forces causing the enhanced dispersion	Required pressure drop	Reagent consumption	Residence time	Band broading
Turbulent flow	Enhanced	Enhanced	Turbulence	Increased	Increased	-	Decreased
Curved channel	Not enhanced	Enhanced	Centrifugal force	Change is negligible	Less or no change	Change is negligible	Decreased
Packed column	Not enhanced	Enhanced	Eddy diffusion	Depends on the packing material	No change	Increased	Decreased

Table 2.8 Comparison of turbulent flow, curved channel and packed column with respect to straight tubing in a laminar flow

Comparison / Approaches	Axial dispersion	Radial dispersion	Forces causing the enhanced dispersion	Required pressure drop	Reagent consumption	Residence time	Band broading
Turbulent flow	Enhanced	Enhanced	Turbulence	Increased	Increased		Decreased
Curved channel	Not enhanced	Enhanced	Centrifugal force	Change is negliglble	Less or no change	Change is negligible	Decreased
Packed columr.	Not enhanced	Enhanced	Eddy diffusion	Depends on the packing material	No change	Increased	Decreased

transition zone is formed in which the concentration changes gradually. For slow radial diffusion in a parabolic profile the transition zone extends over a long axial distance which results in peak spreading. The transition is flatter for fast radial diffusion because concentration differences are readily smoothed out and the sample zone shrinks resulting in a narrower peak.

Turbulent flow not only enhances the radial dispersion but also the axial dispersion which counteracts a decrease in peak broadening. In addition, turbulent flow requires high pressure resulting in large reagent consumption. Packed columns and curved channels on the other hand offer greater advantage without large reagent consumption and axial dispersion and are more frequently adopted as a means of improving analytical results.

(ii) Coiled tubes

The use of coiled tubing to decrease the peak spreading has been reported by many investigators[63-67]. Because of the centrifugal forces in any curved flow channel a secondary flow which is perpendicular to the main flow is generated[65]. In a laminar flow, the secondary flow stimulates radial mass transfer and reduces velocity variation over the cross section of the flow. This is the result of forcing the central streamlines, which are subject to greater centrifugal forces due to greater velocities, towards the outer walls[68]. Consequently, peak spreading can be far less pronounced. This is shown in Figure 2.18. Because of the radial mixing enhancement, the secondary flow is said to prevent sinking effects caused by molecules with higher specific gravity. The secondary flow effect is largest at a flow with a Reynolds number equal to 1000[69]. Presumably this is because a flowrate with a Reynolds number smaller than 1000 is too low to have effective centrifugal forces and to induce a secondary flow and a flowrate with a Reynold's number greater than 1000 is too large to maintain its laminar characteristic. However, coiled tubes tend to stabilise the laminar flow and the critical Reynolds number at which turbulence occurs is higher in coiled tubes than it is in straight tubes[70]. The secondary effect also depends on the tightness of the coil and on the diameter of the tubing used to construct the coil.

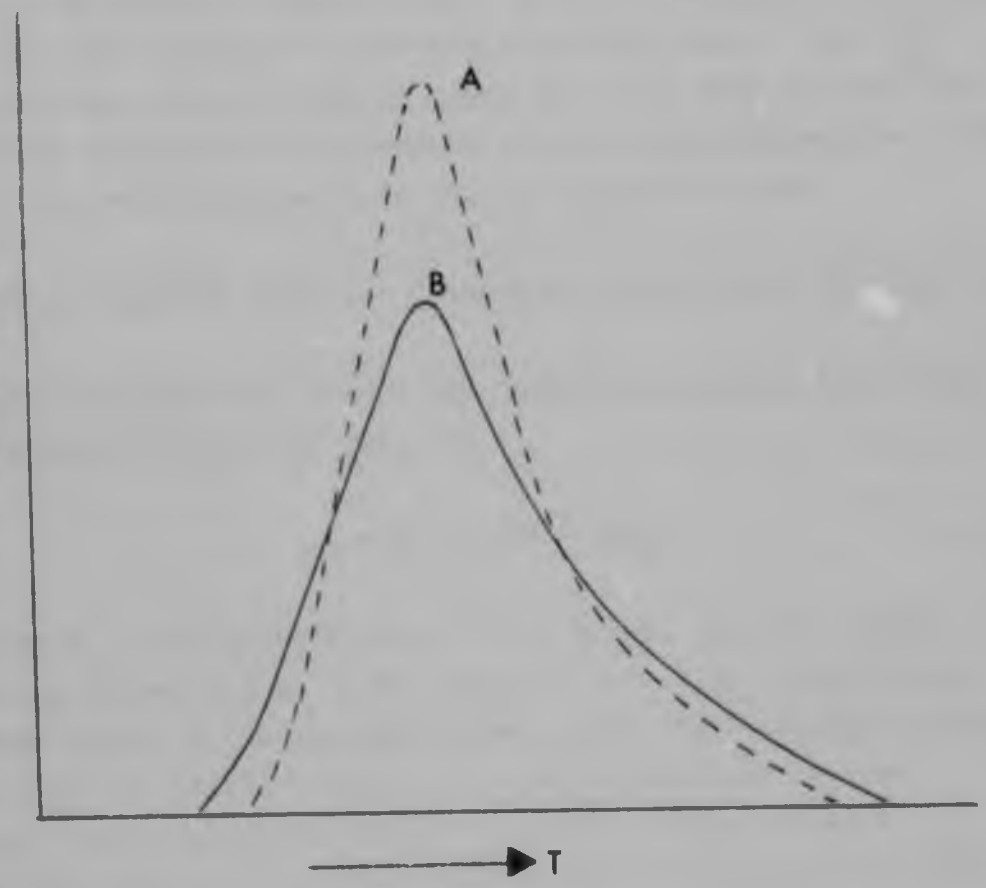


Figure 2.18 Peaks obtained with straight and coiled tubing under identical experimental conditions

Curve A: Obtained with coiled tubing reactor
Curve B: Obtained with straight tubing reactor

The secondary flow effect increases as the ratio of the coil diameter to the tubing diameter (curvature ratio) decreases[29,53]. Consequently, an effective coil is tightly wound from large diameter tubing. Tubing of too large a diameter causes larger axial dispersion, hence there is an upper limit within which the tubing diameter can be selected. Ruzicka and Hansen concluded that only with tube diameters smaller than 1 mm is the dispersion independent of the tube diameter for the same residence time. The first theoretical study of flow in curved tubes was made by Dean[65] who derived an approximate expression for the dimensionless Dean number, Dn, for characterizing fluid flow in a curved channel.

$$Dn = (\text{Reynolds number}) \times (\text{radius of tubing}/\text{radius of coil}) \qquad (2.34)$$

A velocity parameter, Dn^2Sc, was found to be related to the peak spreading in chromatography, and

$$Dn^2Sc = 4a^3\rho u^2/\eta a_c D \qquad (2.35)$$

where Sc is the Schimdt number ($Sc = \eta/D\rho$), ρ is the density of the carrier stream and a_c is the radius of the coil. Let H be the plate height of the straight tubing, H_c be the plate height after coiling this straight tubing, σ_t^2 be the variance in time units for the straight tubing and $(\sigma_t^2)_c$ be the variance in time units for the coiled tubing, then the decrease in sample dispersion by coiling the straight tubing is given by

$$\xi = [(\sigma_t)/(\sigma_t)_c]^2 - 1 = (H/H_c) - 1 \qquad (2.36)$$

The change of (H/H_c) with Dn^2Sc was calculated by Tijssen[65] who concluded that at low Dn^2Sc value (< 10), $H = H_c$, and $\sigma_t = (\sigma_t)_c$, $\xi = 0$, and the coiling effect is negligible.
At $Dn^2Sc > 10$, therefore $\sigma_t > (\sigma_t)_c$ and $\xi > 1$, the secondary flow develops gradually and is well established at $Dn^2Sc > 10^4$.
At $Dn^2Sc = 10^9$, $H = H_c \times 10^4$, $\xi = 10^4$ which

implies a substantial decrease in peak width by a factor of 100.

Snyder[63] found that the mass transfer coefficient for a solute of molecular weight 27 at 25°C in aqueous solution, is four times higher in coiled tubing than in straight tubing. However, the use of coiled tubing has its limitations. Mixing coils function properly only when used in a horizontal position. This is probably because in the vertical position the gravitational force in addition to the centrifugal force would distort the radial mixing that occurs in the coiled tubing.

(iii) Packed-bed reactor

Another approach for enhancing radial dispersion is to disturb the streamline pattern repeatedly by rapidly changing the direction of flow. The most practical way to obtain this effect is to pack the reactor tubing with small spheres of an inert material. A reactor packed with large non-porous beads for FIA systems is called a "single-bead-string reactor"[71]. This reactor is a device which provides efficient mixing (though enhanced radial diffusion) creating a longer residence time by distorting the parabolic profile. It retains the peak height but decreases the peak broadening. Van den Berg[53] found that, for a given length, the efficiency of a single-bead-string reactor, which is directly proportional to the reciprocal of σ_t/T, depends on the particle size chosen. The bead diameter should be greater than 50 per cent of the tubing diameter, but small enough to prevent back pressure problems, and the beads should be packed in a zig-zag pattern to ensure uniformity of packing.

The Reynolds number of a single-bead-string reactor (s.b.s.r) is calculated as follows;

$$(Re)_{s.b.s.r} = 2a_b F / \pi a^2 \nu \qquad (2.37)$$

where ν is the kinematic viscosity.

(e) Chemical Effect on Dispersion

Ruzicka and Hansen[50] stated that the FIA response curve is the result of two processes both kinetic in nature, the physical

process of dispersion of the sample zone within the carrier stream and the chemical process of formation of chemical species. The shape of a peak obtained in FIA which involves a chemical reaction should contain information both on the physical dispersion of the injected sample zone into the carrier stream and on the chemical reaction(s) taking place between the injected sample solution and the carrier reagent solution, i.e., the mechanism of the chemistry involved should have some effects on the overall physical dispersion process. Experimental evidence about the kind of effects that a chemical reaction has on the shape of the peak has been given by Painton and Mottola[66,75]. They tested a numerical model based on the basic dispersion modified by simultaneous consideration of the chemical effect introduced by an assumed pseudo-first-order chemical reaction taking place as the sample plug was dispersed in the flowing stream. The basic concept was that chemical reactions alter the concentration profile within the plug and its boundaries which induces diffusion and convection. The resulting mass transfer dynamics in turn affected the collisional frequency that triggers chemical reactions. The rate coefficient in the chemical kinetics term (if pseudo-first-order conditions were assumed to hold) changed in an oscillating pattern which reflected the complexity of the overall kinetic process that took place inside the plug and its boundaries. The combination of these processes in cyclic form was responsible for the distribution of the monitored chemical species that produced the signal detected as the dispersed sample plug passed through the detector.

2.4.2 Detectors

When evaluating detectors the linearity, noise level and peak broadening effects are important criteria common to all types of detectors. In modern detectors, the only factor requiring consideration is that of peak broadening as it is a result of

(a) the flow velocity in and the hold-up volume of the detector,
(b) the speed of its response and
(c) the time constant of the associated electronics.

The variance of the detector should be no more than 5 per cent of the overall variance[50].

$$\sigma^2_{detector} \leq 0.103\sigma^2_{overall} \qquad (2.38)$$

or $$\sigma_{detector} \leq 0.32\sigma_{overall} \qquad (2.39)$$

that is $$\sigma^2_{overall} + \sigma^2_{detector} \leq (1.05\sigma_{overall})^2 \qquad (2.40)$$

The most common detection techniques in FIA are spectrophotometry, fluorescence, chemiluminiscence, atomic absorption, flame photometry, potentiometry with ion-selective electrodes and voltammetry.

CHAPTER 3

FIA OPTIMIZATION OF URANIUM(VI) DETERMINATION

From an analytical viewpoint, FIA systems with medium dispersion are of greatest interest as they can be applied to a large number of chemical reactions. The magnitude of the dispersion depends on the operating parameters applied to the system, tubing bore size, tubing length, flowrate etc. By varying these parameters the dispersion can be precisely controlled to suit the requirements of the spectrophotometric determination of uranium(VI) with the azo dye, bromo-PADAP, so that optimum response (peak height) is obtained with minimum time and reagent expenditure.

The goal in the design of a FIA system is to maximize response together with sample throughput, to get a practical analytical unit with high precision, minimum baseline drift and as linear and accurate as possible. Ruzicka and Hansen[13] proposed guide lines with respect to sample dispersion and total residence time. These guide lines are based on Taylor's solution of the diffusion-convection equation and are summarized as follows:-

(a) Changing the injection sample volume is a powerful way to change dispersion.

(b) Limited dispersion is obtained by injecting a small sample volume into a manifold consisting of the shortest possible line connecting the injection valve and the detector.

(c) The dispersion of the sample zone increases with the square root of the distance travelled through an open narrow tube and decreases with decreasing flowrate.

(d) Any continuous flow analyzer that includes a mixing chamber generates a large dispersion and therefore yields lower sensitivity of measurement.

(e) To obtain maximum sensitivity, the ratio of the equilibrium constant to the dispersion should be kept as high as possible.

(f) To obtain maximum sampling frequency, the overall axial dispersion should be kept low and the sample volume small.

The aim of this investigation was the assembly of a FIA manifold and the optimization of the physical and chemical parameters by both univariate and simplex methods. The response factor chosen was peak height. The reaction between bromo-PADAP and uranium(VI) gives rise to a peak in absorbance having a height and/or area proportional to the amount of uranium(VI) injected. The maximum reponse will be attained when an optimum balance is reached between dispersion and reaction time. The sensitivity, accuracy and reproducibility of the technique were investigated with a view to its application to the on-line monitoring of uranium(VI) in process streams and effluents.

3.1 Apparatus and Reagents

The peristaltic pump used throughout the study was a Minipuls II, 8-channel (Gilson Medical Electronics, Inc., Middleton. WI). The spectrophotometer was a Jasco UVIDEC-100-IV spectrophotometric detector (wavelength range, 190-600 nm; wavelength accuracy, 2 nm) with a cassette-type flow-through cell of 8 µl capacity (path length 10 mm) and a digital readout (Japan Spectroscopic Co., Ltd. Tokyo, Japan). The recorder was a Laboratory Data Control, single pen, potentiometric strip-chart recorder (Milton Roy Co., Riviera beach, Florida). The injection valve was an air-actuated 6-port injection valve (Dionex P/N 035913) with interchangeable sample loops of varying capacity (Dionex Corp., Sunnyvale, California, U.S.A.). The Tefzel tubing with which the manifolds were constructed had non-collapsible walls and inner diameters of 0.3, 0.5 and 0.8 mm. The tees and tube end fittings were Tefzel. An Apple IIe computer with two disc drives, a CItoH 8510 dot matrix printer and a grappler interface card was used for the simplex optimizations.

All chemicals were of analytical grade. Distilled water was used for all solutions. Two reagent solutions were prepared; the carrier solution was a combined buffer-complex solution (2 per cent) of pH value 8.9 and the reagent solution was 0.01 per cent bromo-PADAP in ethanol. The combined buffer-complex solution was prepared by the suspension 20 g of (1,2-cyclohexylenedinitrilo)-tetraacetic acid (CDTA) and 5 g of sodium fluoride in 400 ml of water. To this suspension,20 ml of ethanolamine was added with stirring and the solution was diluted to 1000 ml with ethanol. A

stock solution of uranium(VI) (1 $g.l^{-1}$ U_3O_8) was prepared as follows. After being dried at 110° C for 1 hour and cooled in a dessicator, 0.5000 g of Specpure U_3O_8 was dissolved in 10 ml of 50 per cent (v/v) nitric acid warming gently to assist dissolution. After evaporation to a moist state, the uranium residue was dissolved in water and diluted to 500 ml. Working standards in the range 0.5 to 20 $mg.l^{-1}$ were prepared by suitable dilution with water.

A schematic diagram of the manifold for the FIA determination of uranium(VI) is shown in Figure 3.1.

3.2 Calibration of the Sample Injector

Because of the manner of its construction, there is an inherent dead volume at the centre bore of the rotary injection valve. The dead volume is independent of the size of the interchangeable sample loops and is additive to the volume of each sample loop. That is

$$S = V_d + \pi r^2 L_s \qquad (3.1)$$

where S represents the actual volume of the injected sample (µl), V_d represents the dead volume of the injection valve (µl), L_s is the length of sample loop tubing in mm and 'r' is the radius of the sample loop tubing (mm).

V_d was determined by calibrating the injection valve with clean mercury. The calibration was performed with sample loops of 0.5 mm inner diameter and of varying lengths (100 mm to 250 mm). The actual volume of the injected sample was calculated from the mass of mercury required to fill the sample loop. The results are shown in Figure 3.2. From the extrapolated intercept point, the value of V_d has been determined as 15.1 µl

3.3 Experimental Procedure

The carrier stream of the combined buffer-complex solution was pumped by the peristaltic pump at a constant flowrate. The flowrate was adjustable by varying either the size of the inner diameter of the pump tubing or the pump revolutions per unit of time. The sample was introduced into the carrier stream by the injection

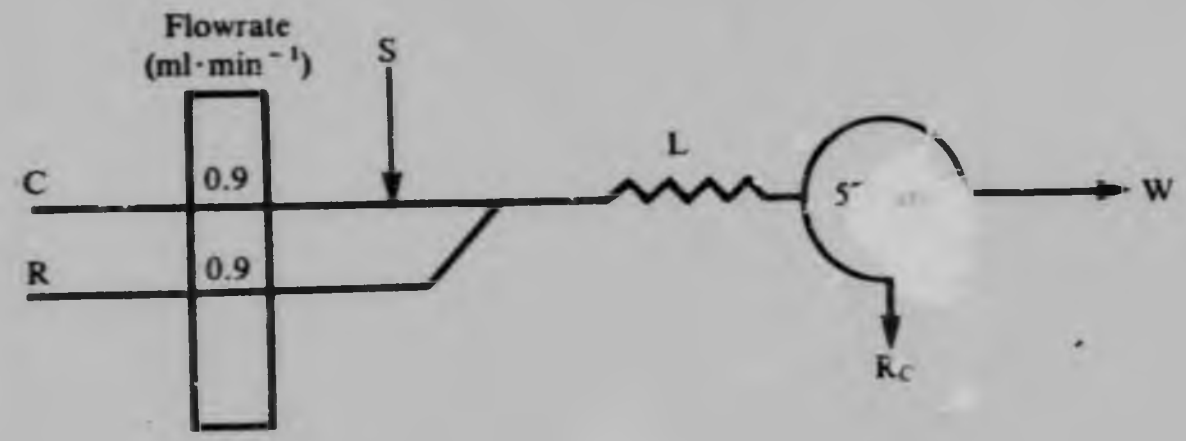


Figure 3.1 Schematic flow diagram for the determination of uranium(VI)

Conditions: (C) 2% buffer-complex solution; (R) 0.01% bromo-PADAP solution; (L) 4 m reaction coil (0.5 mm i.d.); (S) sample injection; (W) waste; (R_C) recorder.

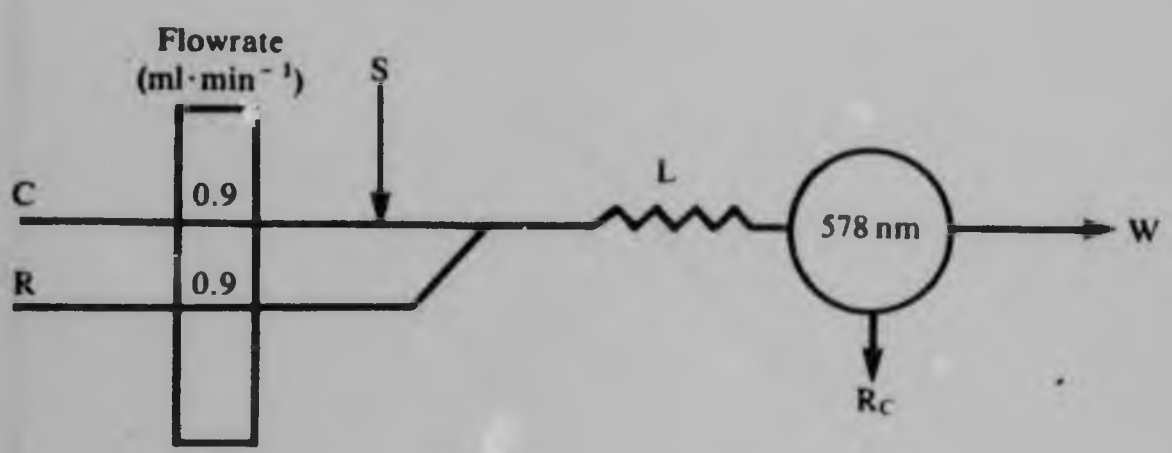


Figure 3.1 Schematic flow diagram for the determination of uranium(VI)

Conditions: (C) 2% buffer-complex solution; (R) 0.01% bromo-PADAP solution; (L) 4 m reaction coil (0.5 mm i.d.); (S) sample injection; (W) waste; (R_C) recorder.

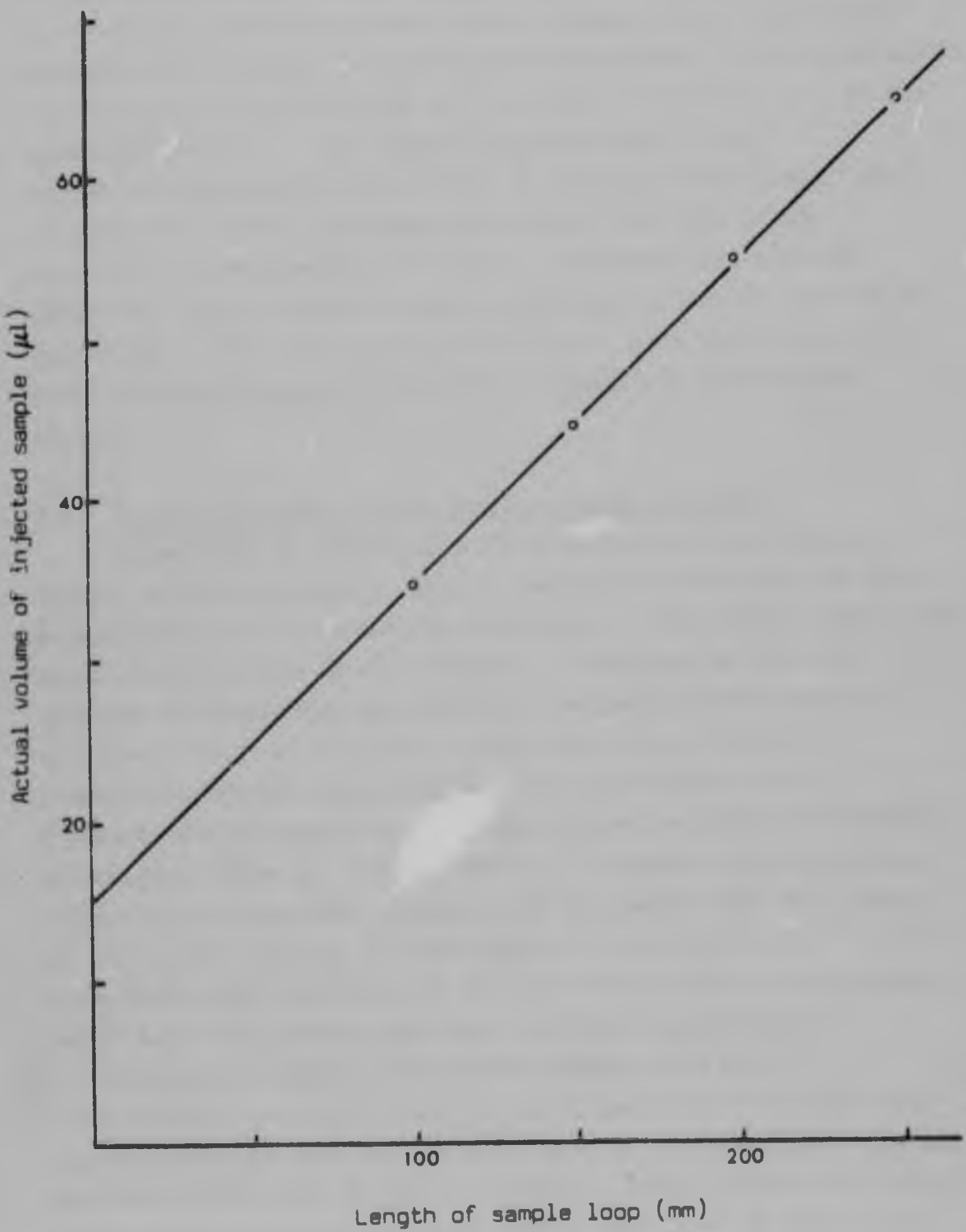


Figure 3.2 Calibration plot for the injection valve

valve and this injection point defined the start of the "reactor". The injected sample, or sample plug, underwent physical dispersion and chemical reaction with the carrier stream and the bromo-PADAP reagent solution as it was transported downstream. This dispersed and chemically reacted sample was monitored at the flow-cell of the spectrophotometer. The complex UO_2(bromo-PADAP$^-$)F was formed in the reaction coil and the absorbance of the complex was monitored at 578 nm The peak heights were recorded on the strip-chart potentiometric recorder. The sample was injected repeatedly until successive peak heights were within 99 per cent of each other. The chart speed and the chart scale were selected in order to ensure adequate resolution of details in the recorded signal.

3.4 Effect of Ethanol in the Buffer-complex Solution

Bromo-PADAP is sparingly soluble in aqueous solution but readily soluble in organic solvents such as ethanol which has been extensively used in uranium determinations. The buffer- complex and sample solutions are usually aqueous. Therefore an ethanolic solution of bromo-PADAP was added to the aqueous buffer-complex solution. In a conventional closed system total mixing, a prerequisite for discrete samples, can be achieved easily. Viscosity effects and changes resulting from the mixing of ethanolic and aqueous phases are not detrimental. However, in FIA complete mixing is not achieved. Injection of the sample into the aqueous carrier stream followed by the addition of an ethanolic solution of bromo-PADAP produced viscosity changes that resulted in an unstable baseline and the sample peaks were difficult to distinguish.

Ethanol was added to the buffer-complex solution at concentrations varying between 10 and 80 per cent. A stable base line was obtained when the carrier stream of buffer-complex solution contained 60 per cent or more of ethanol. When fluoride was present in the buffer solution,it started precipitating out of solution in ethanol solutions containing more than 60 per cent.

3.5 Univariate Method of Optimization

Parameters for the manifold (Table 3.1), such as flowrate,

sample size, length of tubing between sample injection point and the detector and the order of sequential addition of reagents were varied so as to establish a linear relationship between peak height and concentration of the sample. The dispersion of the sample in the flowing stream will be reflected in the shape of the peak as well as the peak height. All but one parameter was kept constant. Only the effect of the variation in this single parameter was established. This optimization gave a set of conditions from which further optimization could proceed to the other parameters in turn.

Table 3.1 Experimental parameters with chosen levels (for discrete adjustable parameters) or ranges (for continuous adjustable parameters)

Factor	Adjustable	Ranges
Injection volume	discrete	> 10 μl
Maximum pumping rate	discrete	2-20 ml.min^{-1}
Coil length	discrete	> 0.1 m
Tube diameter	discrete	0.3-1.0 mm
Pumping rate x	continuous	10-60% of max.flow

x By choice of peristaltic pump tubing

3.5.1 Results and Discussion

(a) Effect of Sample Loop Size

The sample loops were made of varying lengths of Teflon tubing of 0.5 mm inner diameter. The required lengths of tubing for the sample loops were calculated from the formula

$$S = \pi r^2 L_s \qquad (3.2)$$

The sample loop volumes (consisting of the loop but excluding the dead volume of the rotary valve) were 15, 25, 40, 50 and 70 μl.

After the sample loop of the rotary valve was filled with the sample solution, the sample zone was stationary until the valve was switched such that the sample loop was placed in the manifold and the carrier solution pushed the sample plug along the manifold. The effect of sample volume on the peak height is shown in Figure 3.3.

If only one mixing stage is involved in the injection process, the ascending part of the peak would be the reversal of the descending part and both would be exponential:

$$\text{rising curve:} \quad C = C_o^o(1 - e^{-ks}) \qquad (3.3)$$

$$\text{falling curve:} \quad C = C_o^o e^{-ks} \qquad (3.4)$$

$$S_{1/2} = 0.693/k \qquad (3.5)$$

where $S_{1/2}$ is the volume of sample required to obtain $C = C^{max} = 50$ per cent of C_o^o corresponding to $D_i = 2$. By sampling for two $S_{1/2}$, 75 per cent of C_o^o is obtained ($D = 1.33$), etc. The maximum sample volume required in practice is of the order of one $S_{1/2}$ volume even for systems with limited dispersion[13]. The injection of a sample with a volume of a fraction of $S_{1/2}$ is sufficiently reproducible to allow direct analysis of concentrated sample solutions which otherwise would have to be diluted manually prior to analysis.

Using log to the base 10 when $\log(1 - C^{max}/C_o^o)$ was plotted versus S, a curve was obtained (Figure 3.4) from which $S_{1/2} = 29\ \mu l$ was read off[13]. The value of C_o^o corresponding to the concentration of 10 $mg.l^{-1}$ of uranium(VI) was determined by filling the flow cell with the solution of UO_2(bromo-PADAP$^-$)F and measuring the absorbance and the corresponding peak height. Approximately 50 μl were needed to reach $D_t = 2$ and 82 μl to reach $D_t = 1.5$, whereas the steady state is reached at about $S = 250\ \mu l$ as shown in Figure 3.3.

The experiment was repeated with sample loops made from Teflon tubing with an inner diameter of 0.8 mm (20, 45 and 70 μl). All the measured C^{max} values were plotted according to equation (3.3). The results (Figure 3.4) were on the line with a slope corresponding to $S_{1/2} = 29\ \mu l$. Thus if D_f is kept constant D_i

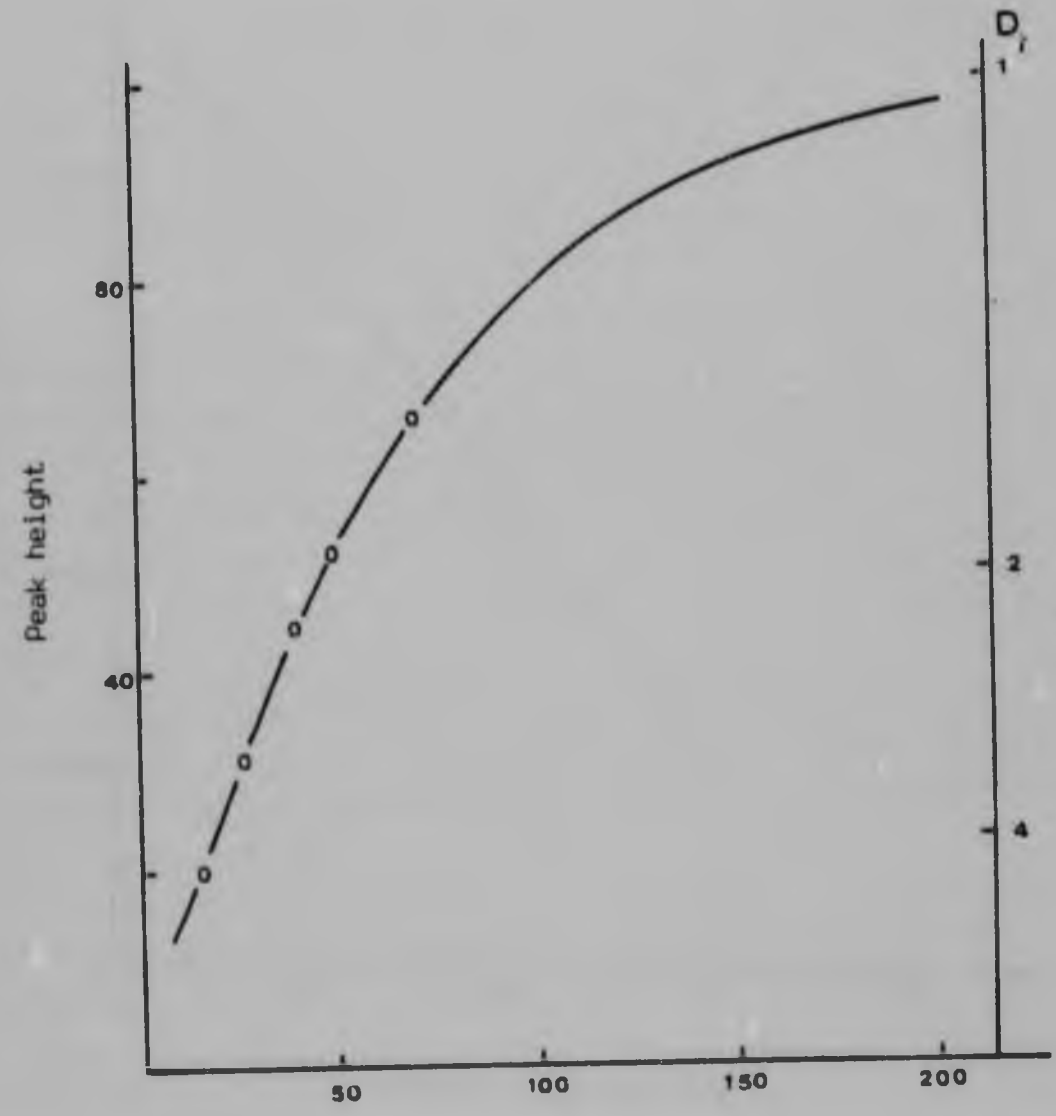


Figure 3.3 Effect of sample loop size on peak height

Conditions: 2% buffer-complex solution; 0.05% bromo-PADAP; sample concentration, 10 $mg.l^{-1}$; coil length, 1 m; flowrate, 0.9 $ml.min^{-1}$; sample loop diameter, 0.5 mm.

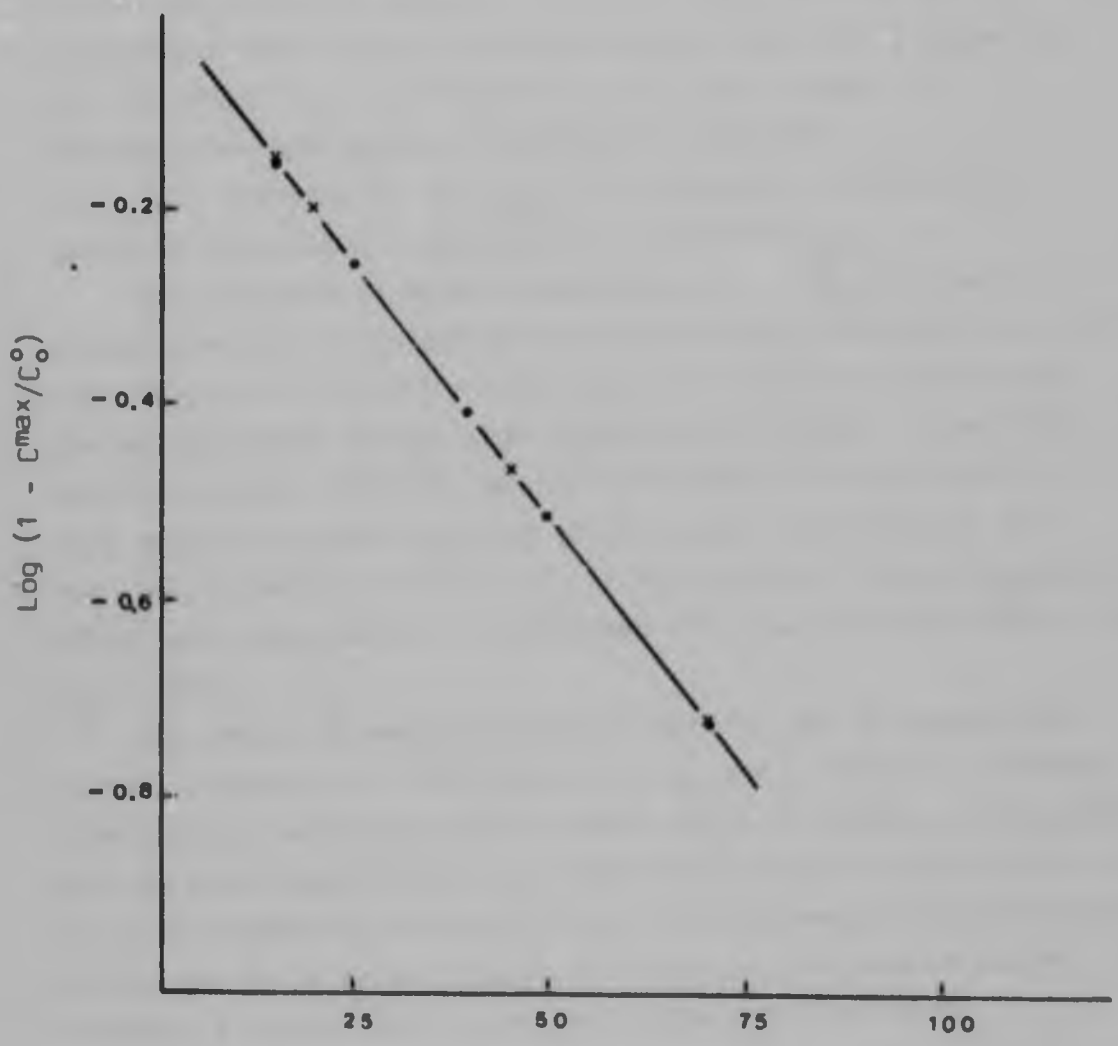


Figure 3.4 Effect of sample loop size on S

Conditions: 2% buffer-complex solution; 0.05% bromo-PADAP; sample concentration, 10 $mg.l^{-1}$; coil length, 1 m; flowrate, 0.9 $ml.min^{-1}$; sample loop diameter, (o) 0.5 mm, (x) 0.8 mm.

is independent of the geometry of the sample zone prior to injection. For the same linear velocity, F the residence time, T is proportional to the length of the system, L which is also true for the relationship between the residence time of one mixing stage, t_i, and its length L_i. A shorter t_i and L_i will result in a steeper curve and because $S = \pi r^2 L_s$ the ratio of L_i/L_s will decrease as will $S_{1/2}$. In contrast, increasing the volume of the mixing stage will also increase $S_{1/2}$.

The influence of medium dispersion on the $S_{1/2}$ value was investigated by the injection of various sample volumes into varying coil lengths (4, 6 and 8 m) and recording the C^{max} values, (all the samples loops had an inner diameter of 0.5 mm). When the resulting $\log(1 - C^{max}/C_o^o)$ was plotted versus S for all of the coil lengths, the same $S_{1/2}$ value of 52 μl was found (Figure 3.5). If the inner diameter of the tubing is increased to 1 mm, a $S_{1/2}$ value of 200 μl was obtained which corresponds to a four-fold increase in the $S_{1/2}/L_s$ ratio.

The choice of sample size is a powerful way of varying the overall dispersion of the system and $S_{1/2}$ is an important parameter especially in analyses where a small amount of sample is available. Because the flowrate and coil length are fixed, equations (3.3) and (3.4) are expressed in terms of S. Flow geometry has an important effect on the D_i value because, for example, the sample volume ($S = \pi r^2 L_s$) would occupy a portion of the tube four times longer if the radius were halved. Thus, if the dispersion of the flow, D_f, depends only on the residence time and not on the tube diameter, which is an acceptable approximation within the range of r = 0.2-0.5 mm, $S_{1/2}$ will decrease with the square root of the tube radius because the length of the mixing stage L_i will remain practically constant and consequently the volume of the sample solution required to reach 50 per cent of C_o^o ($S_{1/2}$) will be four times smaller. Thus the radius of the tube should be kept small if limited or medium dispersion is required. An increase in the sample volume has a gradually diminishing effect on the decrease in the total dispersion of the system.

At a constant flowrate (0.9 ml.min^{-1}) and coil length (2 m),

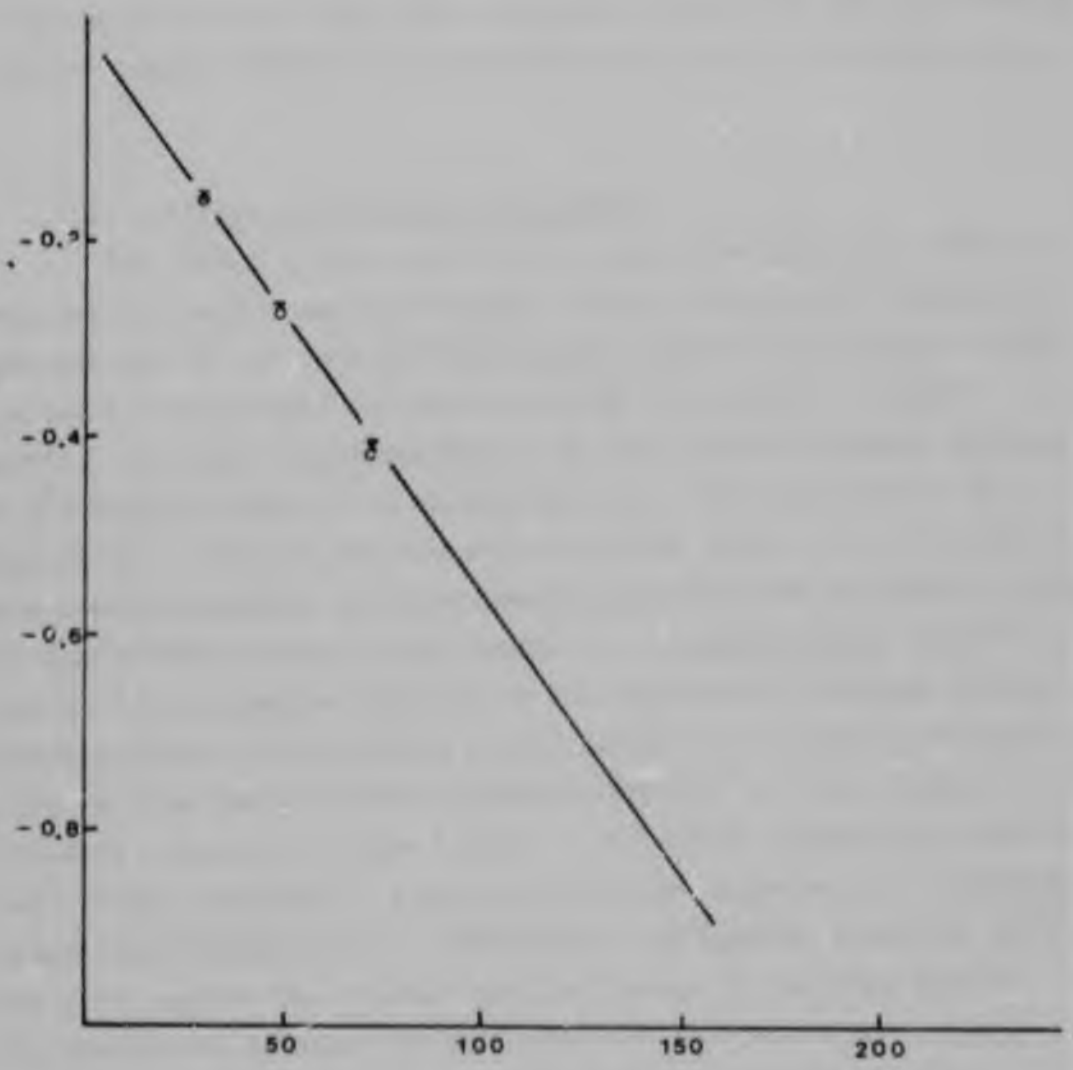


Figure 3.5 Effect of coil length

Conditions: 2% buffer-complex solution; 0.05% bromo-PADAP; sample concentration, 5mg.l^{-1}; coil length, (x) 4m, (o) 6m, (-) 8m; flowrate, 0.9ml.min^{-1}; tube diameter,0.5 mm.

double peaks were obtained in this investigation when sample sizes larger than 70 µl were used. Karlberg et al.[72] and Krug et al.[73] attributed the formation of double-humped peaks when using large samples to the fact that adequate mixing with the surrounding carrier reagent stream occurs only at each end of the sample plug.

(b) Effect of Reaction Coil Length

The effect of the length of the reaction coil was tested by the use of lengths varying between 1 and 7 m while the flowrate of the carrier (2 per cent buffer-complex solution) and reagent (0.01 per cent bromo-PADAP) was maintained at 0.9 ml.min^{-1} (Figure 3.6). The peak height decreased for coil lengths between 0.5 and 3 m and then increased to a maximum at 4 m. This phenomenon is explained by Johnson and Florence who noted that, at a pH value of 8, the unstable complex with absorbance maxima at 546 and 580 nm formed initially but decayed fairly rapidly. It would appear that the decay of this complex resulted in the decrease of the peak height for reaction coils <3 m, whereas a coil length of 4 m gave sufficient time for the stable complex U_2(bromo-PADAP$^-$)F to form, with a resulting increase in peak height. A further increase in reaction coil length resulted in a decrease in peak height due to increased dispersion (Section 2.4). Because of the precise timing of a FIA manifold, either the initial complex formed or the more stable complex can be measured to determine the analyte concentration. To increase the sampling rate, shorter reaction coils should be employed.

The range of D_t values that can be obtained under the given conditions (flowrate 0.9 ml.min^{-1}, inner diameter of the manifold tubing 0.5 mm, S = 30, 50 and 70 µl) when measuring the more stable complex, varied from 1.6 to 10 within the coil lengths of 4, 6 and 8 m and the results are shown in Figure 3.7. The relationship between L and D_f is given by the equation

$$D_f = 2L^{\frac{1}{2}}L_i^{\frac{1}{2}}/W_o \qquad (3.6)$$

where W_o is the peak width. The residence time, T can be used

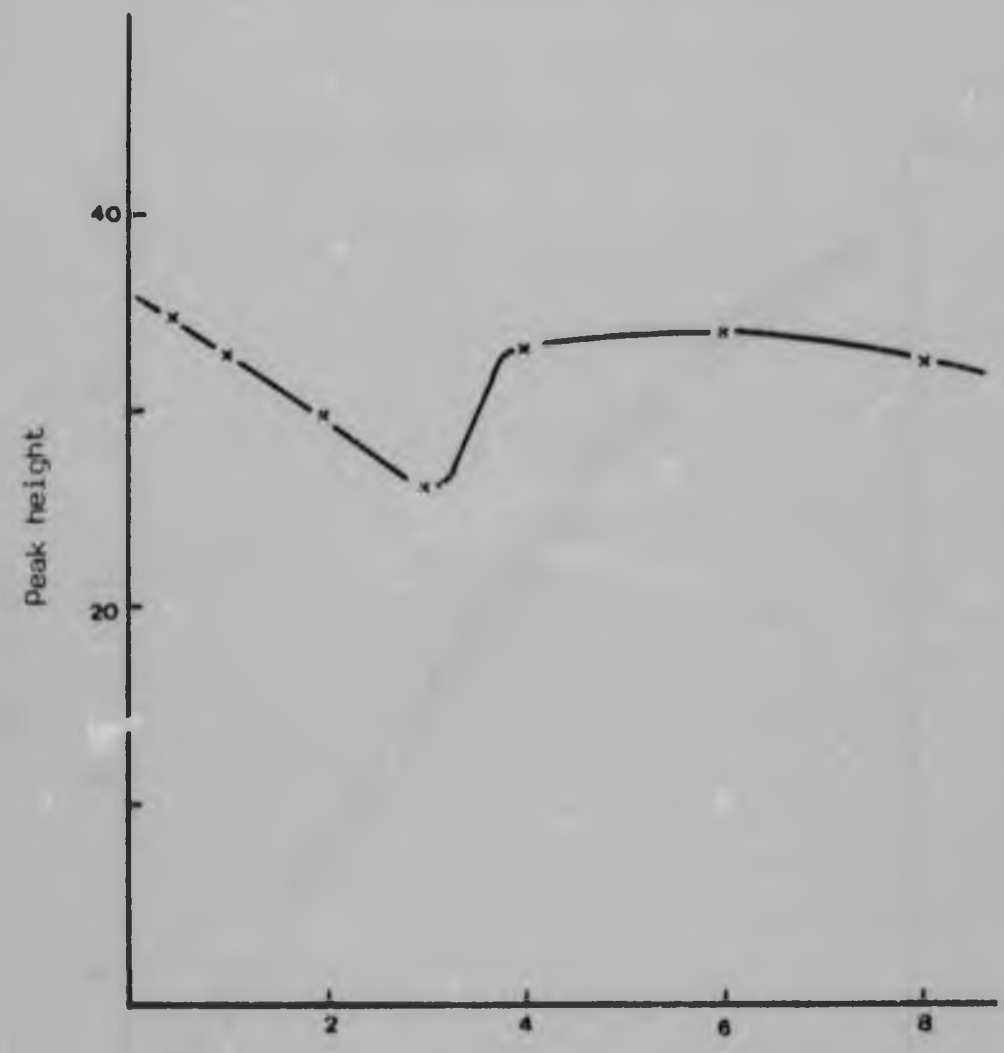


Figure 3.6 Effect of length of reaction coil

Conditions: 2% buffer-complex solution;
0.08% bromo-PADAP; sample volume, 50μl;
sample concentration, 5mg.l^{-1};
flowrate, 0.9ml.min^{-1}.

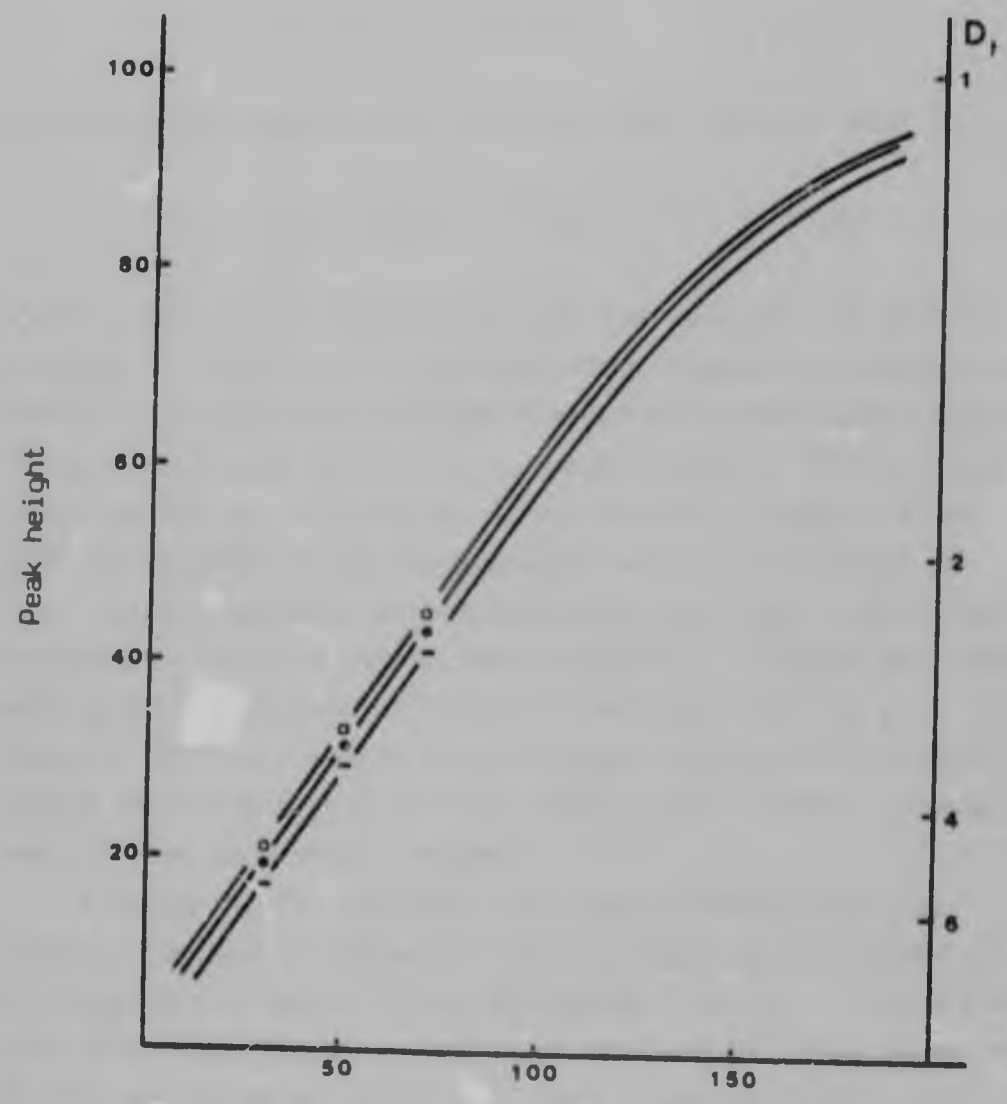


Figure 3.7 Effect of coil length and sample size on peak height

Conditions: 2% buffer-complex solution; 0.05% bromo-PADAP; sample concentration, 5mg.l^{-1}; coil length, (o) 4m, (•) 6m, (-) 8m; flowrate, 0.9ml.min^{-1}; tube diameter, 0.5mm.

in place of L as the main parameter. The peak heights are then plotted against the square root of the time between the injection and the peak maximum.

$$D_f = 2QT\ t_i^{1/2}/W_o \pi r^2 \qquad (3.7)$$

Replacing the pumping rate Q by the linear flow velocity F

$$D_f = (2/W_o)\ F\ T^{1/2} t_i^{1/2} \qquad (3.8)$$

where L_i or t_i are system constants that describe the mixing in terms of tube length, residence time, viscosity, temperature, etc. The coil lengths varied between 4 and 8 m and the sample size was 50 µl The experiment was repeated with sample sizes of 30 and 70 µl. Extrapolation of the straight lines obtained (Figure 3.8) to the C_o^{max} values (C_o^{max} becomes the concentration of the element of fluid at peak maximum, extrapolated to t = 0 mol^{-1}) gave the D_f values. Plotting these values against T (Figure 3.9) shows that D_f is independent of S within the range 30 to 70 µl. The value of C^{max} in a sample under dynamic flow conditions where the colour development does not have time to go to completion was 95 per cent of that in a static system.

Although D_i is dependent on S, tube diameter and flow velocity for medium dispersion, the D_f value is independent of D_i provided the sample volume is smaller than $S_{1/2}$. Thus the same coil length and flowrate would give the same D_f value regardless of the sample volume and it will take a progressively longer time to reduce the peak height even further.

(c) Effect of Flowrate

There was a decrease in the peak height with increased flowrate (Figure 3.10; equation 3.8) indicating that at increased flowrates there was increased dispersion. This dependence on the flow velocity was investigated by injecting a given sample size into a manifold at flowrates ranging from 0.45 to 1.8 $ml.min^{-1}$. Peak heights and residence times for gradually increasing coil lengths were recorded for each flowrate. Figure 3.11 shows the curves

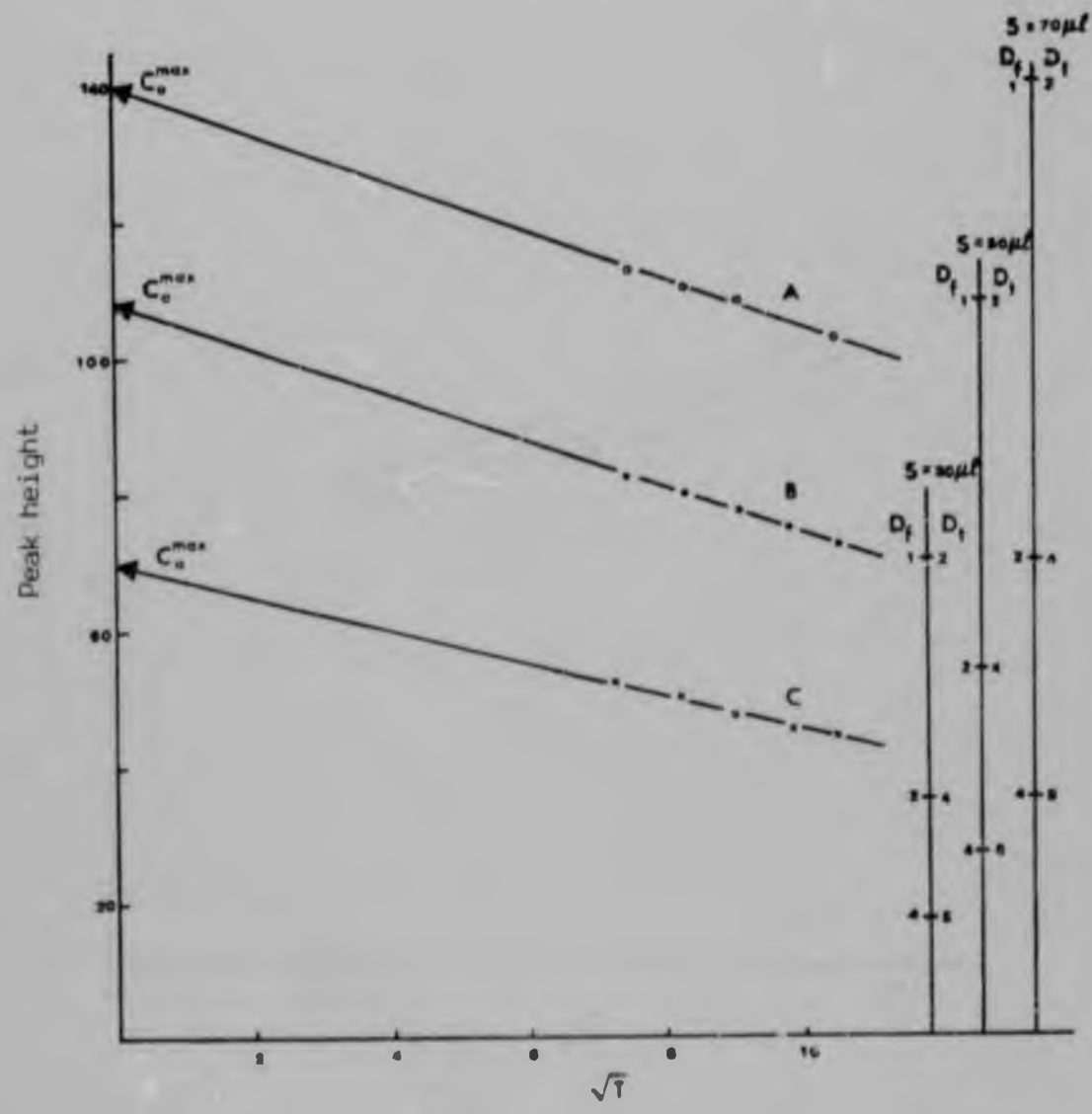


Figure 3.8 Relationship between peak height, extrapolated peak height and residence time for varying sample sizes

Conditions: 2% buffer-complex solution; 0.05% bromo-PADAP; sample volumes, A 70, B 50 and C 30µl; sample concentration, 5mg.l^{-1}; coil lengths, 4, 5, 6, 7 and 8m; flowrate, 0.9ml.min^{-1}; tube diameter, 0.5mm.

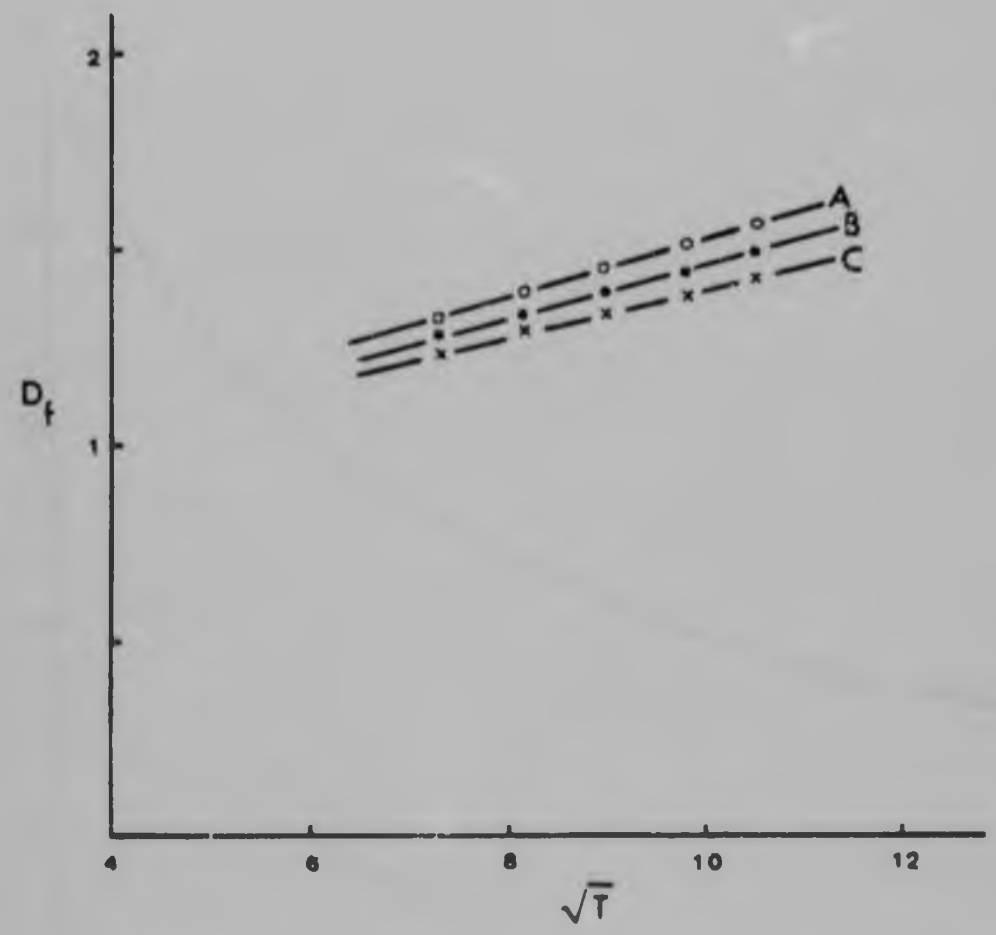


Figure 3.9 Influence of sample size on the D_f value

Conditions: 2% buffer-complex solution; 0.05% bromo-PADAP; sample volumes, A 70, B 50 and C 30 μl; sample concentration, 5mg.l^{-1}; coil lengths, 4, 5, 6, 7 and 8m; flowrate, 0.9ml.min^{-1}; tube diameter 0.5mm.

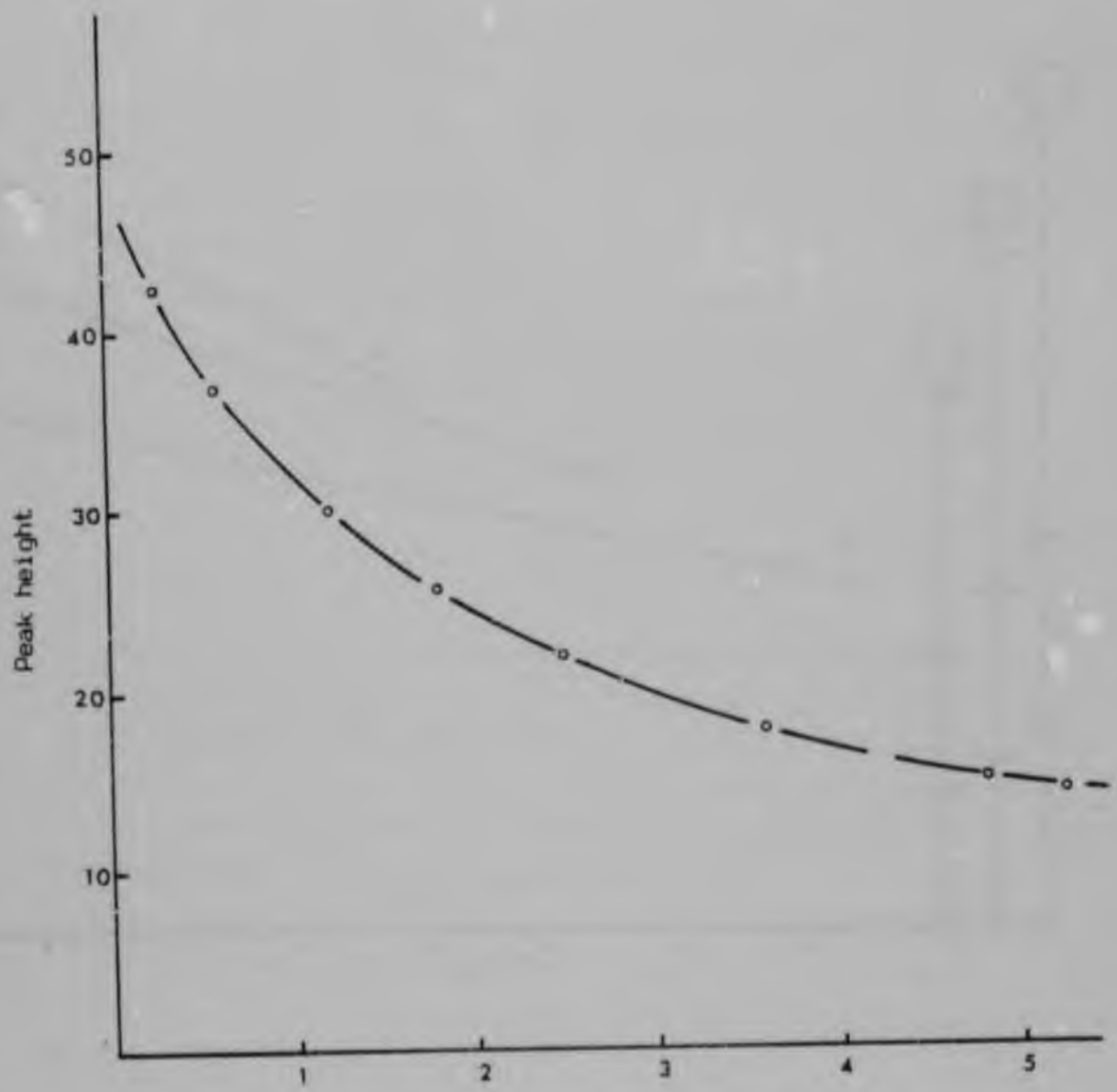


Figure 3.10 Effect of flowrate

Conditions: 2% buffer-complex solution; 0.08% bromo-PADAP; sample volume, 50μl; sample concentration, 5mg.l^{-1}; coil length, 2m.

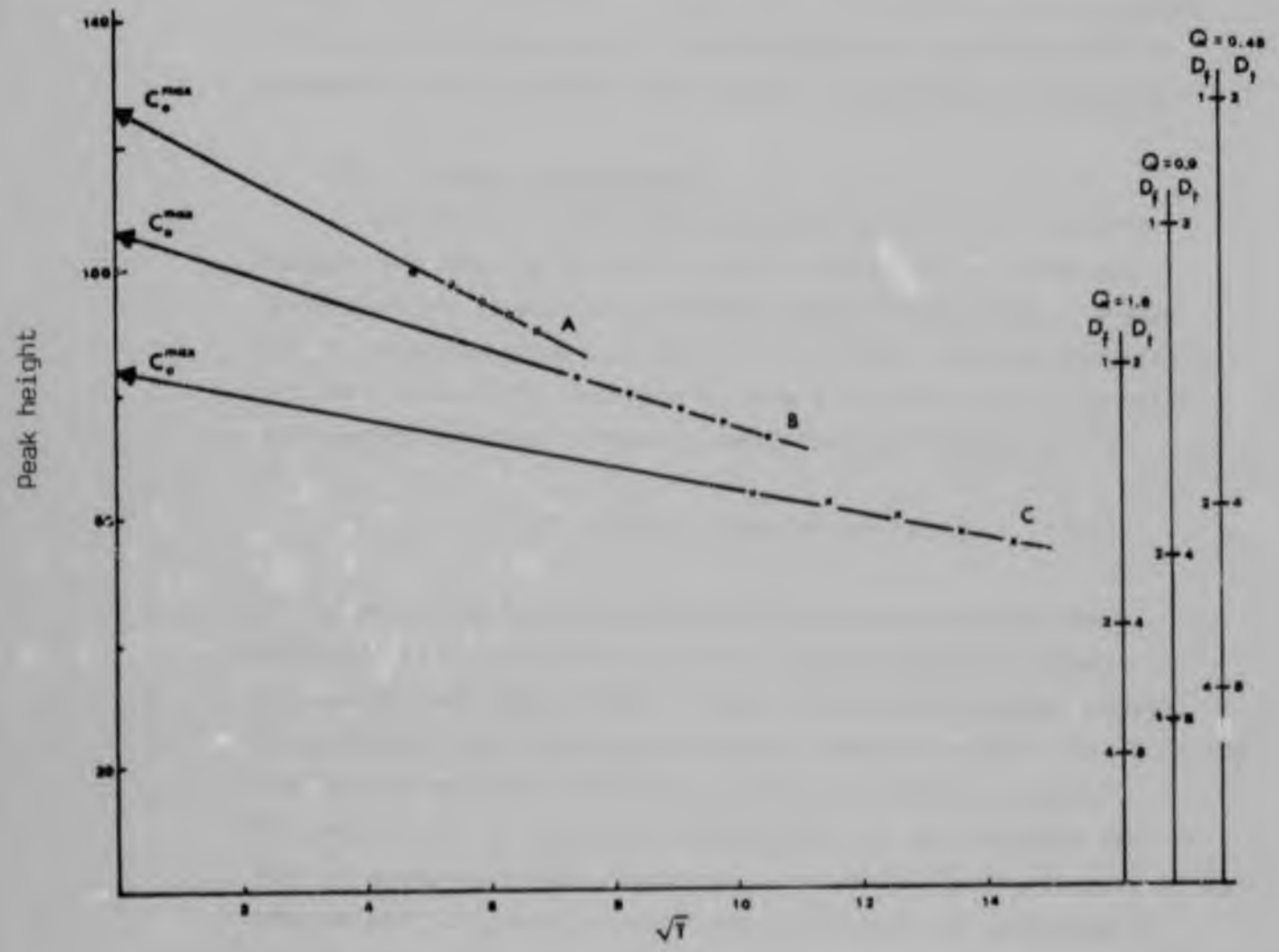


Figure 3.11 Relationship between peak height, extrapolated peak height and residence time for varying flowrates

Conditions: 2% buffer-complex solution; 0.05% bromo-PADAP; sample volume, 50μl; sample concentration, 5mg.l^{-1} ; coil lengths, 4, 5, 6, 7 and 8m; flowrates, A 0.45, B 0.9 and C 1.8ml.min^{-1}; tube diameter, 0.5mm.

obtained and the extrapolated C_o^{max} from which the corresponding D_f values were obtained. From the plot of the D_f against T (Figure 3.12) it can be seen that the flow velocity has a marked effect on the dispersion of the sample plug or zone and that a decrease in the flowrate will lead to a decrease in dispersion.

(d) Sampling Frequency

In FIA, one or more samples zones can be in the manifold between the point of injection and the detector. In manual operations, one sample at a time is usually determined. A peak height measured at a time $t_f = T + 1.5\ W$ will be approximately 1 per cent of the C^{max} recorded at time T if the curve is Gaussian. The maximum sampling frequency would then be (Figure 3.13):

$$S^{max} = 3600/T \text{ (samples per hour)} \qquad (3.9)$$

In the determination of uranium(VI), the residence time was sufficiently long to allow for the chemical reaction between uranium(VI) and bromo-PADAP to start forming the stable complex. The analysis rate for large batches of samples ranged from 16 to 180 samples per hour for flowrates between 0.3 and 5.4 $ml.min^{-1}$. The sensitivity is inversely proportional to the flowrate and, so that an acceptable peak height and a reasonable analysis rate of 40 samples per hour could be obtained, a flowrate of 0.9 $ml.min^{-1}$ was chosen. The recorder trace of peak height for varying residence time is shown in Figure 3.14.

(e) Effect of bromo-PADAP Concentration

Variation in the concentration of the bromo-PADAP (Figure 3.15) gave a maximum absorbance reading for the UO_2(bromo-PADAP$^-$)F complex at 0.08 per cent bromo-PADAP in ethanol. With a concentration of 0.002 per cent bromo-PADAP as recommended for the use in static batch analysis, the peak height for 10 $mg.l^{-1}$ under the dynamic conditions of FIA was 56 per cent of that obtained using 0.08 per cent bromo-PADAP. For the 0.01 per cent solution of bromo-PADAP, chosen because of the much lower interference effects with this concentration (Section 4.1.3(b)), the

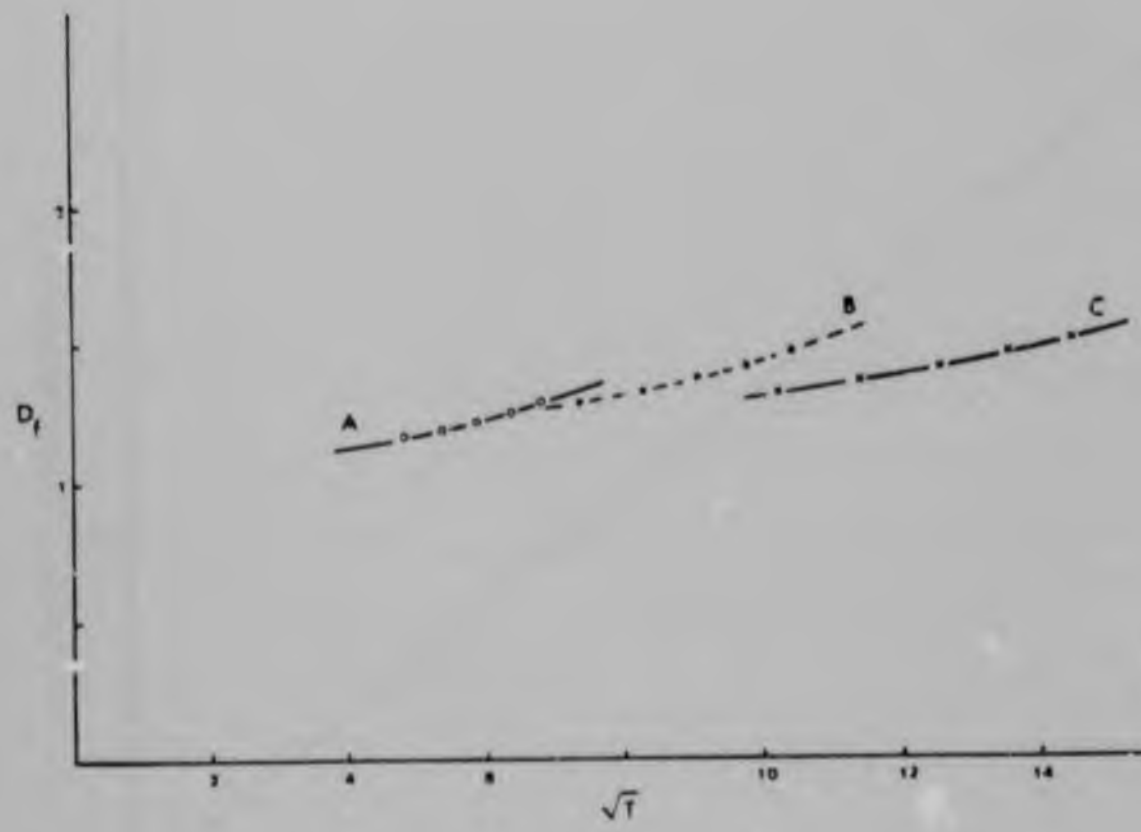


Figure 3.12 Influence of flowrate on the D_f value

Conditions: 2% buffer-complex solution; 0.05% bromo-PADAP; sample volume, 50μl; sample concentration, 5mg.l^{-1}; coil lengths, 4, 5, 6, 7 and 8m; flowrates, A 0.45, B 0.9 and C 1.8ml.min^{-1}; tube diameter, 0.5 mm.

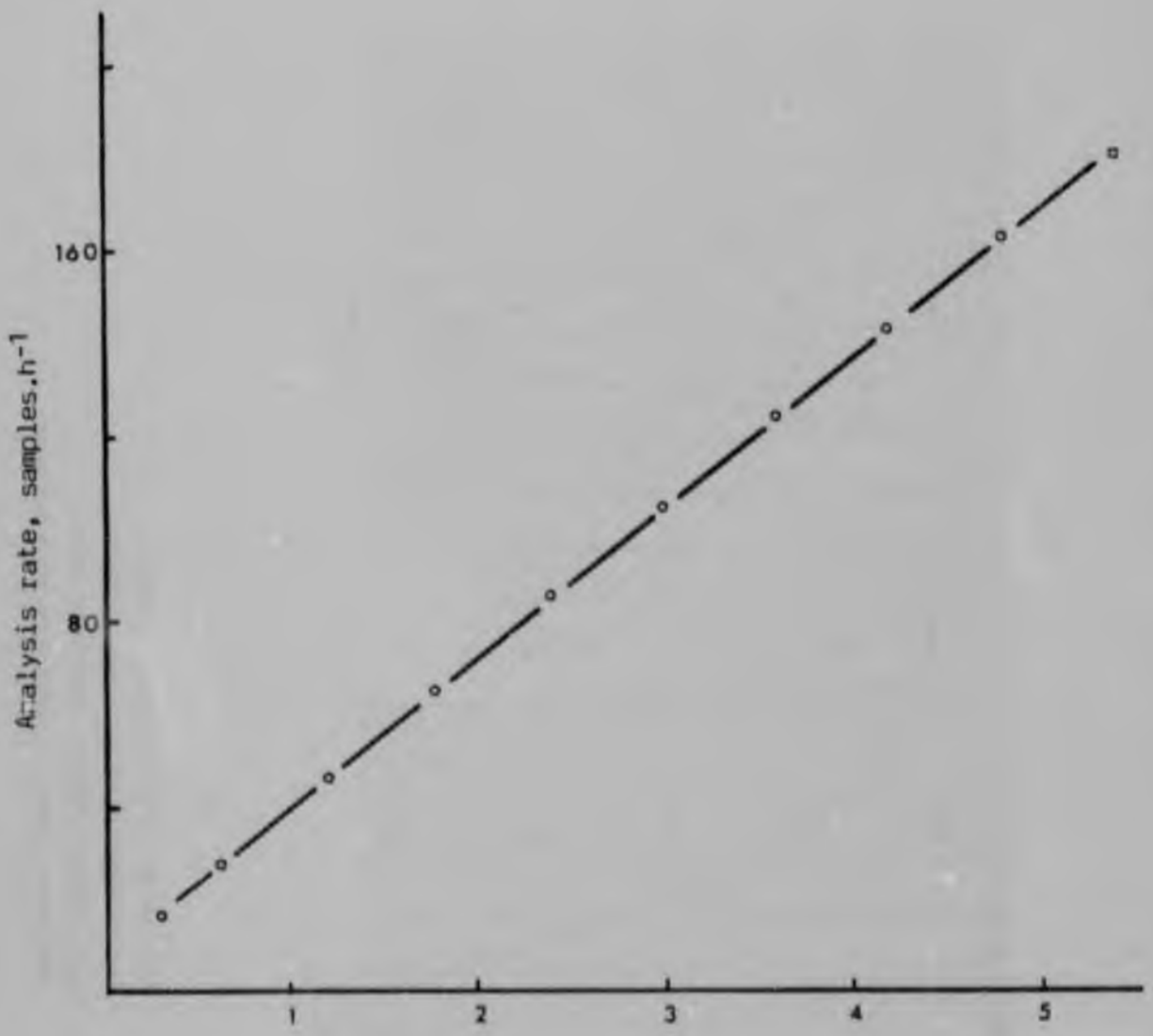


Figure 3.13 Sampling rate

Conditions: 2% buffer-complex solution; 0.01% bromo-PADAP solution; sample volume, 50μl; sample concentration; 10mg.l^{-1} in 10g.l^{-1} H_2SO_4; coil length, 4m.

Figure 3.14 Recorder trace for sampling rate

Conditions: 2% buffer-complex solution; 0.01% bromo-PADAP solution; sample volume, 50µl; sample concentration, 10 mg l^{-1} in 10 g.l^{-1} H_2SO_4; coil length, 4 m; chart speed, 30 mm.min^{-1}

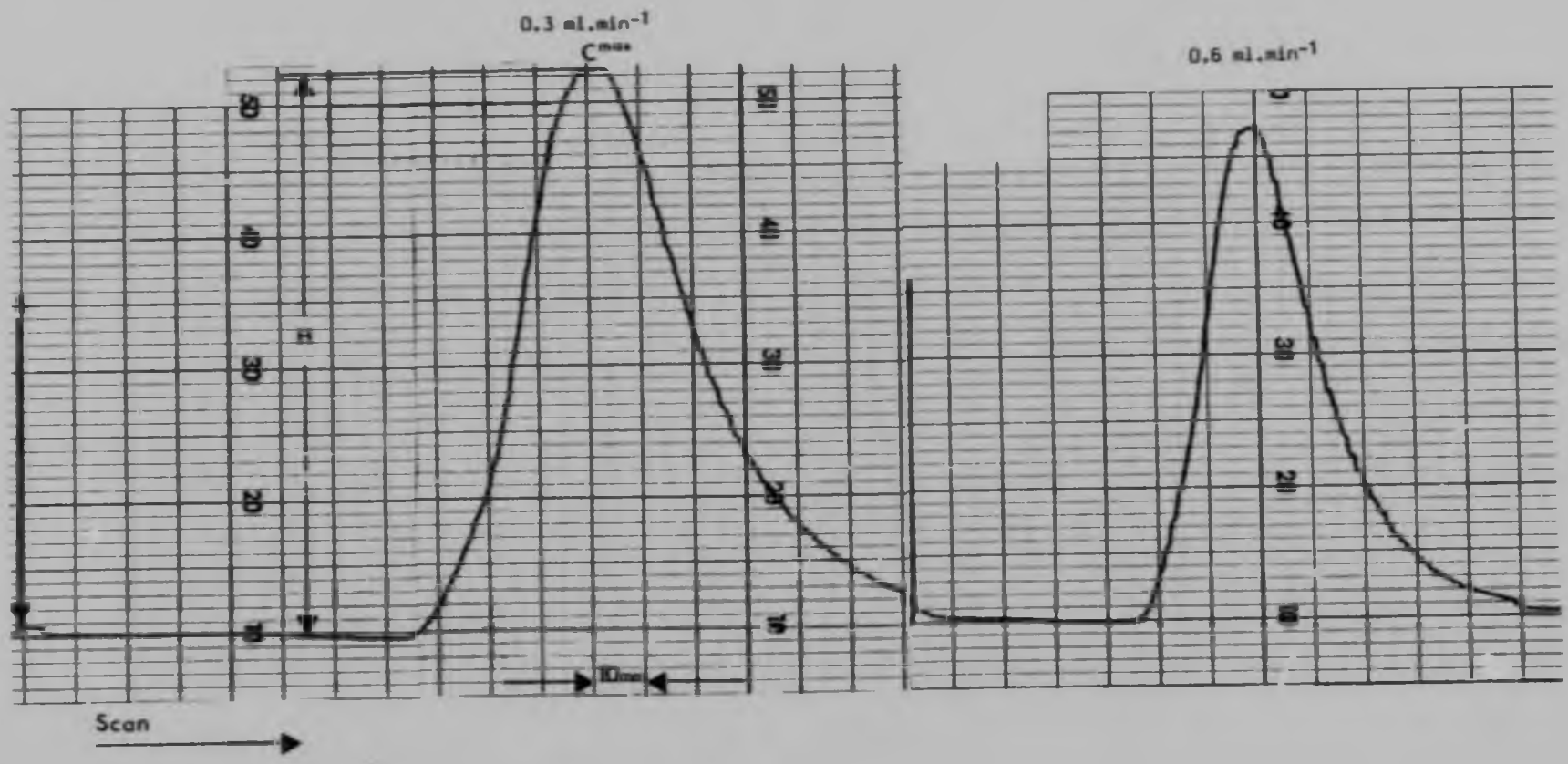
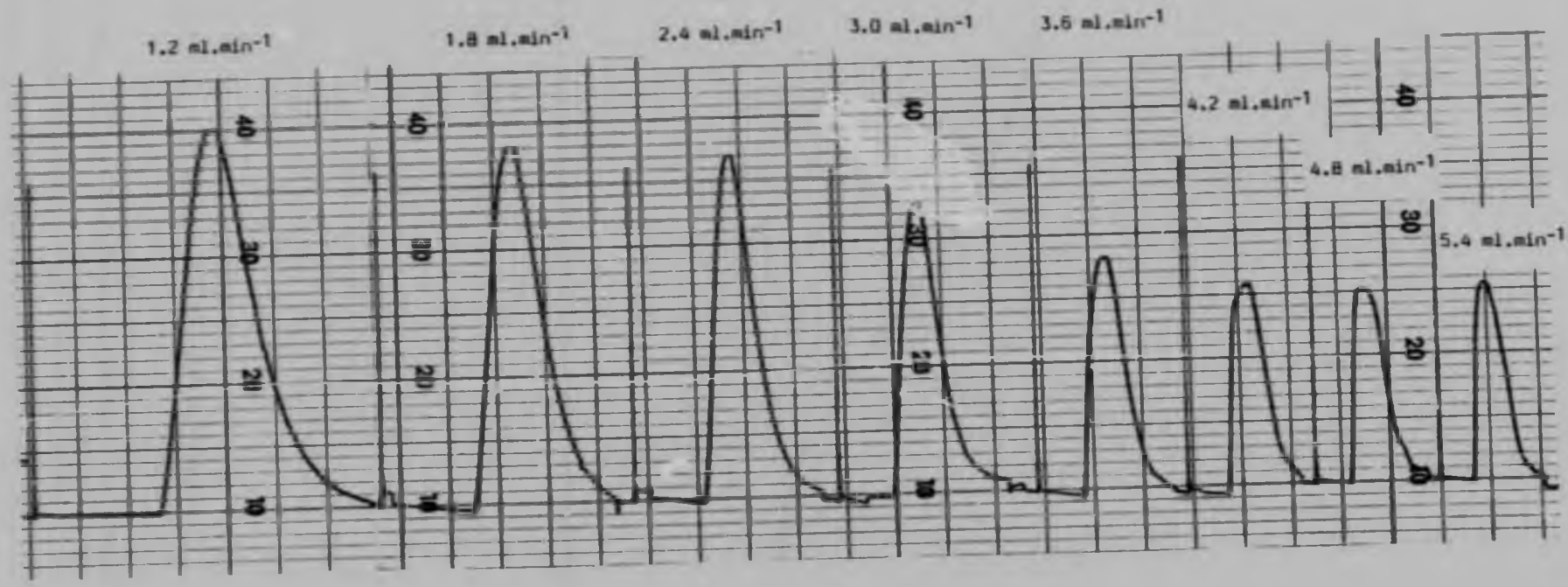


Figure 3.14 continued:-



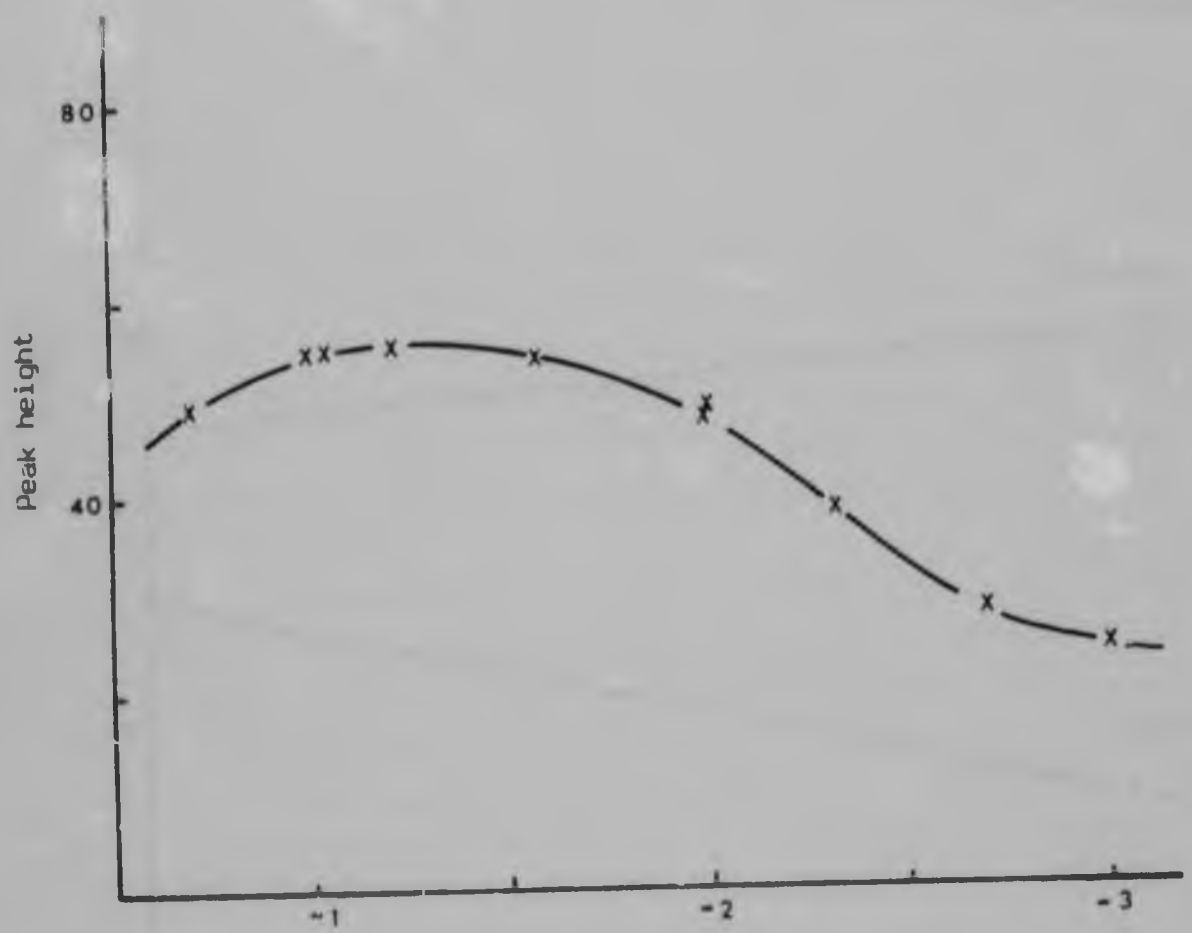


Figure 3.15 Effect of varying bromo-PADAP concentration

Conditions: 2% buffer-complex solution; sample volume, 50μl; sample concentration, 5 $mg.l^{-1}$; coil length, 4 m; flowrate, 0.9 $ml.min^{-1}$.

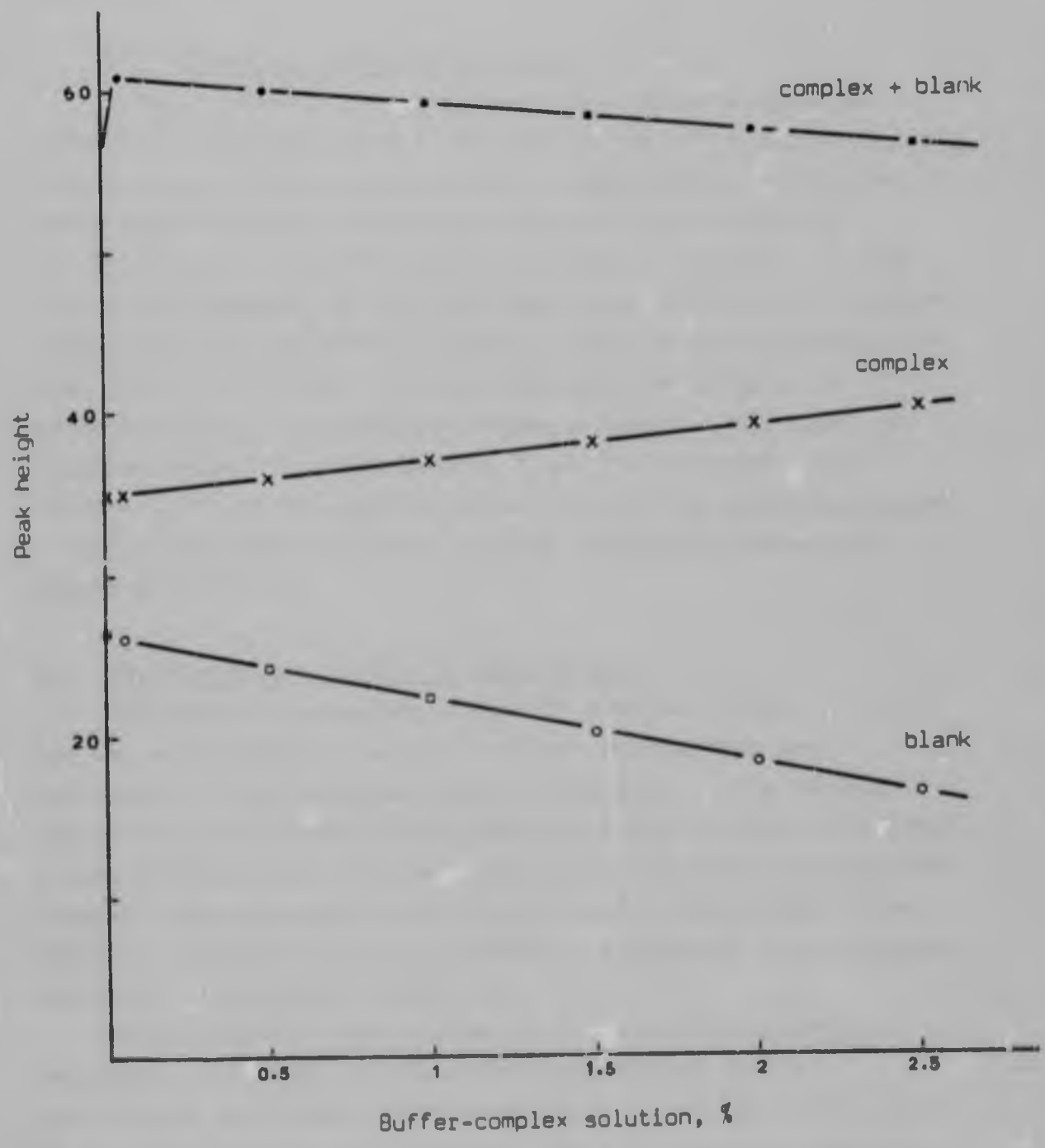


Figure 3.16 Effect of concentration of buffer solution

Conditions: 0.01% bromo-PADAP; sample volume, 50 µl; sample concentration, 10 $mg.l^{-1}$; in 10 $g.l^{-1}$ H_2SO_4; coil length, 4 m; flowrate, 0.9 $ml.min^{-1}$.

peak height was 94 per cent of that obtained with a 0.08 per cent solution.

(f) Effect of Buffer Concentration

The pH value of the combined buffer-complex solution was constant at a pH value of 8.9 when varying the buffer between 0.5 and 2.5 per cent. There was a decrease in peak height for both the gross signal (complex + blank) and the blank with increasing concentration of the buffer-complex solution (Figure 3.16). The rate of the decrease for the blank was higher than that of the gross signal, thus the net signal (complex - blank) showed an increase in peak height with increasing concentration of the buffer. A concentration of 2 per cent was chosen because, at this level, an injected sample (50 µl) containing 20 $g.l^{-1}$ of sulphuric acid (Figure 3.16) did not suppress the pH value of the sample and reagent stream to less than 8.6 which is within the optimum range of pH values of 8.5 to 9.5.

3.6 Modified Simplex Method of Optimization

The physical parameters of the FIA manifold (Figure 3.1) used for the determination of uranium (VI) and which affect the performance of the system are shown in Table 3.1. The chemical variables of the system (buffer-complex solution of pH value 8.9 and a bromo-PADAP solution of concentration 0.01 per cent in 50 per cent ethanol) were maintained at the levels found to be optimum in the presence of mineral acids and interfering elements in the univariate method of optimization (Chapter 4).

The optimizations were carried out in terms of experimental variables, coil length and flowrate (pump setting) in the two-variable optimization with the addition of the sample loop size in the three-variable optimization. The FIA system was assembled with the required coil length, pump setting (and sample size) and the carrier and reagent streams were allowed to flow for a few minutes. When a stable chart base line on the recorder was obtained, a sample was injected, the reaction took place and the resulting peak was recorded.

The boundaries for each variable are shown in Table 3.1. These were chosen on the grounds of experimental experience. For example,

the higher flowrate limit specified was the fastest flow that could be obtained from the given pump. The lower limit was the slowest flow possible from which a peak could be obtained. The optimizations started from a set of experimental conditions chosen by the operator on the basis of experience.

The names of the variables were entered into the microcomputer together with their ranges (Table 3.1). A n+1 set of variables, (see vertex 1 to 3 in the two-variable optimization and vertex 1 to 4 in the three-variable optimization), were chosen by the operator and n+1 peak heights were recorded. After the experiments were performed the actual values of the variables used and the peak heights obtained were entered into the microcomputer (Appendix II) and a further experiment was carried out. The process was continued, the programme calculator giving a new set of conditions each time.

3.6.1 Results and Discussion

The response factor chosen for optimization was peak height sensitivity as in the univariate optimization.

(a) Two-Variable Simplex Optimization

The results of a two-variable optimization are given in Tables 3.2 to 3.4. In the Tables, "Vertex No." refers to the point in factor space defined by the values of the variables shown in that row. It therefore corresponds to an actual experiment the response of which is shown as a peak height. A running account of the current simplex is recorded in the Tables the points being ranked in order of the magnitude of the response. The cycle for generating a new point usually varies from one to three experiments and these are recorded in the Tables. After 24, 26 and 18 experiments in Tables 3.2 to 3.4 respectively, the optima for the two-variable systems appeared to have been reached. This is also shown in Figures 3.17 to 3.19 where the net signals after the final experiments were the maxima indicated by the approach to a horizontal line.

Where sample dispersion is suboptimal (under the prevailing chemical and physical conditions), double peaks can occur. In the FIA system these peaks tend to be eliminated from the simplex since,

Table 3.2 Optimization using a Modified Simplex approach with two variables

Simplex Move	Vertex No.	Current Vertex points (ranked)	Violations	Type of Simplex Move	Flowrate $m..min^{-1}$	Coil length m	Peak height	SD	Opt. %
	1				0.60	1	32		58
	2				0.90	2	40		71
1	3	2,3,1		R	0.60	3	33	4.36	59
2	4	2,4,3		R	0.90	4	37	3.51	66
	5			R	1.20	3	27		49
3	6	2,3,4		-C	0.75	3	28	80.04	50
	7	7,3,2		R	0.90	2	40*		72
	8			R	0.60	1	30		54
4	9	9,7 3		+C	0.68	2	49	8.02	88
	10			R	0.98	1	25		43
5	11	9,11,7		-C	0.96	2.5	48	4.92	86
	12			R	0.47	2.5	54		97
6	13	12,9,11	BV	E	0.25	2.5*		3.21	
7	14	12,14,9		R	0.45	1.5	51	2.52	92
8	15	12,14,15	BV	-C	0.57	2	48	3.00	86
	16	16,14,15		R	0.47	2.5	56*		101
9	17	16,17,14		R	0.35	2	53	2.00	95
	18			R	0.37	2.5	50		90
10	19	16,19,17		-C	0.43	2	52	98.83	94
	20	20,19,17		R	0.47	2.5	55*		99
	21			R	0.54	2.2	51		92
11	22	20,21,19		+C	0.50	2	52	94.41	94
	23	23,22,19		R	0.47	2.5	56*		101
	24	23,24,22		R	0.54	2.5	54	1.76	97

+ Vertex repeated n+1 times reevaluated and averaged; * failed expansion; C contraction; R reflection; E expansion; BV boundary violation; SD standard deviation; Opt. optimization.

Conditions: Tube diameter 0.5mm; flow cell capacity 8μℓ; sample size 50μℓ; sample concentration $10mg.l^{-1}$ in sulphuric acid ($10g.l^{-1}$); 2% buffer- complex solution; 0.01% bromo- PADAP solution.

FINAL SIMPLEX

Flowrate 167 ($0.5ml.min^{-1}$)

Coil length 2.3 m

Table 3.3 Optimization using a Modified Simplex approach with two variables

Simplex Move	Vertex No.	Current Vertex points (ranked)	Violations	Type of Simplex Move	Flowrate $ml.min^{-1}$	Coil length m	Peak height	SD	Opt. %
	1				0.90	5	30		71
	2				1.50	4	24		57
1	3	1,3,2		R	1.20	3	29	3.21	69
	4			R	0.60	4	35		83
2	5	4,3,1	BV	E	0.15	4*		3.21	
3	6	4,6,1		R	0.30	6	33	2.52	79
4	7	4,6,7	BV	-C	0.68	5	28	3.61	67
	8	8,6,7		R	0.60	4	41+		98
5	9	8,6,9	BV	-C	0.56	5	29	4.51	69
	10			R	0.34	5	31		74
6	11	8,11,6		+C	0.39	5	32	80.99	76
	12	12,11,6		R	0.60	4	40+		95
	13			R	0.69	3	31		74
7	14	14,12,11		+C	0.60	4	42	5.31	100
	15			R	0.80	3	32		76
8	16	14,16,12		-C	0.49	4.5	40	1.53	95
	17			R	0.49	4.5	40		95
9	18	14,17,16		+C	0.52	4	39	86.03	93
	19	19,17,16		R	0.60	4	42		100
10	20	19,20,17		R	0.59	3.5	41	1.00	98
	21	21,20,17		R	0.60	4	42+		100
	22			R	0.70	3	33		79
11	23	21,23,20		-C	0.54	4	41	87.47	98
	24	24,23,20		R	0.60	4	41+		98
	25			R	0.55	4	41		98
12	26	24,25,23		+C	0.56	4	40	87.90	95

+ Vertex repeated n+1 times reevaluated and averaged; * failed expansion; C contraction; R reflection; E expansion; BV boundary violation; SD standard deviation; Opt. optimization.

Conditions: Tube diameter 0.5mm; flow cell capacity 8µℓ; sample size 50µℓ; sample concentration $10mg.l^{-1}$ in sulphuric acid ($10g.l^{-1}$); 2% buffer-complex solution; 0.01% bromo-PADAP.

FINAL SIMPLEX

Flowrate 187 ($0.57ml.min^{-1}$)

Coil length 4 m

Table 3.4 Optimization using a Modified Simplex approach with two variables

Simplex Move	Vertex No.	Current Vertex points (ranked)	Violations	Type of Simplex Move	Flowrate $ml.min^{-1}$	Coil length m	Peak height	SD	Opt. %
	1				1.20	1	21		47
	2				0.30	4	45		100
1	3	2,3,1		R	1.50	7	22	13.56	49
2	4	2,4,3	BV	-C	1.05	3.5	29	11.79	64
3	5	2,4,5	BV	-C	1.09	5.5	28	9.53	62
	6	6,4,5		R	0.30	4	45+		100
4	7	6,7,4	BV	-C	0.88	4.5	37	8.00	82
	8	8,7,4		R	0.30	4	43+		96
5	9	8,9,7	BV	-C	0.82	4	38	3.79	84
6	10	8,10,9	BV	-C	2.88	4	39	3.21	87
	11	11,10,9		R	0.30	4	45+		100
7	12	11,10,12	BV	-C	0.67	4	38	3.50	84
8	13	11,13,10		R	0.36	4	44	3.04	98
	14	14,13,10		R	0.30	4	45+		100
9	15	14,13,15	BV	-C	0.53	4	44	0.43	98
10	16	14,13,16	BV	-C	0.43	4	44	0.43	98
	17	17,13,16		R	0.30	4	44+		98
	18	17,13,18	BV	-C	0.38	4	44	0.21	98

+ Vertex repeated n+1 times reevaluated and averaged; * failed expansion; C contraction; R reflection; E expansion; BV boundary violation; SD standard deviation; Opt. optimization.

Condition: Tube diameter 0.5mm; flow cell capacity 8μℓ; sample size 50μℓ; sample concentration 10mg.l^{-1} in sulphuric acid (10g.l^{-1}); 2% buffer-complex solution; 0.01% bromo-PADAP.

FINAL SIMPLEX

Flowrate 115 (0.35ml.min^{-1})

Coil length 4 m

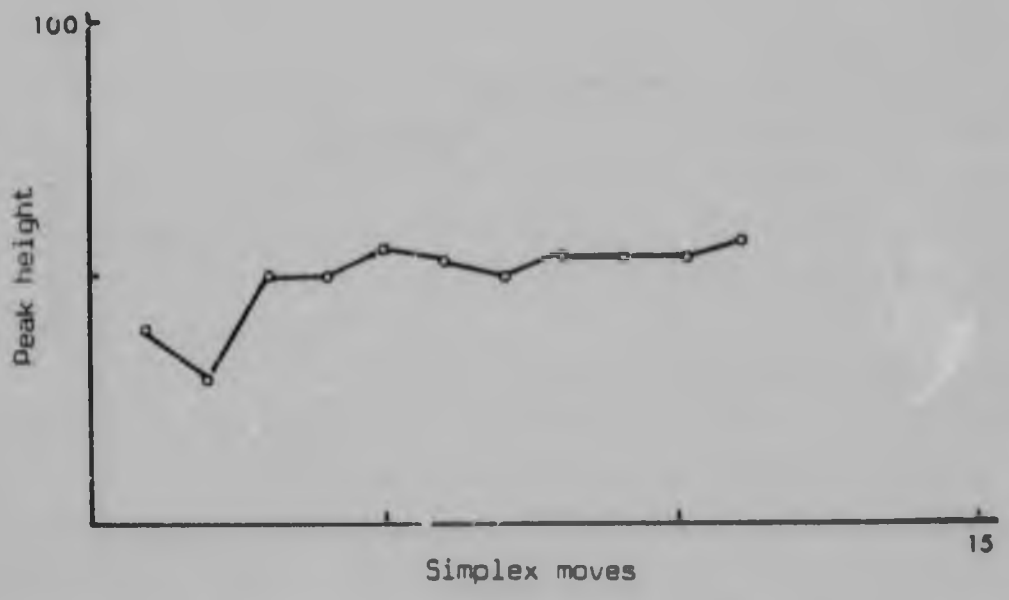


Figure 3.17 Optimization using a Modified Simplex approach with two variables

Conditions: Initial simplex and peak heights as in Table 3.2

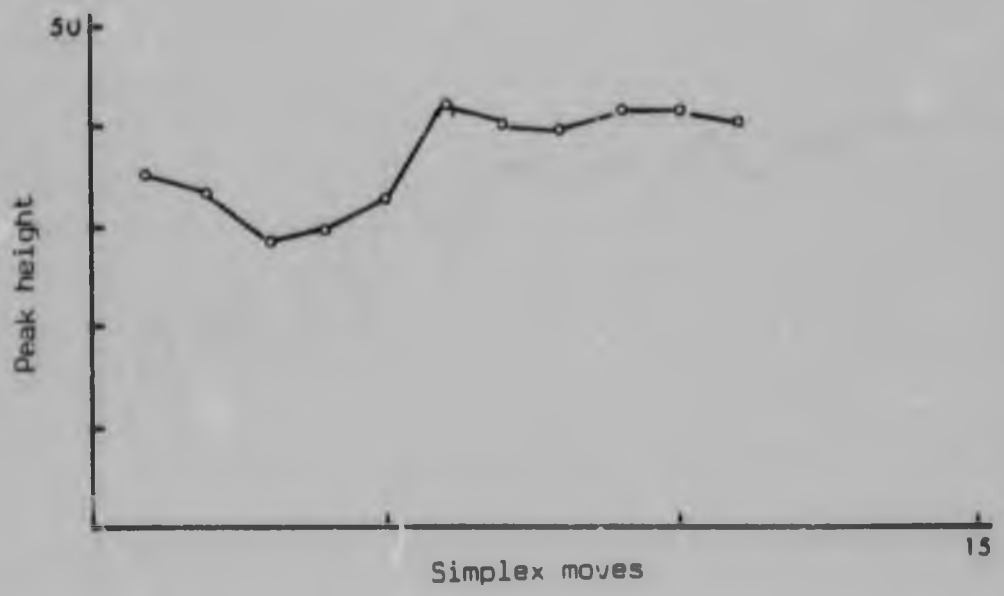


Figure 3.18 Optimization using a Modified Simplex approach with two variables

Conditions: Initial simplex and peak heights as in Table 3.3

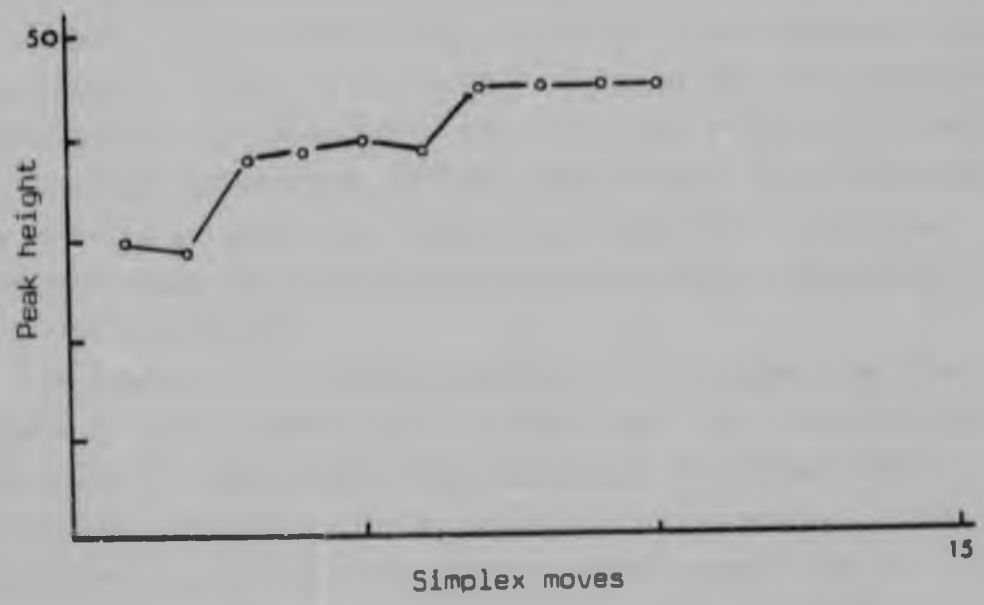


Figure 3.19 Optimization using a Modified Simplex approach with two variables

Conditions: Initial simplex and peak heights as in Table 3.4

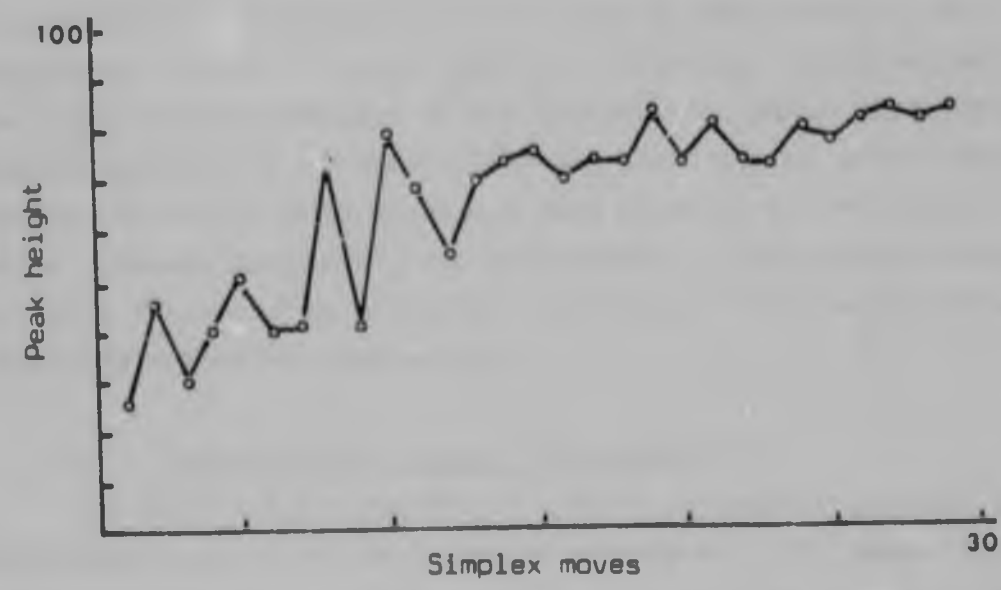


Figure 3.20 Optimization using a Modified Simplex approach with three variables

Conditions: Initial simplex and peak heights as in Table 3.5

within the ranges specified, single peaks give maximum peak height. The expected trend in peak shape from that of low double to high shouldered, to high single and then to low single with increasing dispersion is also observed in the univariate optimization results.

In this optimization, a fixed sample size of 50 μl was used. It was selected initially as a sample loop size for FIA because reasonable peak heights were obtained for samples containing 1 to 10 $mg.l^{-1}$ of uranium(VI).

In Tables 3.2 to 3.4, the flowrates in the final simplices were between 0.35 and 0.57 $ml.min^{-1}$ giving total flowrates of 0.7 and 1.14 $ml.min^{-1}$ respectively after merging of the bromo-PADAP stream with the buffer-complex solution carrier stream. The difference is not significant and an average total flow of 0.9 $ml.min^{-1}$ would be optimum (0.45 $ml.min^{-1}$ for both the buffer-complex and the bromo-PADAP streams).

The first simplex (Table 3.2) was started with coil lengths between 1 and 3 m and an optimum was obtained with a coil length of 2.3 m. The second simplex, (Table 3.3) starting with coil lengths between 3 and 5 m, gave an optimum with a coil length of 4 m whilst a third (Table 3.4) starting with a larger simplex i.e., a wider range of coil lengths of between 1 and 7 m gave an optimum with 4 m. The optimum obtained with a coil length of 2.3 m was, in all probability, the result of the formation of the initial 1:1 complex that forms between uranium(VI) and bromo-PADAP and which decays fairly rapidly whereas the optima obtained at 4 m were given by the more stable complex between uranium(VI) and bromo-PADAP. These optima produced the curve shown in Figure 3.6 for the effect of coil length using the univariate method of optimization.

(b) Three-Variable Simplex Optimization

In Table 3.5, the results of a three-variable (flowrate, coil length and sample size) optimization are shown. The peaks obtained from the first twenty vertices and the improvements made thereafter are shown in Figure 3.20. The procedure followed the same pattern as for the two-variable simplex and resulted in a further increase in sensitivity indicating that the 50 μl sample size used in the two-variable optimization was not optimal. The simplex moved

Table 3.5 Optimization using a Modified Simplex approach with three variables

Simplex Move	Vertex No.	Current Vertex points (ranked)	Violations	Type of simplex move	Flowrate $ml.min^{-1}$	Coil length m	Sample size $\mu\ell$	Peak height	SD	Opt. %
	1				1.50	1	50	20		24
	2				0.30	3	70	45		55
	3				0.90	5	40	29		35
1	4	2,4,3,1			0.60	7	60	36	10.60	44
2	5	2,4,3,5	BV	-C	1.05	3	55	25	8.77	30
3	6	2,6,4,3	BV	-C	0.83	4	55	45	7.76	55
4	7	2,6,4,7	BV	-C	0.74	5	50	30	7.35	37
	8	8,6,4,7		R	0.30	3	70	50*		61
5	9	8,6,9,4	BV	-C	0.66	4.5	55	40	5.14	49
	10			R	0.39	1	60	50		61
6	11	10,8,6,9	BV	E	0.58	-2.3	60*		4.27	
	12			R	0.49	0.5	65	40		49
7	13	10,8,9,6		-C	0.61	3.5	60	39	76.04	48
8	14	10,8,9,14	BV	-C	0.67	3.5	60	40	5.15	49
	15			R	0.36	2.5	66	74		90
9	16	15,10,8,9	BV	E	0.20	1.7	70*		14.71	
10	17	15,10,8,17	BV	-C	0.54	3.5	60	40	14.71	49
11	18	18,15,10,8	BV	-C	0.48	2.5	65	78	15.85	95
	19			R	0.65	1	55	49		60
12	20	18,15,20,10		+C	0.56	1.5	60	67	12.37	82
	21			R	0.34	3.5	65	53		65
13	22	18,15,22,20		+C	0.40	2.5	65	54	90.94	66
14	23	18,15,23,22	BV	-C	0.49	2	60	69	10.50	84
	24	24,15,23,22		R	0.48	2.5	65	79+		96
15	25	24,15,25,23		R	0.48	2	65	72	3.99	88
16	26	24,15,26,25		R	0.39	2.5	65	74	2.75	90
	27			R	0.34	3	65	57		69
17	28	24,15,25,26		-C	0.44	2	65	69	95.46	84
	29	29,15,25,24		R	0.48	2.5	65	80+		98
	30			R	0.49	2	60	70		85
18	31	29,15,31,25		+C	0.46	2	65	73	3.29	89
	32			R	0.39	3	65	53		65
19	33	29,15,25,31		-C	0.46	2	65	72	96.59	88
	34			R	0.41	2.5	65	80		98
20	35	35,29,15,25		E	0.39	2.5	65	82	4.62	100
	36			R	0.34	3	65	58		71
21	37	35,29,25,15		-C	0.44	2	65	72	98.96	88
22	38	35,38,29,25		R	0.53	2.5	65	80	4.37	98
	39			R	0.46	3	65	53		65
23	40	35,38,25,29		-C	0.47	2	65	72	100.09	88
	41	41,38,25,29		R	0.39	2.5	65	80+		98

Table 3.5 (continued)

Simplex Move	Vertex No.	Current Vertex Violations points (ranked)	Type of Simplex Move	Flowrate $ml.min^{-1}$	Coil length m	Sample size $\mu\ell$	Peak height	SD	Opt. %
	42		R	0.46	2	65	72		88
24	43	41,38,42,43	+C	0.44	2	65	71	100.41	87
25	44	41,38,44,42	R	0.44	2.5	65	78	4.03	95
	45		R	0.45	3	65	55		67
26	46	41,38,46,44	-C	0.46	2	65	76	102.02	93
	47	47,38,46,44	R	0.39	2.5	65	80+		98
	48		R	0.48	2	65	74		90
27	49	47,38,49,46	+C	0.47	2.5	65	80	2.10	98
	50		R	0.47	2.5	65	81		99
28	51	51,47,49,38	E	0.48	3	65	82	0.94	100
	52		R	0.35	2.5	65	78		95
29	53	51,47,38,49	-C	0.49	2.5	65	80	100.42	98
	54		R	0.47	3	65	80		98
30	55	51,55,47,38	+C	0.47	2.5	65	81	0.85	99

+ Vertex repeated n+1 times reevaluated and averaged; * failed expansion; C contraction; R reflection; E expansion; BV boundary violation; SD standard deviation; Opt optimization.

Conditions: Tube diameter 0.5mm; flow cell capacity 8$\mu\ell$; sample concentration 10mg.l^{-1} in sulphuric acid (10g.l^{-1}); 2% buffer-complex solution; 0.01% bromo-PADAP solution.

FINAL SIMPLEX

Flowrate 155 (0.47ml.min^{-1})
Coil length 2.5 m
Sample size 65 $\mu\ell$

towards the larger sample size of 65 µl.

In the three-variable optimization, the flowrate in the final simplex was 0.5 ml.min^{-1} and the coil length was 2.5 m. The initial complex between uranium(VI) and bromo-PADAP is more intense in colour at that point in time than the more stable complex which develops some time later. If the latter complex was given more time to develop than was the case in this FIA manifold, the colour would be more intense than the initial complex. However, a longer manifold even with slow flowrates, would result in a larger dispersion with correspondingly lower peak heights and the increase in absorbance of the stable complex would not be apparent.

3.7 Comparison of the Optimization Procedures

The parameters chosen for optimization by the univariate method were the coil length, flowrate and the concentrations of the bromo-PADAP and buffer solutions. The coil length and the concentrations of the reagent and buffer sulutions were optimized to provide maximum sensitivity. A fixed total flowrate of 1.8 ml.min^{-1} was chosen to give an acceptable compromise between sensitivity and sampling rate, and the sample size was chosen so as to give suitable sensitivity without double peaks.

It should be mentioned that the univariate procedure adopted was the commonly applied single cycle optimization.

For the simplex optimization procedure, the concentrations of the bromo-PADAP and buffer solutions were not varied. The concentration of bromo-PADAP was fixed at 0.1% as this gave the minimum interference from iron(III), an important consideration in the determination of uranium(VI) in plant solutions, and there is a relatively narrow pH range (8.5 to 9.5) for the development of the UO_2(bromo-PADAP)F complex[34].

The optima obtained by the MSM algorithm are improved over those obtained by the conventional univariate procedure where the optimization is terminated at the end of one cycle. In the MSM, a rapid initial improvement is observed until a peak or ridge is obtained and this is followed by a slower "tuning" stage corresponding to the contraction of the simplex on to the top of the peak or ridge. When operating at near optimum conditions, a

relatively large change in flowrate resulted in a smaller change in sensitivity than might be expected. Thus, using a faster flowrate, an improved sampling rate can be obtained while still keeping a satisfactory sensitivity.

There is a difference in speed of the univariate and the MSM methods which may be explained as follows. The MSM approaches the optimum by varying all the factors simultaneously and therefore zigzags along the line of highest gradient. The univariate method approaches the optimum by varying one factor at a time. In a system with n variables where k experiments are used and the whole process repeated r times, the number of experiments required in a univariate method is krn. Application of Pythagoras's theorem shows that a straight line ascending directly to the optimum (using the same step size) would need $\sqrt{n}$ to $kn^{1/2}$ experiments. A substantial improvement in speed can therefore be forecast for methods which vary several or all of the variables simultaneously. As the number of variables considered increases so is there a saving in the time required to achieve the optimum.

In the MSM, one trades off detailed investigation of individual experimental parameters in favour of reaching the optimum operating conditions in the minimum number of experiments. The univariate results show the variation in sensitivity obtained over a wider range than do the MSM results. In Figure 3.20, the data are represented in a series of "scatter diagrams", an unconventional method which nevertheless enables qualitative assessments to be made. The presence of interactions is likely to decrease the rate of climb since the optimization procedure may require that one or more of the variables should revert to earlier values. The peak height versus reaction coil length shows such behavior as do the simplex data. As can been seen from the scatter diagrams and the Tables, the optimum reaction coil length of 2.5 m and flowrate of the carrier and reagent streams of 0.45 and 0.5 $ml.min^{-1}$ for the univariate and MSM optimization procedures respectively were in agreement. The optimum coil length of 4 m obtained by the univariate method was a local optimum.

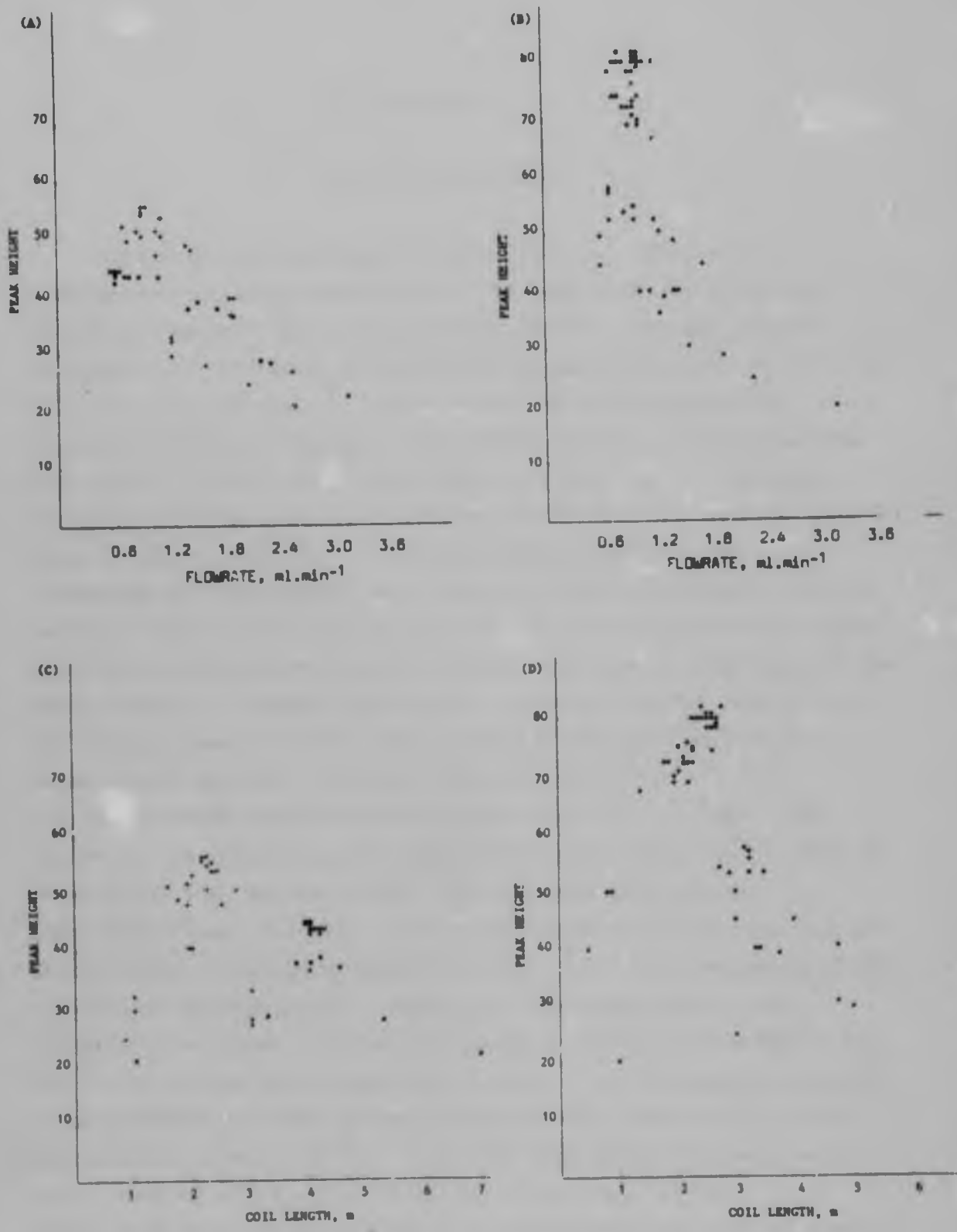


Figure 3.21 Scatter diagrams of peak heights vs. variable values for the Modified Simplex optimizations

Conditions: A and C, two-variable optimization; B and D, three-variable optimizations; initial simplexes as in Tables 3.2 to 3.5.

CHAPTER 4

INTERFERENCE STUDIES

The principal advantage of bromo-PADAP over PAR is its considerably improved sensitivity. It must rank among the most sensitive reagents known. The spectral data for the bromo-PADAP complexes with different elements determined at the optimum pH values are listed in Table 4.1. The measured spectra indicated the formation of single complexes with double maxima. The double peaks for cobalt(II) and zinc(II) are shown in Figure 4.1. The peak separation for the copper(II) complex is not as well resolved as the other complexes shown[34]. A general observation from the comparison of the spectral data (Table 4.2) of bromo-PADAP, PAR and o-PAP is that the more electronegative the substitution in the 'para' position on the benzene ring the higher the molar absorptivity of the metal complex. Hammett substituent constants for the diethylamino and hydroxy groups in the 'para' positions are -0.70 and -0.37 respectively and that for the O^- group is -0.52[34].

Bromo-PADAP has the same chelating structure as PAR. The maxima of the complexes with bromo-PADAP occur over a wider range of wavelengths than the maxima with PAR and some simultaneous measurements are possible. For example cobalt(II) and zinc(II) can be determined simultaneously at a pH value of 2.8 by measuring at 590 and 520 nm respectively[34]. Cobalt can be determined in the presence of at least a fifty-fold excess of zinc(II), the Beer's Law plot being linear to at least this level. The improved sensitivity of bromo-PADAP over PAR for most elements is a factor of 2 and for bismuth(III) a factor of 5. The transition metal complexes have molar absorptivities of the order of 10^5 and many of the bromo-PADAP metal complexes are extractable enabling a far greater selectivity than with PAR, the complexes of which are usually charged and non-extractable.

Since it is so general a reagent, the potential for interference is great and the selectivity is the key to its application. In this investigation, the selectivity of the method for the determination of

Table 4.1 Spectral Data of metal-bromo-PADAP complexes

Metal ion	pH*	Absorption max. nm A	B	Molar absorptivity 10^4 l.mole^{-1}.cm^{-1} A	B	Absorbance ratio A/B	Mole ratio M:L
Mn(II)	10	525	560	8.8	8.8	1.00	1:2
Fe(II)	8	523	557	6.6	8.2	0.81	1:2
Co(II)	8	554	588	8.7	9.3	0.97	1:2
Ni(II)	8	526	559	9.8	11.7	0.88	1:2
Zn(II)	8	522	553	11.6	13.3	0.87	1:2
Cu(II)	8	NR+	560	--	11.6	--	1:2
Fe(III)	8	542	594	7.2	8.2	0.88	--
Eu(III)	8	536	568	5.3	5.5	0.96	--
Zr(IV)	4.8	544	580	2.4	3.1	0.79	--
V(V)	8	NR+	600	--	6.0	--	--
U(VI).F	8	546	578.5	5.5	7.3	0.76	1:1
U(VI).OH	8	547	580	4.9	6.4	0.77	1:1
U(VI)	4	552	586	4.5	5.6	0.77	1:1

* pH for maximum absorbance

+ NR - not resolved

Note. Justification for visually estimating peaks is demonstrated by a computer analysis of a spectrum by using a curve-resolution program. There is no difference between the visually estimated peak separation and the computed value

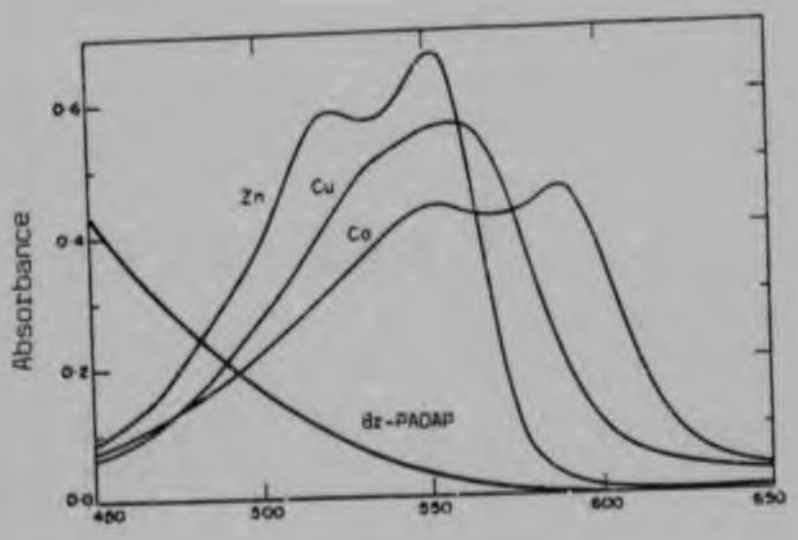


Figure 4.1 Spectra of bromo-PADAP complexes of zinc, copper, and cobalt

Conditions: 1×10^{-5} M bromo-PADAP; 2×10^{-4} M metal; solution pH 8

Table 4.2 Comparative spectral data for complexes of bromo-PADAP, PAR AND o-PAP

Metal	bromo-PADAP		PAR		o-PAP	
	ε, 10^4 l.mole^{-1}.cm^{-1}	λ_{max} nm	ε, 10^4 l.mole^{-1}.cm^{-1}	λ_{max} nm	ε, 10^4 l.mole^{-1}.cm^{-1}	λ_{max} nm
Cu(II)	11.6	560	5.89	510	1.98	547
Ni(II)	11.7	559	7.3	494	2.26	543
Co(II)	9.3	558	5.6	510	1.28	533
Zn(II)	13.3	553	6.34	495	2.30	520
Mn(II)	8.80	560	-	-	-	-
U(VI)	7.3	578	3.85	530	-	-
Bi(III)	5.8*	590	1.07	515	-	-
V(V)	6.0	600	3.6	550	-	-

* Reference 32

* " 34

Table 4.2 Comparative spectral data for complexes of bromo-PADAP, PAR AND o-PAP

	bromo-PADAP		PAR		o-PAP	
Metal	ε, 10^4 l.mole^{-1}.cm^{-1}	λ_{max} nm	ε, 10^4 l.mole^{-1}.cm^{-1}	λ_{max} nm	ε, 10^4 l.mole^{-1}.cm^{-1}	λ_{max} nm
Cu(II)	11.6	560	5.89	510	1.98	547
Ni(II)	11.7	559	7.3	494	2.26	543
Co(II)	9.3	558	5.6	510	1.28	533
Zn(II)	13.3	553	6.34	495	2.30	520
Mn(II)	8.80	560	-	-	-	-
U(VI)	7.3	578	3.85	530	-	-
Bi(III)	5.8*	590	1.07	515	-	-
V(V)	6.0	600	3.6	550	-	-

* Reference 32

+ " 34

uranium(VI) was established with respect to mineral acids and selected ions. The acids included hydrochloric, sulphuric, nitric, perchloric and phosphoric. The elements, listed in Table 4.3, included those that could be present in a leach solution.

4.1 Interferences in the FIA Determination of Uranium(VI)

4.1.1 Apparatus and Reagents

The manifold shown in Figure 3.1 was used. The carrier solution was the buffer-complex solution (2 per cent) and the reagent solution was 0.01 per cent bromo-PADAP in 60 per cent ethanol. Solutions of the interferent elements were made by dissolving the appropriate amount of the metal salt in water.

4.1.2 Procedure

Increasing amounts of the inorganic acids and the interferent elements were individually added to the uranium standard (10 $mg.l^{-1}$) and the effect on the FIA determination of uranium was established.

4.1.3 Results and Discussion

(a) Effect of Acids

In the FIA system, the presence of the buffer in the carrier stream maintained the pH level (8.5 to 9.5) required for the development of the UO_2(bromo-PADAP$^-$)F complex when the concentration of inorganic acids (such as hydrochloric, sulphuric, nitric, perchloric and phosphoric acids) in the injected sample was 30 $g.l^{-1}$ or less. When the effect of these acids was tested it was observed that, with the exception of phosphoric acid, they all initially enhanced the peak height (Figure 4.2) but increasing amounts progessively decreased the peak heights to varying degrees dependant upon the particular acid. Because the pH value was maintained at approximately the same level by the buffer it was assumed that these effects were mainly caused by the various anions. At levels beyond those shown as the maximum tested for the individual acids, double peaks developed because the buffer concentration was too low to maintain the pH value required for maximum colour

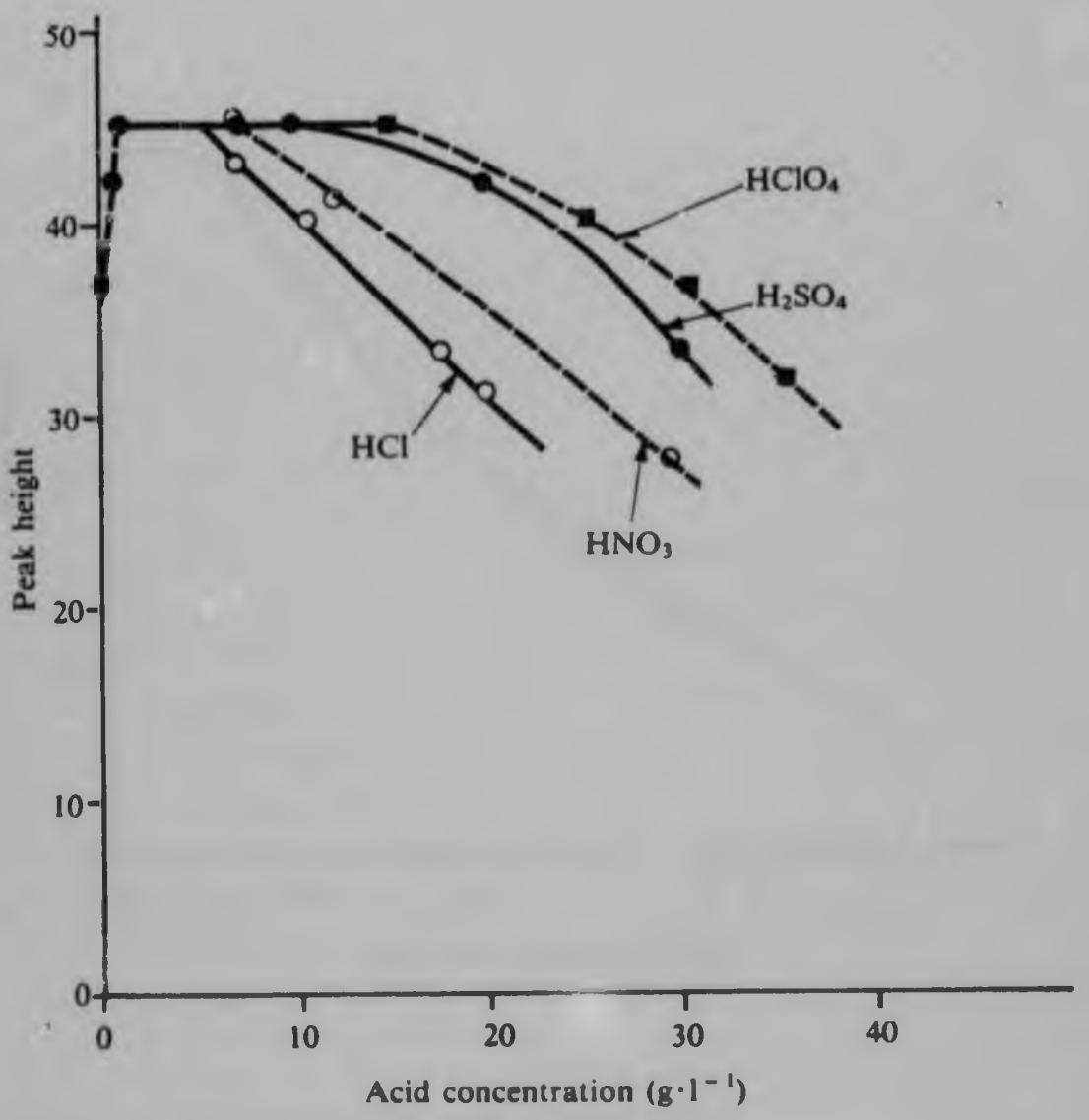


Figure 4.2 Interference from inorganic acids

Conditions: 2% buffer-complex solution; 0.01% bromo-PADAP; sample size 50$\mu\ell$; sample concentration 10mg.l^{-1}; coil length 4m; flowrate 0.9ml.min^{-1}

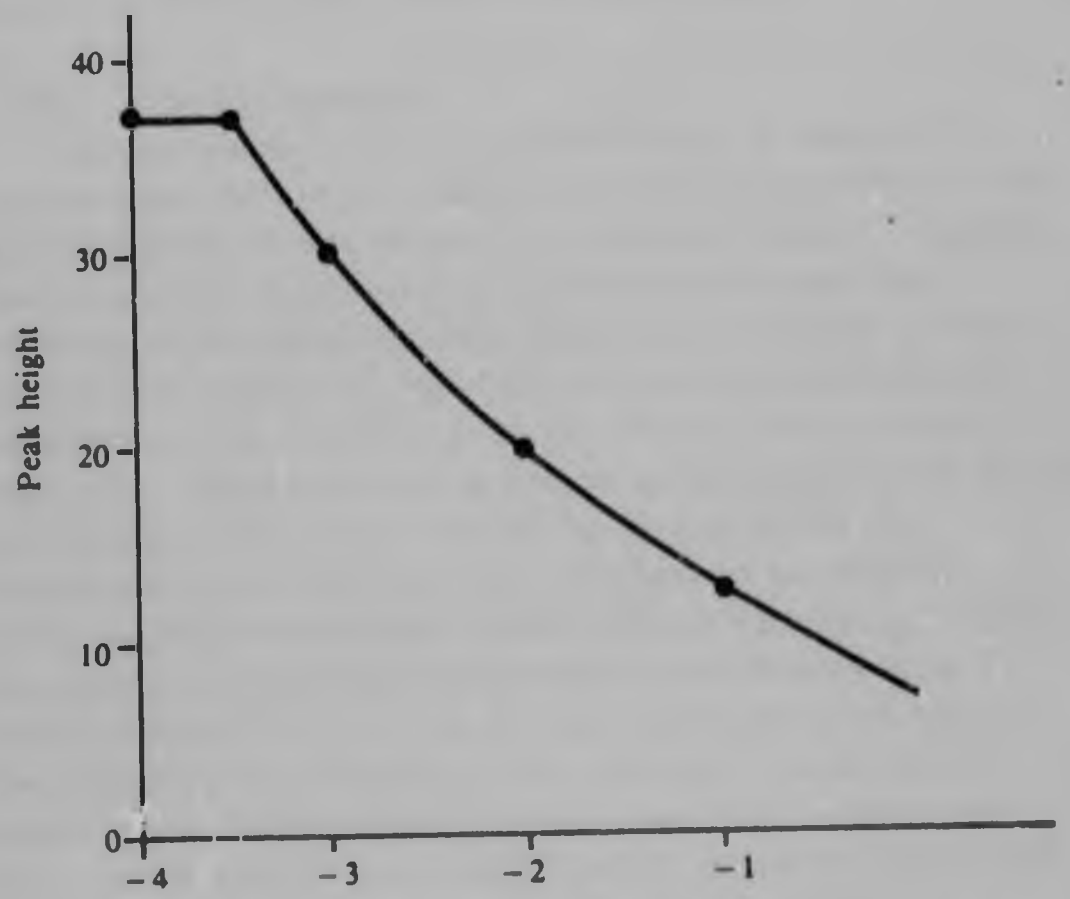


Figure 4.3 Response vs log H_3PO_4 concentration
(Concentration in $g.l^{-1}$)

Conditions: 2% buffer-complex solution; 0.01% bromo-PADAP; sample size, 50μl; sample concentration, 10 $mg.l^{-1}$; coil length, 4m; flowrate, 0.9 $ml.min^{-1}$.

development. The presence of trace amounts (1 $mg.l^{-1}$) of phosphoric acid inhibited the development of the coloured complex UO_2(bromo-PADAP$^-$)F as shown in Figure 4.3.

Solutions in which uranium(VI) is to be determined must be free of phosphate ions and the concentration of chloride, nitrate, sulphate and/or perchlorate anions should not exceed 30 $g.l^{-1}$.

(b) Effect of Elements

Leach solutions in which the determination of uranium(VI) is required would contain the commonly occurring element iron(III) and hence the effect of this element is an important factor. Elements such as iron(III) form a complex with bromo-PADAP under the conditions of the method and make a positive contribution to the absorbance at 578 nm[37]. The effect of varying concentrations of bromo-PADAP on the interference of iron(II) and (III) is shown in Figure 4.4. Uranium(VI) can be determined in solutions with an iron concentration of $< 1.5\ g.l^{-1}$ by the use of bromo-PADAP at concentrations of < 0.01 per cent. The optimum bromo-PADAP concentration was established as 0.08 per cent (Section 3.5.1.(e)) when sensitivity alone was concerned and it was found that at a concentration of 0.01 per cent the peak height was 94 per cent of that obtained with the 0.08 per cent solution. However at a concentration of 0.01 per cent for the bromo-PADAP solution, the tolerance for iron(II) and iron(III) was significantly greater than at 0.08 percent with only a slight reduction in sensitivity. Consequently a concentration of 0.01 per cent was used in the subsequent interference studies.

The selectivity of the method was investigated by the determination of uranium(VI) at a concentration of 10 $mg.l^{-1}$ in the presence of varying amounts of different ions, examined individually. An ion was considered not to interfere if it caused a change of less than 2 per cent in the absorbance obtained for uranium(VI) alone. The effects of the elements on the determination of uranium(VI) are shown in Figures 4.5(a) to (d).

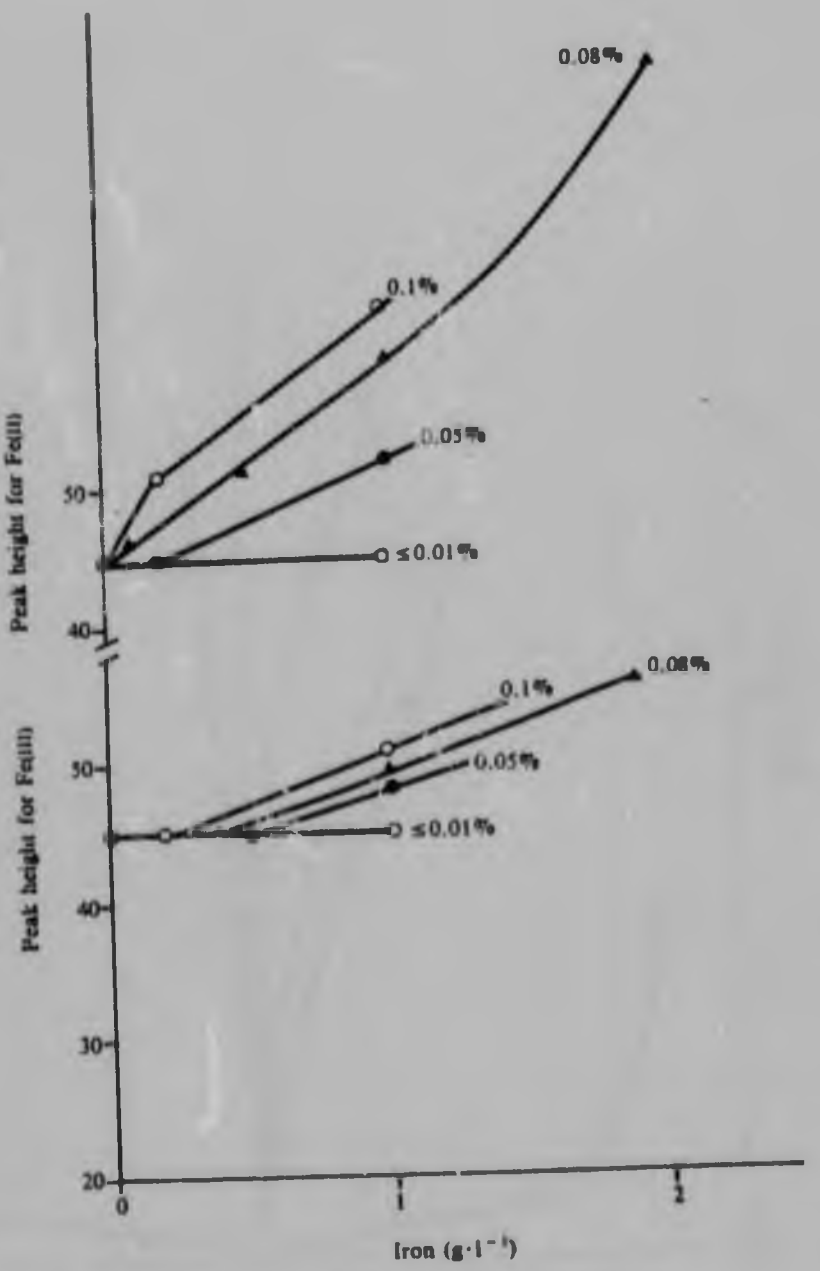


Figure 4.4 Effect of bromo-PADAP concentration on iron interference

Conditions: 2% buffer-complex solution; sample size 50µℓ; sample concentration 10mg.l^{-1} in sulphuric acid (10g.l^{-1}); coil length 4m; flowrate 0.9ml.min^{-1}

Figure 4.5(a)

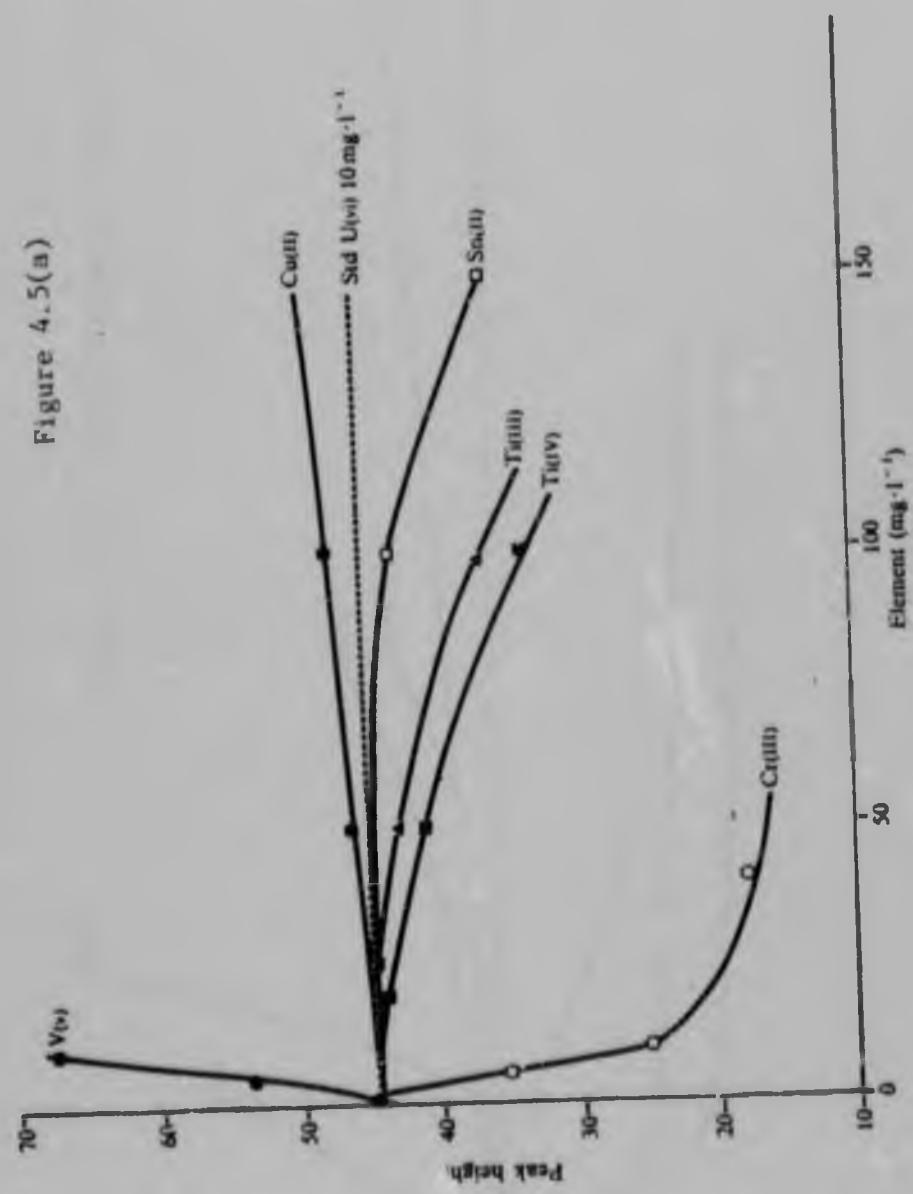
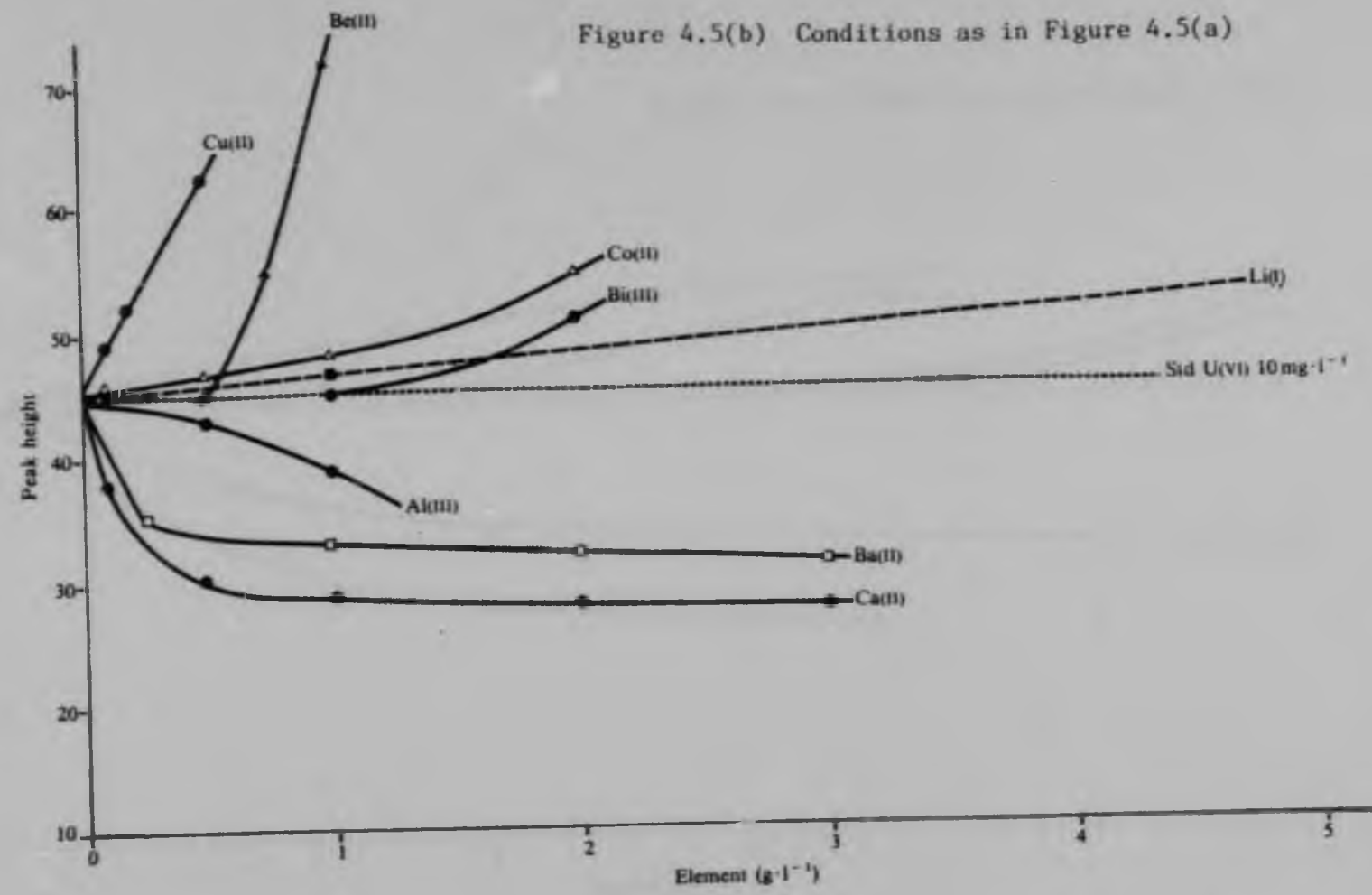


Figure 4.5 Interferences in direct bromo-PADAP method

Conditions: 2% buffer-complex solution; 0.01% bromo-PADAP; sample size 50µℓ; sample concentration 10mg.l^{-1} in sulphuric acid (10g.l^{-1}); coil length 4m; flowrate 0.9ml.min^{-1}

Figure 4.5(b) Conditions as in Figure 4.5(a)



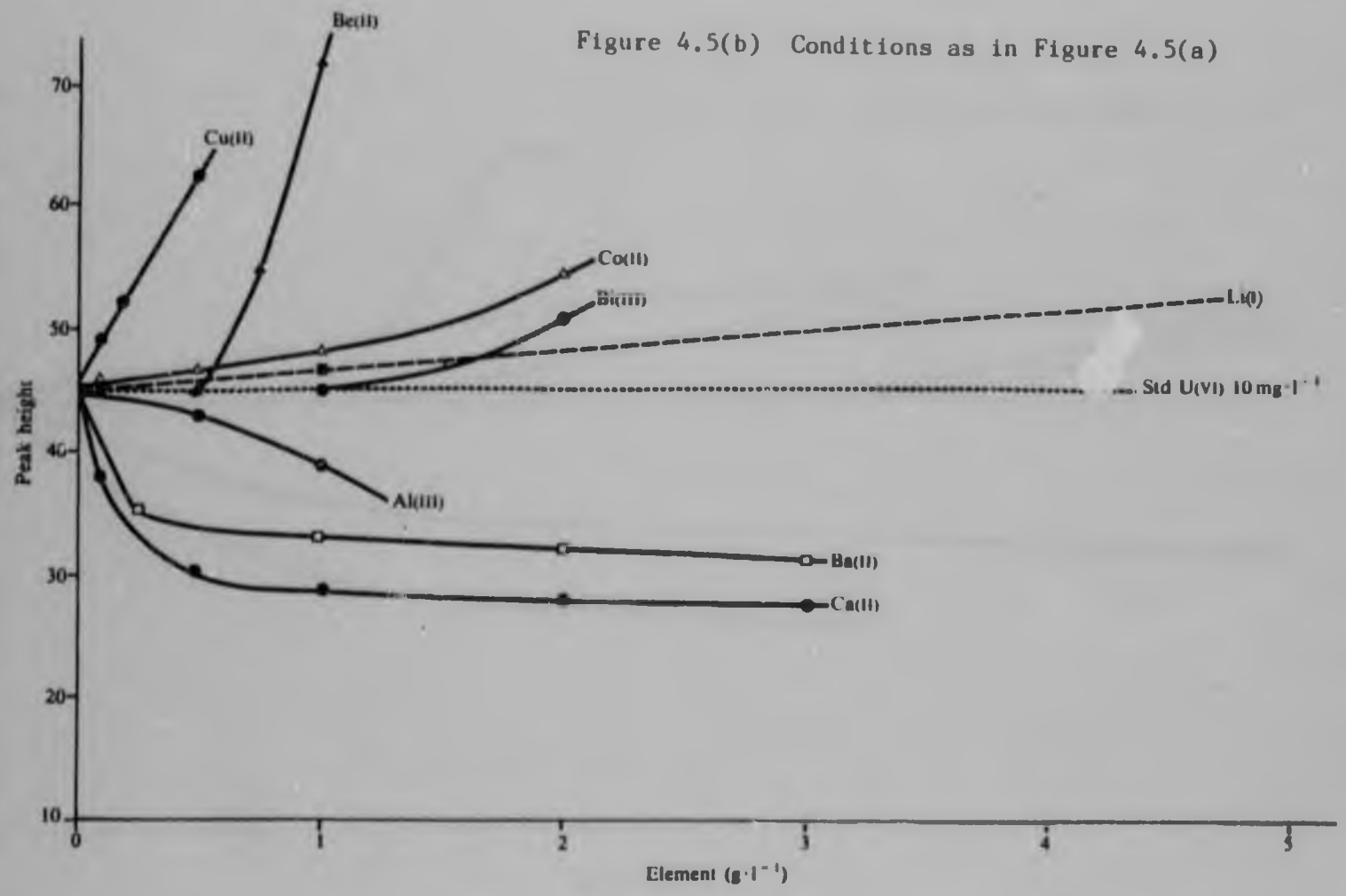


Figure 4.5(b) Conditions as in Figure 4.5(a)

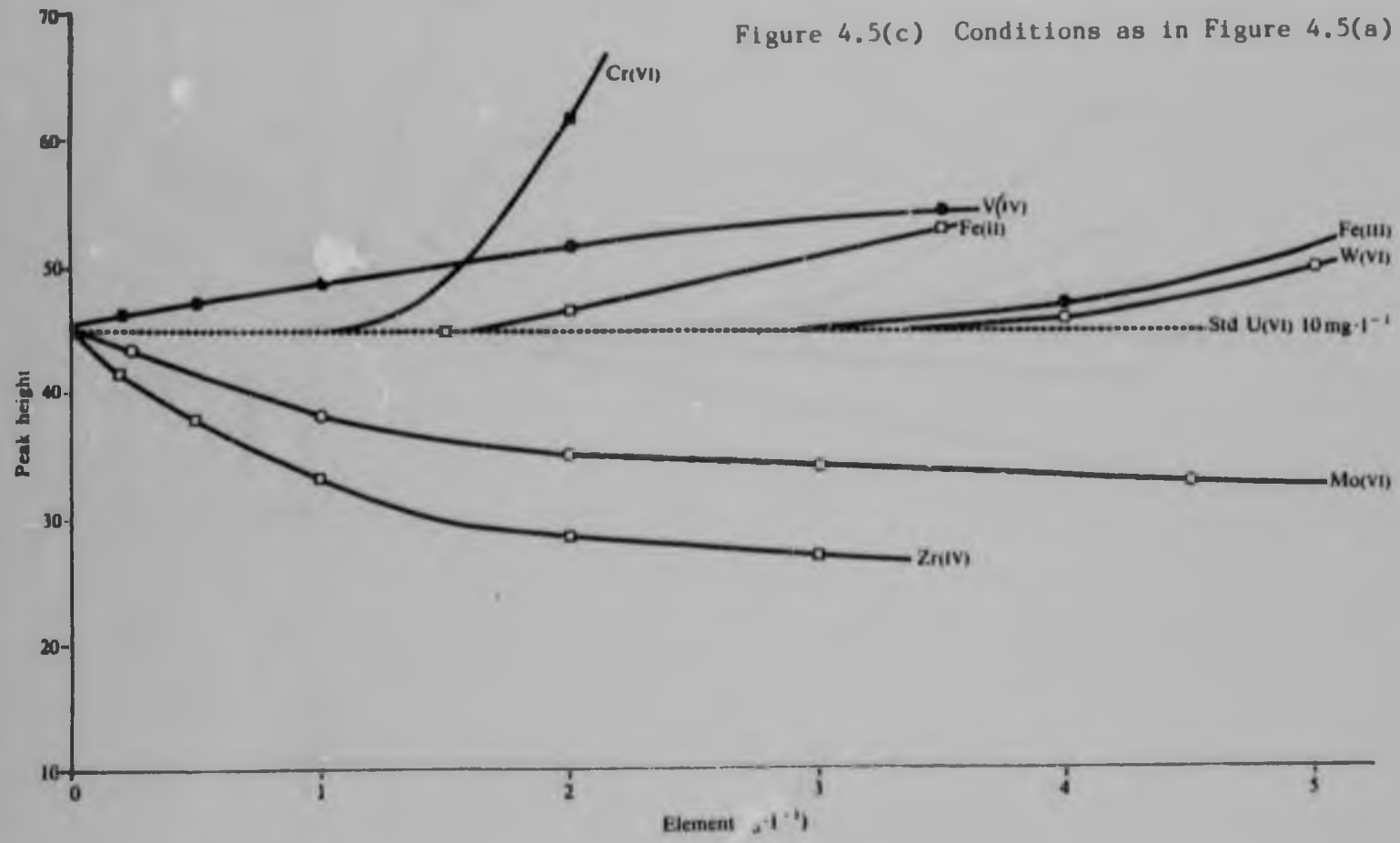


Figure 4.5(c) Conditions as in Figure 4.5(a)

Figure 4.5(d) Conditions as in Figure 4.5(a)

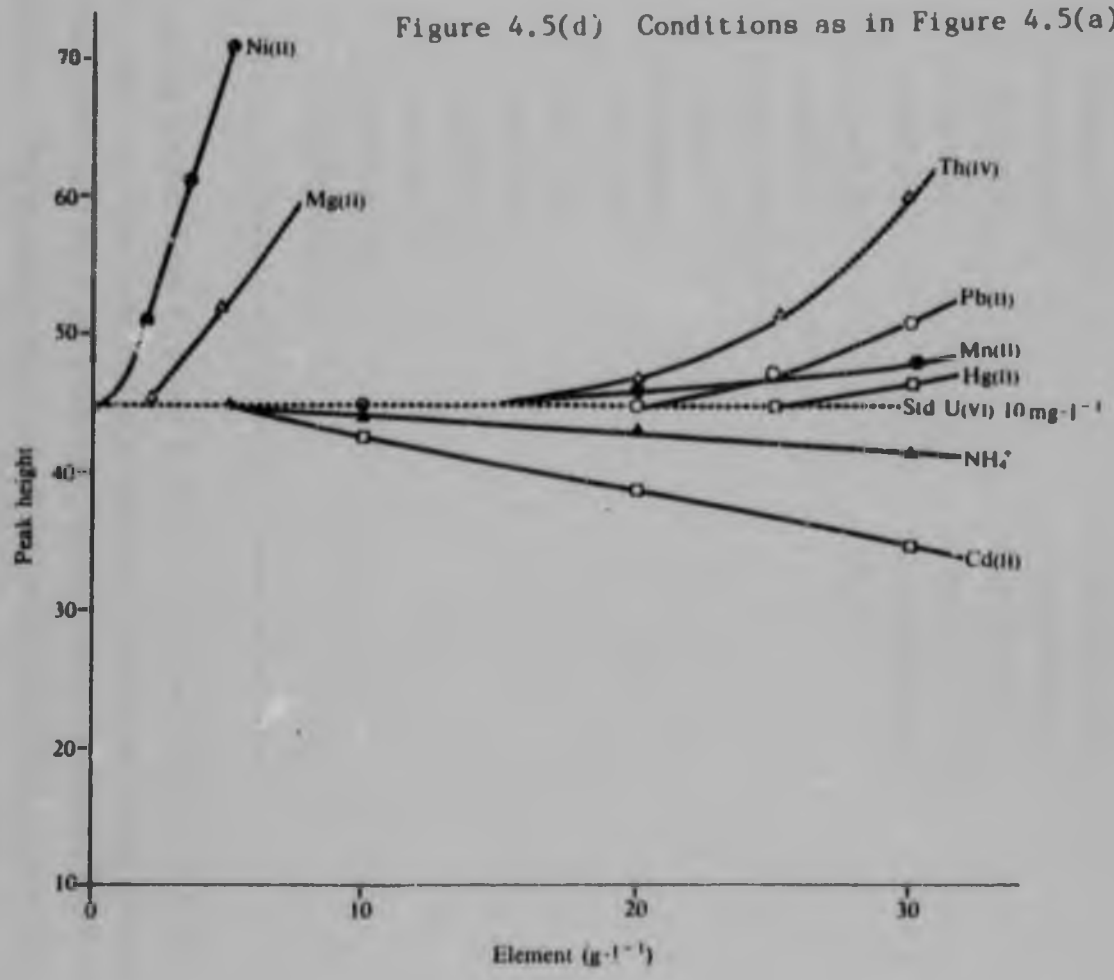


Table 4.3 Elemental interferences

Enhancement	Depression
Lithium(I)	Tin(II)
Sodium(I)	Cadmium(II)
Beryllium(II)	Chromium(III)
Magnesium(II)	Aluminium(III)
Calcium(II)	Titanium(III)
Barium(II)	Titanium(IV)
Copper(II)	Zirconium(IV)
Cobalt(II)	Molybdenum(VI)
Nickel(II)	NH_4^+
Lead(II)	
Manganese(II)	
Mercury(II)	
Bismuth(III)	
Iron(II)	
Iron(III)	
Thorium(IV)	
Vanadium(IV)	
Vanadium(V)	
Chromium(VI)	
Tungsten(VI)	

It would appear from Figures 4.5(a) to (d) and Table 4.3 that elements that have positive redox potentials form a coloured complex with bromo-PADAP and have an enhancing effect on the determination of uranium(VI). The elements with negative redox potentials generally have a depressing effect on the determination of uranium(VI). Elements with more than one oxidation state have an enhancing or a depressing effect on the determination depending on the redox potential of the particular oxidation state present as shown by chromium. A general observation from the interference studies is that bromo-PADAP can be used for the spectrophotometric determination of elements with positive redox potentials.

The concentrations of elements that can be tolerated in the determination of 10 $mg.l^{-1}$ of uranium(VI) are shown in Table 4.4.

Table 4.4 Tolerance limits of interfering elements in bromo-PADAP method

⩽2 $mg.l^{-1}$	⩽1 $g.l^{-1}$	⩽2 $g.l^{-1}$
Arsenic(V) *	Cobalt(II)	Aluminium(III)
Beryllium(II)	Vanadium(IV)	Bismuth(III)
Chromium(III)	Zirconium(IV)	Cadmium(II)
Copper(II)		Chromium(VI)
Silica(IV) *		Lead(II)
Tin(II)		Lithium(II)
Titanium(III)		Magnesium(II)
Titanium(IV)		Manganese(II)
Vanadium(V)		Mercury(II)
		Molybdenum(VI)
		NH_4^+
		Nickel(II)
		Thorium(VI)
		Tungsten(VI)

* From reference 33

Cook[42] investigated the interference of several elements. In the presence of aluminium(III) ions, the tolerance for arsenic(V) ions and phosphoric acid anions is higher. In the presence of aluminium(III) at a concentration of 0.12 $g.l^{-1}$, arsenic (V) at a concentration of 0.04 $g.l^{-1}$ does not cause an interference of more than 3 per cent and, according to Cook, in the presence of 0.04 $g.l^{-1}$ of aluminium(III), a phosphoric acid anion content of 0.02 $g.l^{-1}$ does not interfere to an extent greater than 2 per

cent with uranium(VI) at 1 $mg.l^{-1}$. A positive interference is given by vanadium(V) at a concentration of 0.04 $g.l^{-1}$, but the addition of iron(II) at 0.4 $g.l^{-1}$ reduces this interference to about 1 per cent. The interference of calcium(II) and magnesium(II) is as a result of the insolubility of their sulphates in ethanol. In the absence of sulphuric acid the interferences are greatly reduced and uranium(VI) was determined in the presence of these elements at concentrations of $\leq$ 20 $g.l^{-1}$.

Compounds such as EDTA and CDTA form complexes with some elements and prevent their interference in the determination of uranium(VI). CDTA forms metal complexes that are generally more stable than the corresponding complexes formed by EDTA[27]. The tolerance levels for many of the metal ions can be increased by the addition of more CDTA as masking agent but its concentration must not exceed 0.067 $g.l^{-1}$ in the carrier stream since it also forms a complex with uranium and low results are obtained[27]. The presence of fluoride in the complexing reagent solution not only enhances the intensity of the absorption of the UO_2(bromo-PADAP$^-$)F complex but also forms complexes with zirconium and titanium increasing the tolerance of the method to these metals[33,37].

4.2 Analysis of a Synthetic Leach Solution

As plant leach solutions were not available, uranium was determined in a synthetic leach solution by the proposed procedure. The accuracy and precision were established by replicate analyses. The solution contained 10 $mg.l^{-1}$ of uranium(VI) and the following elements at the concentrations indicated (in $g.l^{-1}$): iron(LII) 1.5, aluminium(III) 1, nickel(II) 0.2, copper(II) 0.2, manganese(II) 2, calcium(II) 2, magnesium(II) 1 and nitric acid 5. This solution is similiar in composition to that obtained from the leaching of a low-grade ore with nitric acid.

The mean of twelve replicate determinations for uranium(VI) in this solution by the proposed FIA scheme was 10.1 $mg.l^{-1}$ with a relative standard deviation of 0.019. The recorder output for the uranium(VI) standards and the synthetic leach solution is shown in Figure 4.6. The calibration curves are shown in Figure 4.7. The

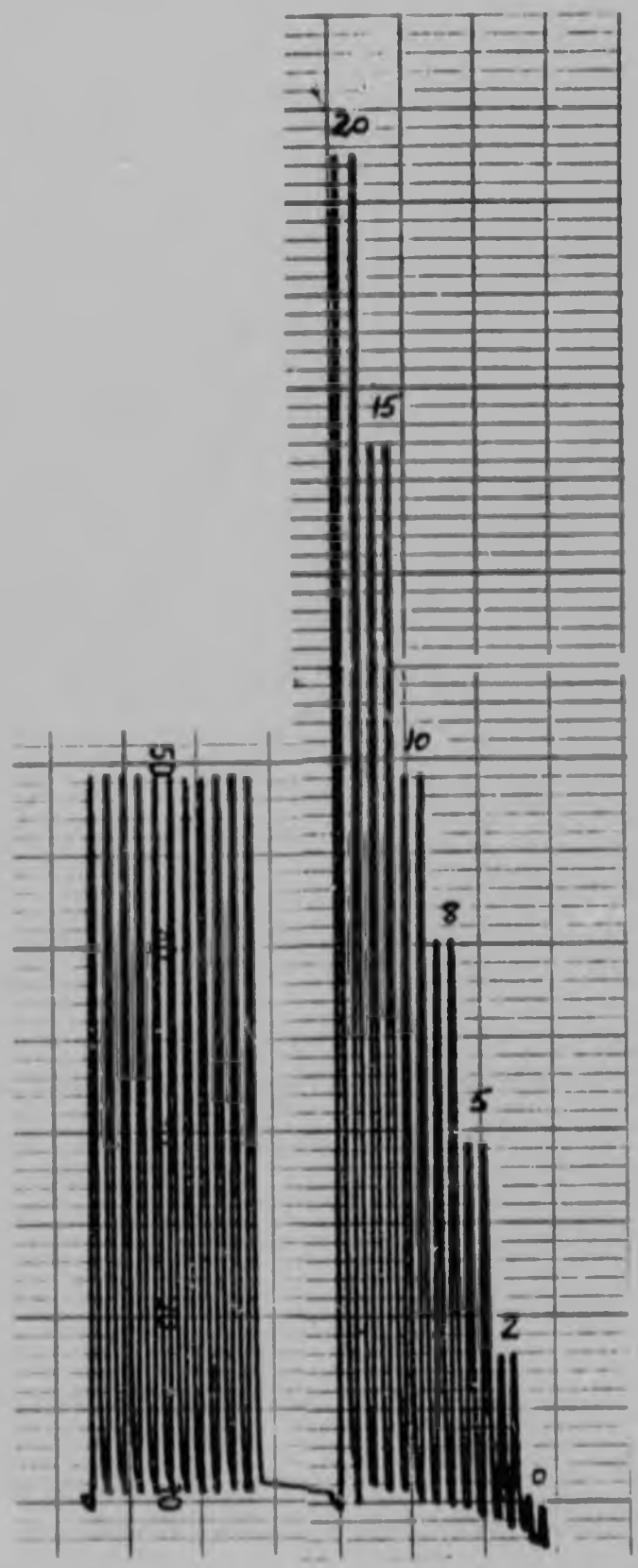


Figure 4.6 Recorder output for RSD of uranium (V1)

Conditions: 2% buffer-complex solution; 0.01% bromo-PADAP; sample size 50μℓ; coil length 4m; flowrate 0.9ml.min^{-1}; chart speed 2mm.min^{-1}; spectrophotometer sensitivity range 0.64; peak numerals represent mg.l^{-1} of uranium (V1) in sulphuric acid (10g.l^{-1})

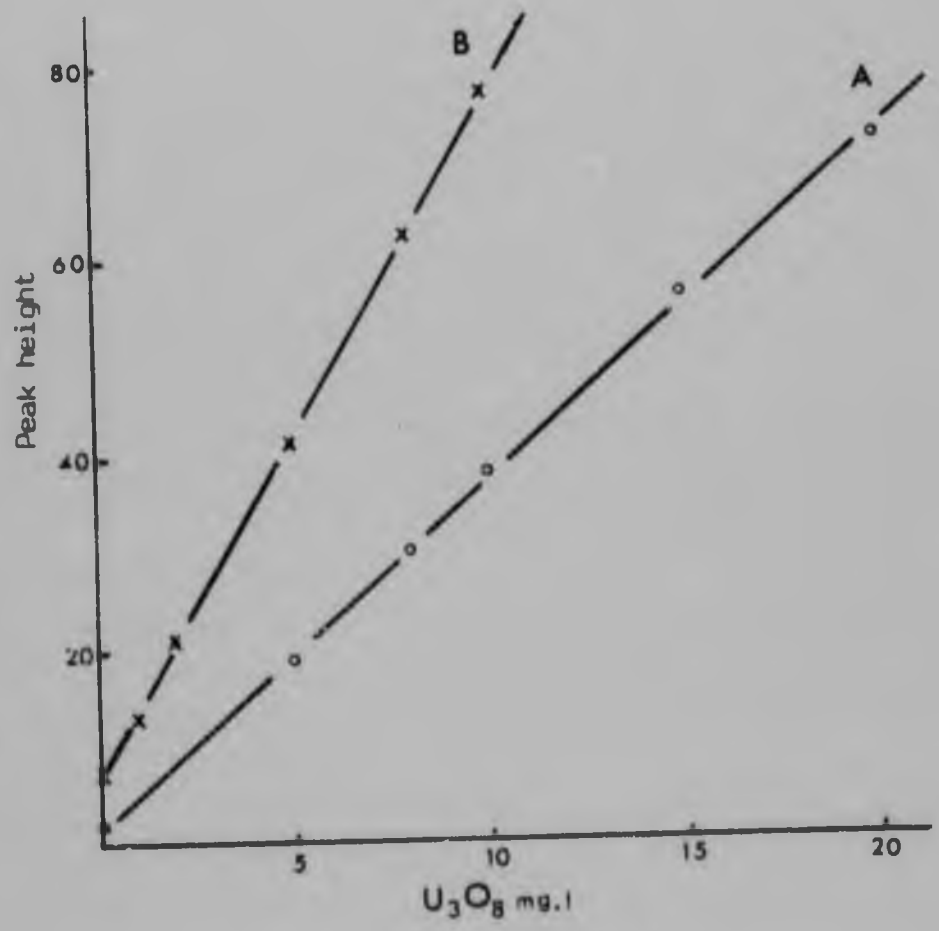


Figure 4.7 Calibration curves for U_3O_8

Conditions: 2% buffer-complex solution; 0.01% bromo-PADAP; sample volume, 50µl; coil length, 4m; flowrate, 0.9ml.min^{-1}, concentration H_2SO_4 10g.l^{-1}; sensitivity range of recorder, 0.64 for A, 0.32 for B

levels of the elements in the synthetic solution were such that they did not interfer in the determination of uranium under the conditions employed in the method.

CHAPTER 5

CONCLUSION

Flow injection analysis was used for the direct determination of uranium(VI) using a simple manifold consisting of a carrier stream of a buffer-complex solution (ethanolamine and CDTA) and merging the reagent solution (bromo-PADAP) with the sample solution after injection. The FIA procedure is based on the spectrophotometric measurement at 578 nm of the UO_2(bromo-PADAP)F complex after reaction of the uranyl ion (UO_2^{2+}) with bromo-PADAP at a pH value of 8.6 in the presence of fluoride.

The manifold used in this investigation was less complicated than those by previous investigators[40,41]. Lynch et al.[40] incorporated a liquid-liquid separation procedure into their experimental system thereby necessitating the removal of an organic phase prior to colour development. Silfwerbrand-Lindh et al.[41] made use of packed beds to mix the aqueous and ethanolic streams and thereby overcame viscosity effects. In the present study, the buffer was prepared in 60 per cent ethanolic solution and viscosity effects were obviated without the use of the more complicated manifold. In addition to mechanical and chemical considerations, a further aim of the present study was to design an analytical system which would be suitable for on-line plant process monitoring. Obviously, the more complicated the system the greater the possibility of encountering problems with both computer control and robustness in a non-laboratory environment. With these aspects as major considerations, a single system is to be preferred but a limiting factor could have been the reduction in analytical sensitivity using the simple system. However, when this aspect was investigated, a limit of determination of 0.5 mg l^{-1} was established which is the same as previously published data[40,41].

The physical parameters of the manifold such as the length of tubing between the injection and detection points and the flowrate have been optimized by both univariate and simplex methods, and the sample size by a simplex method. The chemical parameters of pH

value of the buffer solution and bromo-PADAP concentration were maintained at levels found to be optimum for the determination of uranium(VI) in the presence of elements that form complexes with bromo-PADAP. The univariate method approaches the optimum by altering one variable at a time whereas in the simplex method all the parameters are varied simultaneously. A rapid initial improvement is observed followed by a slower "tuning" stage corresponding to the contraction of the simplex onto the optimum. Potential applications of the simplex method in analytical chemistry are unlimited. The inherent simplicity of the method makes otherwise difficult experimental optimizations more attractive.

In this investigation, both the univariate and simplex methods of optimization gave optima at a coil length of 4 m which probably measures the more stable comple[illegible]romo-PADAP)- that developes relatively slowly. [illegible]plex method gave optima at 2.3 m (2-variable) and 2.5 m (3-variable) which probably measures the initial complex that forms between uranium(VI) and bromo-PADAP and decays fairly rapidly. The precise timing of FIA allows either the initial unstable complex or the more stable complex that develops later to be measured depending on the sensitivity and rate of sampling required.

The interference caused by many commonly occurring elements and the effects of mineral acids were studied and their tolerance levels under optimum conditions were established. The relative standard deviation obtained on a synthetic leach solution containing several elements and uranium(VI) at the 10 $mg.l^{-1}$ level was 0.019. The calibration curve was linear over the range 0.2 to 20 $mg.l^{-1}$. Increased sensitivity is obtained with lower flowrates as the dispersion is kept low and the colour of the UO_2(bromo-PADAP)F complex developes relatively slowly.

The method can be automated to measure uranium(VI) in acid leach solutions or waste waters, the rate of analysis depending on the flowrate of the carrier and reagent solutions. This rate is directly proportional to the flowrate and ranges from 16 to 180 samples per hour for flowrates of 0.3 and 5.4 $ml.min^{-1}$ respectively. The sampling rate under optimum conditions is up to 40 samples per hour.

REFERENCES

1. PALEI, P.N. Analytical chemistry of uranium. London, Ann Arbor-Humphrey Science Publishers. 1970.

2. KOLTOFF, I.M., and ELVING, P,J. Treatise on analytical chemistry. Part II. Analytical chemistry of the elements. vol.9. New York, Interscience Publishers. 1962. pp.1-188.

3. CORDFUNKE, E.H.P. Chemistry of uranium including its applications in nuclear technology. Amsterdam, Elsevier Publishing Company. 1969. pp.1-20.

4. KATZ, J.J., and RABINOWITCH, E. The chemistry of uranium. Part I. The element, its binary and related compounds. New York, McGraw-Hill Book Company, Inc. 1951.

5. SKEGGS, L.T. An automatic method for colorimetric analysis. Am.J.Clin.Pathol. vol.28. 1957. pp.311-322.

6. RUZICKA, J., and HANSEN, E.H. Flow injection analysis. Part I. A new concept of fast continuous flow analysis. Anal.Chim.Acta. vol.7[illegible]. 1975. pp.145-157.

7. STEWART, K.K., BEECHER, G.R., and HARE, P.E. Rapid analysis of discrete samples: The use of nonsegmented, continuous flow. Anal.Biochem. vol.70. 1976. pp.167-173.

8. STEWART, K.K. Flow injection analysis. A review of earlier history. Talanta. vol.28. 1981. pp.789-797.

9. GOTO, M. Monitoring of environmental water using continuous flow. Tr.Anal.Chem. vol.2. 1983. pp.92-94.

10. RANGER, C.B. Flow injection analysis: A new approach to near-real-time process monitoring. Anal.Proc. Con. vol.1. 1982. pp.39-67.

11. STEWART, K.K. Flow injection analysis. New tool for old assays. New approach to analytical measurements. Anal.Chem. vol.55. 1983. pp.931A-935A.

12. VAN DER LINDEN, W.E. Flow injection analysis; the manipulation of dispersion. Tr.Anal.Chem. vol.1. 1982. pp.188-191.

13. RUZICKA, J., and HANSEN, E.H. Flow injection analysis. Part X. Theory, techniques and trends. Anal.Chim.Acta. vol.99. 1978. pp.37-76.

14. RUZICKA, J., and HANSEN, E.H. Flow injection analysis, principles, applications and trends. Anal.Chim.Acta. vol.114. 1980. pp.19-44.

15. FRITZ, J.S., and SCHENK, G.H. Quantitative analytical chemistry. 3rd edition. Boston, Allyn and Bacon Inc. 1976. pp.69-106.

16. ANDERSON, R.G., and NICKLESS, G. Heterocyclic azo dyestuffs in analytical chemistry. Analyst. vol.92. 1967. pp.207-238.

17. SAVVIN, S.B. Analytical [illegible]ications of arsenazo III. The mechanism of complex formation between arsenazo III and certain elements. Talanta. vol.11. 1964. pp.7-19.

18. GUSEV, S.I., and SHCHUROVA, L.M. Pyridylazo compounds as metallochromic indicators. Comm.I. 5-(2-pyridylazo)-2-monoethylaminoparacresol as as analytical reagent. J.Anal.Chem.USSR. vol.19. 1964. pp.743-745.

19. GUSEV, S.I., and SHCHUROVA, L.M. Pyridylazo compounds as metallochromic indicators. Comm.II. Complexometric determination of bismuth in the presence of 5-(2-pyridylazo)-2-monoethylaminoparacresol as indicator. J.Anal.Chem.USSR. vol.19. 1964. pp. 898-901.

20. GUSEV, S.I., and NIKOLAEVA, E.M. A study of pyridylazo compounds as reagents for indium. Comm.III. Complexometric and spectrophotometric determination of indium with brominated pyridylazoaminocresol derivatives. J.Anal.Chem.USSR. vol.21. 1966. pp.1053-1058.

21. ANDERSON, R.G., and NICKLESS, G. Metal complexes of some azo and azomethine dyestuffs. Part III. Metal complexes of 2-(2-pyridylazo)phenol and 4-(2-pyridylazo)phenol. Anal.Chim.Acta. vol.39. 1967. pp.469-477.

22. GUSEV, S.I., and NICKOLAEVA, E.M. A study of pyridylazo compounds as reagents for indium. Comm.II. Complexometric and photometric determination of indium with pyridylazoaminophenols. J.Anal.Chem.USSR. vol.21. 1966. pp.248-254.

23. GUSEV, S.I., and NICKOLAEVA, E.M. A study of pyridylazo compounds as reagents for indium. Comm.I. Complexometeric and extraction-photometric determination of indium with 2-(2-pyridylazo)-4-naphthol. J.Anal.Chem.USSR. vol.21. 1966. pp.147-152.

24. GEARY, W.J., NICKLESS, G., and POLLARD, F.H. The metal complexes of some azo dyes and azomethine dyestuffs. Part I. Spectra in water, and in dioxan/water in the wavelength range 320-600mu. Anal.Chim.Acta. vol.26. 1962. pp.575-582.

25. SOMMER, L., IVANOV, V.M., and NOVOTNA, H. The reaction of uranyl ions with 4-(2-pyridylazo)rescorcinol. Talanta. vol.14. 1967. pp.329-343.

26. SAVVIN, S.B., GROBOV, L.A., and LEBEDEV, V.L., and LIKHONINA, E.A. Electronic structure of azo compounds and their complexes with the elements. Comm.10. Study by the Huckel simple MO LCAO method of the ionic states of 4-(2-pyridylazo)-rescorcinol and its lanthanum complexes. J.Anal.Chem.USSR. vol.26. 1971. pp.1884-1894.

27. FLORENCE, T.M., and FARRAR,Y. Spectrophotometric determination of uranium with 4-(2-pyridylazo)rescorcinol. Anal.Chem. vol.35. 1963. pp.1613-1616.

28. SHIBATA, S., FURUKAWA, M., and TOEI, K. Synthesis and spectrophotometric studies of azo dyes containing m-dimethylaminophenol as analytical reagents. Anal.Chim.Acta. vol.66. 1973. pp.397-409.

29. FLORENCE, T.M., JOHNSON, D.A., and FARRAR, Y. Spectrophotometric determination of uranium(VI) with 2-(2-pyridylazo)-5-dimethylaminophenol. Anal.Chem. vol.41. 1969. pp.1652-1654.

30. FLORENCE, T.M., and FARRAR, Y. Rapid spectrophotometric determination of uranium in ores. Anal.Chem. vol.42. pp.271-273.

31. GUSEV, S.I., and SHALAMOVA, G.G. Pyridylazodiethylaminophenols as reagents for determining vanadium(V). J.Anal.Chem.USSR. vol23. 1968. pp.591-595.

32. GUSEV,S.I., and SHCHUROVA, L.M. Pyridylazo compounds as metallochromic indicators. Comm. 3. New azo compounds of the pyridine series and their use as indicators for the complexometric determination of bismuth. J.Anal.Chem.USSR. vol.21. 1966. pp.927-933.

33. JOHNSON, D.A., and FLORENCE, T.M. Spectrophotometric determination of uranium(VI) with 2-(5-bromo-2-pyridylazo)-5-diethylaminophenol. Anal.Chim.Acta. vol.53. 1971. pp.73-79

34. JOHNSON, D.A., and FLORENCE, T.M. A study of some pyridylazo dyestuffs as chromogenic reagents and the elucidation of the nature of their metal complex spectra. Talanta. vol.22. 1975. pp.253-265.

35. PALKANS, P., and MCALLISTER, B.R. Spectrophotometric determination of uranium in selective organic extractants with 2-(5-bromo-2-pyridylazo)-5-diethylaminophenol. Anal.Chim.Acta. vol62. 1972. pp.207-209.

36. PALKANS, P. Spectrophotometric determination of uranium in ores after decomposition in a Teflon pressure bomb. Anal.Chim.Acta. vol.69. 1974. pp.211-215.

37. LYLE, S.J., and TAMIZI, M. A study of the direct spectro photometric determination of uranium(VI) in trialkylamine extracts with 2-(5-bromo-2-pyridylazo)-5-diethylaminophenol. Anal.Chim.Acta. vol.108. 1979. pp.267-275.

38. LYLE, S.J., and TAMIZI, M. An automatic spectrophotometric method for the determination of uranium(VI) extracted into a liquid-exchanger medium. Anal.Chim.Acta. vol.121. 1980. pp.341-344.

39. HUNG, S., QU, C., and WU, S. Spectrophotometric determination of uranium (VI) with 2-(3,5-dibromo-2-pyridylazo)-5-diethylaminophenol in the presence of an ionic surfactant. Talanta. vol.29. 1982. pp.629-631.

40. LYNCH, T.P., TAYLOR, A.F., and WILSON, J.N. Fully automatic flow injection system for the determination of uranium at trace levels in ore leachates. Analyst. vol.108. 1983 pp.470-475.

41. SILFWERBRAND-LINDH, C., NORD, L., DANIELSSON, L., and INGMAN, F. The analysis of aqueous solutions with ethanol-soluble reagents in a flow injection system. Spectrophotometric determination of uranium. Anal.Chim.Acta. vol.160. 1984. pp.11-19.

42. COOK, E.B.T. The determination of acid soluble uranium in silicate ores and solutions. Randburg, Council for Mineral Technology, Report 1841. July 1976. 4pp.

43. ROUTH, M.W., SWARTZ, P.A., and DENTON, M.B. Performance of the super modified simplex. Anal.Chem. vol.49. pp.1422-1428.

44. MORGAN, S.L., and DEMMING, S.N. Simplex optimization of analytical chemical methods. Anal.Chem. vol.46. pp.1170-1181.

45. RYAN, P.B., BARR, R.L., and TODD, H.D. Simplex techniques for nonlinear optimization. Anal.Chem. vol.52. pp.1460-1467

46. SPENDLEY, W., HEXT, G.R., and HIMSWORTH, F.R. Sequential application of simplex designs in optimization and evolutionary operation. Technometrics. vol.4. pp.441-461.

47. NELDER, J.A., and MEAD, R. A simplex method for function minimization. Comp.J. vol.7. 1965. pp.308-313.

48. DEMING, S.N., and MORGAN, S.L. Simplex optimization of variables in analytical chemistry. Anal.Chem. vol.45. 1973. pp.278A-283A.

49. BETTERIDGE, D., SLY, T.J., and WADE, A.P. Computer-assisted optimization for the flow injection analysis of isoprenaline. Anal.Chem. vol.55. 1983. pp.1292-1299.

50. RUZICKA, J. and HANSEN, E.H. Chemical Analysis. A series of monographs on analytical chemistry and its applications. Volume 62. Flow injection analysis. New York, Interscience Publishers. 1981

51. BETTERIDGE, D., and RUZICKA, J. The determination of glycerol in water by flow injection analysis - a novel way of measuring viscosity. Talanta vol.23. 1976. pp.409-410.

52. RUZICKA, J., HANSEN , E.H., MOSBAEK, H., and KRUG, F.J. Exchange of comments: Pumping pressure and reagent consumption in flow injection analysis. Anal.Chem. vol.49. 1977. pp.1858-1861.

53. VAN DEN BERG, J.H., DEELDER, R.S., and EGBERINK, H.G.M. Dispersion phenomena in reactors for flow analysis. Anal.Chim.Acta. vol.114. 1980. pp.91-104.

54. RANGER, C.B. Flow injection analysis. Principles, techniques, applications, designs. Anal.Chem. vol.53. 1981. pp.20A-32A.

55. VANDERSLICE, J.T., STEWART, K.K., ROSENFELD, A.G., and HIGGS, D.J. Laminar dispersion in flow-injection analysis. Talanta. vol.28. 1981. pp.11-18.

56. RUZICKA, J., HANSEN, E.H., and MOSBAEK, H. Flow injection analysis. Part IX. A new approach to continuous flow titrations. Anal.Chim.Acta. vol.92. 1977. pp.235-249.

57. HANSEN, E.H. Flow injection analysis: New analytical methods based on the use of potentiometric and spectrophotometric flow-through detectors. Anal.Proc. 1981. pp.261-263.

58. TYSON, J.F., and IDRIS, A.B. Flow injection sample introduction for atomic absorption spectrometry: Applications of a simplified model for dispersion. Analyst. vol.106. 1981. pp.1125-1129.

59. GOLAY, M.J.E., and ATWOOD, J.G. Early phases of the dispersion of a sample injected in Poiseuille flow. J.Chromatog. vol.186. 1979. pp.353-370.

60. BETTERIDGE, D. Flow injection analysis. Anal.Chem. vol.50. 1978. pp.832A-846A.

61. REIJN, J.M., VAN DEN LINDEN, W.E., and POPPE, H. Transport phenomena in flow injection analysis with chemical reaction. Anal.Chim.Acta. vol.126. 1981. pp.1-13.

62. LEVENSPIEL, O. Chemical reactor engineering, 2nd ed. New York, John Wiley & Sons. Inc. 1972.

63. SNYDER, L.R. Reaction colorimeters as detectors in high performance liquid chromatography. Extra-column band broadening with segmented flow through the reaction coil. J.Chromatog. vol.125. 1976. pp.287-306.

64. SNYDER, L.R., LEVINE, J., STOY, R., and CONETTA, A. Automated chemical analysis: Update on continuous-flow approach Anal.Chem. vol.48. 1976. pp.942A-956A.

65. TIJSSEN, R. Axial dispersion and flow phenomena in helically coiled tubular reactors for flow analysis and chromatography. Anal.Chim.Acta. vol.114. 1980. pp.71-89.

66. PAINTON, C.C., and MOTTOLA, H.A. Chemical kinetic contributions to practical dispersion in flow injection analysis. Anal.Chem. vol.53. 1981. pp.1713-1715.

67. STEWART, J.W.B., and RUZICKA, J. Flow injection analysis Part.V. Simultaneous determination of nitrogen and phosphorus in acid digests of plant material with a single spectrophotometer. Anal.Chim.Acta. vol.82. 1976. pp.137-144.

68. TIJSSEN, R. Axial dispersion in helically coiled open columns for chromatography. Thesis, Delft, The Netherlands. 1979. p.62.

69. CARO, C.G. The dispersion of indicator flowing through simplified models of the circulation and its relevance to velocity profile in blood vessels. J.Physiol. vol.185. 1966. pp.501-519.

70. HOFMANN, K., and HALASZ, I. Mass transfer in ideal and geometrically deformed open tubes. 1. Ideal and coiled tubes with circular cross section. J.Chromatog. vol.173. 1979. pp.211-228.

71. REIJN, J.M., VAN DEN LINDEN, W.E., and POPPE, H. Dispersion in open tubes and tubes packed with large glass beads. Anal.Chim.Acta. vol.123. 1981. pp.229-237.

72. KARLBERG, B., JOHANSSON, P., and THELANDER, S. Extraction based on the flow-injection principle. Part 2. Determination of codeine as the picrate ion-pair in acetylsalicylic acid tablets. Anal. Chim. Acta. vol.104. 1979. pp.21-28.

73. KRUG, F.J., RUZICKA, J., and HANSEN, E.H. Determination of ammonia in low concentrations with Nessler's Reagent by flow injection analysis. Analyst. vol.104. 1979. pp.47-54.

74. FLASCHKA, H.A., abd BARNARD, A.J. Chelates in analytical chemistry. New York, Marcel Dekker Inc. 1972. pp.194-202.

75. PAINTON, C.C., and MOTTOLA, H.A. Kinectics in continuous flow sample processing. Chemical contributions to dispersion in flow-injection techniques. Anal.Chim.Acta. vol.158. 1384. pp.67-84

APPENDIX I

The Preparation of bromo-PADAP
[2-(5-bromo-2-pyridylazo)-5-diethylaminophenol]

1. OUTLINE OF METHOD

The method is a scaled up adaptation of that described by Johnson and Florence.[33] The preparation is conducted in three stages. Sodium 5-bromo-pyridyldiazotate is prepared by a diazotisation procedure carried out in an atmosphere of nitrogen under reflux conditions. This compound is coupled with m-diethylaminophenol under an atmosphere of carbon dioxide. The impure product is then recrystallised.

2. APPLICATION OF THE REAGENT

The reagent is applicable to the spectrophotometric determination of uranium in aqueous and organic media. The reagent is more sensitive and selective than 2-(2-pyridylazo)-5-diethyl-aminophenol (PADAP) in the determination of uranium.

3. REAGENTS

(1) Sodium amide (K and K Lab. Inc.)

(2) 2-amino-5-bromopyridine (Aldrich Chem. Co. Inc.)

(3) Iso-amyl nitrite (Riedel de Haen)

(4) m-diethylaminophenol (Aldrich Chem. Co. Inc.)

(5) Degassed benzene. Transfer 900 ml of A.R. benzene to a dry 1 litre volumetric flask. Pass nitrogen through the benzene for 1 hour. Stopper the flask. The degassed benzene is used for the diazotisation.

(6) Toluene (A.R.)

(7) Ethyl ether (A.R.)

(8) Ethanol (aerosol brand)

(9) Nitrogen gas (high purity)

(10) Carbon dioxide gas

4. APPARATUS

The apparatus is shown in Figure I-1. To assemble the apparatus proceed as follows:

(a) Place a flat bottomed 1 litre distillation flask (A), provided with a thermometer-sleeve (B), on a stirring hot-plate (C).

(b) Attach a dual adapter (D) to the flask and insert a pear-shaped funnel of 50 ml capacity (E) into the adapter as shown. The funnel should have a gas-inlet tube immediately below the tap through, which nitrogen can be passed.

(c) Connect a condenser (F) to the side arm of the adapter (D) and connect the top of the condenser to a length of tubing leading to the drainpipe of a sink.

5. PROCEDURE

5.1 Diazotization

(a) Remove the flask (A) and add 6 ml of toluene. Place the flask on a reagent balance and, without delay, add 6.24 g of sodium amide. (This reagent should be taken from a well-sealed bottle which should be immediately resealed).

(b) Transfer a magnetic paddle (45 mm) to the flask and place the flask on the stirring hot-plate. Fit the funnel (E) into place and start the flow of nitrogen.

(c) Transfer 27.68 g of 2-amino-5-bromopyridine to a dry 250 ml beaker. Add 80 ml of benzene, stir and pour the suspension into the distillation flask. Wash the beaker with successive portions of benzene and transfer the washings to the flask. A total volume of 680 ml of benzene should be added to the flask. Mark the level on the flask and adjust the nitrogen flow to 2 bubbles per second.

(d) Connect the condenser system and start the flow of cooling water. Introduce about 30 mm of water into the thermometer sleeve and insert a thermometer. Adjust the stirrer until the solid material is maintained in

suspension. Switch on the heating element and raise the temperature of the suspension to 40°C. Maintain this temperature (±2°C) for 40 minutes or more until evolution of ammonia has ceased. (Test the gas at the top of the condenser with moist litmus paper).

(e) Add, through the funnel (E), 18.72 g of iso-amyl nitrite and continue stirring for a further 90 minutes. Maintain the benzene volume by occasional increments of benzene added through the funnel (E).

(f) Filter the precipitated diazotate under vacuum on a 7 cm Whatman filter paper supported on a Buchner funnel. Wash the precipitate twice with 20 ml of ethyl ether. Place the paper and the precipitate onto a 15 cm cover glass. Dry in a vacuum oven at 40°C until no further loss in mass occurs when the cover glass and the contents are weighed on a reagent balance. (To assist the drying process, break up large lumps of material with a nickel spatula).

(g) Transfer the dried product to a weighed sample tube and close with a tight-fitting stopper.

5.2 Coupling

(a) The mass of coupling agent, m-diethylaminophenol, required is 0.7433 x the mass of sodium 5-bromo-2-pyridyldiazotate available. Transfer the required mass of the compound to a 500 ml beaker. Add 3 ml of ethanol per gram of the compound, introduce a gas delivery tube and a thermometer and place the beaker on a steam bath. Pass a fairly rapid stream of carbon dioxide through the solution and raise the temperature to 60°C (±5°C)

(b) Dilute 114 ml of ethanol with distilled water to 200 ml in a 250 ml beaker. Raise the temperature to 65°C. Transfer all the diazotate prepared to a dry 250 ml separating funnel and add 8 ml of the hot ethanol solution per gram of diazotate to the funnel. Shake to dissolve the compound and add to the coupling solution prepared as

described in Section 5.2(a). Pass carbon dioxide through the coupling solution during and after this addition until the ethanol has all evaporated. Maintain the temperature at 60°C (±5°C) during the evaporation procedure.

(c) Dissolve the oily residue in 10M hydrochloric acid (1.8 ml per gram of diazotate coupled). Pour the solution into a 2 litre beaker and wash the beaker with 5 x 100 ml portions of water, adding the washings to the 2 litre beaker. Dilute the solution to 1400 ml, stir and allow to stand overnight. Decant the solution through a 7 cm Whatman paper, supported on a Buchner funnel subjected to vacuum, while retaining the precipitate in the beaker. Place the beaker under an infrared lamp and heat until all the superficial water has evaporated. At the same time dry the Buchner funnel and paper in the vacuum oven at 80°C.

(d) Suspend the Buchner funnel over the beaker and pour 50 ml of hot (±60°C) ethanol on to the paper. Allow the ethanol to run down the sides of the beaker. Place the beaker on a hot plate and heat until most of the residue has dissolved. Pour the solution into a 250 ml graduated beaker and wash the paper and beaker with successive portions of hot ethanol. Do not exceed 100 ml (total volume).

5.3 Recrystallisation

(a) Evaporate the solution to between 45 and 50 ml. Add 50 ml of water, cool in ice and allow to stand overnight to recrystallise. Decant the supernatant liquor and wash the crystals with a volume of 1:1 ethanol equal to half that of the mother liquor and again decant the supernatant liqour. Finally wash the crystals twice with similar volumes of water and decant as before.

(b) Dry the crystals in the beaker under an infrared lamp until superficial moisture has been driven off. Finally dry the crystals in the beaker at 80°C in a vacuum

oven until no further condensation of moisture is evident on the window of the oven when the vacuum pump is disconnected. Transfer the crystals to a sealed glass container. The yield is between 5 and 7 g and the melting point 153-154°C.

6. ELEMENTAL ANALYSIS

Calculated: C 51.6%; H 4.9%; N 16.0%; O 4.6%; Br 22.9%.

Found: C 51.6%; H 4.9%; N 16.2%; O 4.9%; Br 22.4%.

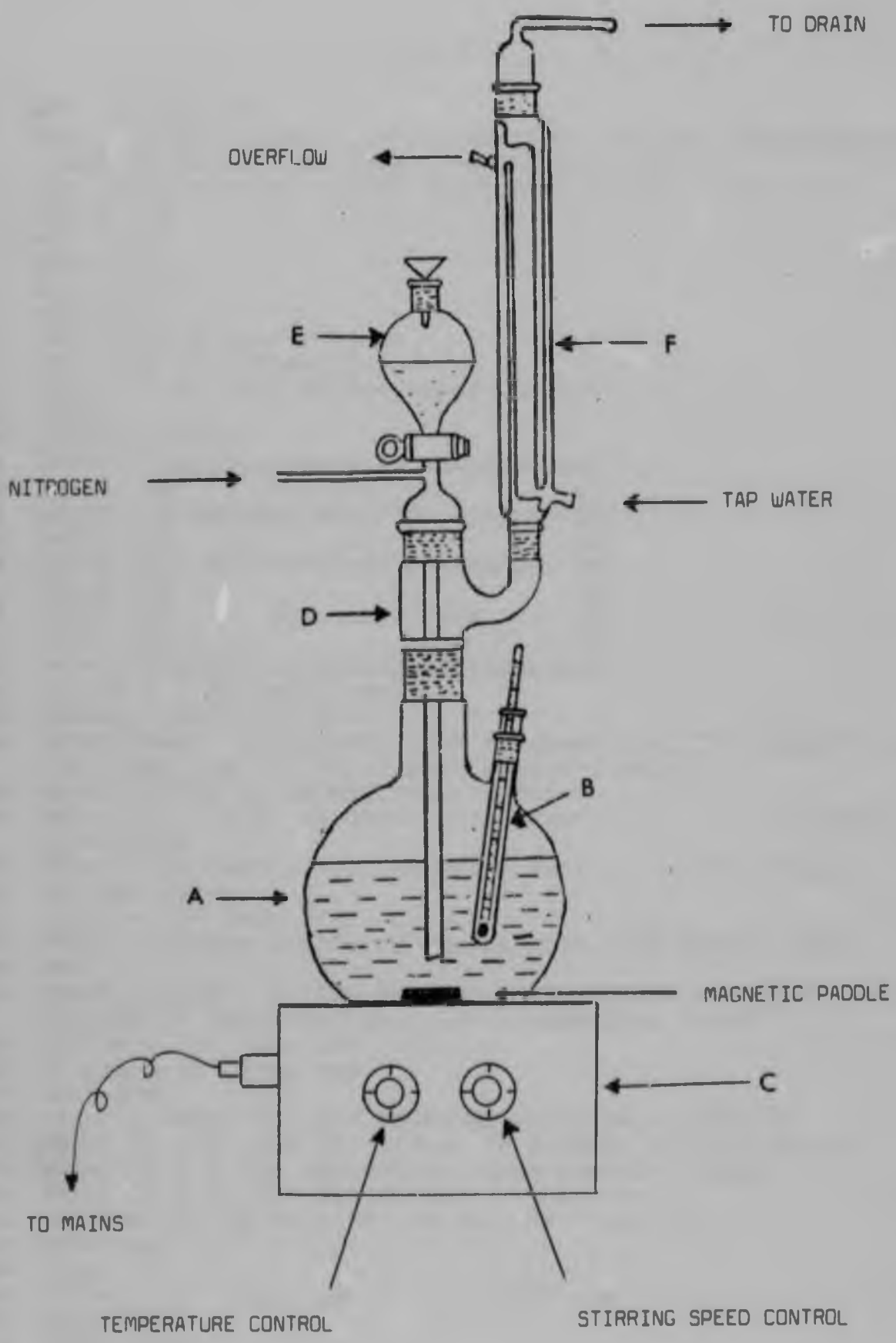


Figure I-1 The apparatus
(Diagrammatic - not to scale)

```
10  REM   GENMOD.PROG
20  REM    LOWER & UPPER LIMITS (BOUNDARY VALUES) OF VARIABLES
      MUST BE ENTERED AS DATA LINES, LINES 40-99
30  REM   PROG MUST BE LOADED ABOVE HGR2 USING GENMOD PROG
40  DATA 0.8,5
50  DATA 5,30
60  DATA 0,60
70  DATA 10,23
80  DATA -2,2
100  REM  MAX 20 ANALYT LINES
110  REM  MAX 10 VARIABLES
120  PRINT  CHR$ (4);"BLOADALPHABET,A$4000"
130  TEXT
140  HOME : INVERSE
150  PRINT "ØØØØØØØØØØØØØØØØØØØØØØØØØØØØØØ"
160  PRINT "ØØ                          ØØ"
170  PRINT "ØØ GENERAL MODIFIED SIMPLEX  ØØ"
180  PRINT "ØØ                          ØØ"
190  PRINT "ØØ  OPTIMIZATION PROGRAMME   ØØ"
200  PRINT "ØØ                          ØØ"
210  PRINT "ØØ       GLM-MARCH 1984     ØØ"
220  PRINT "ØØ                          ØØ"
230  PRINT "ØØØØØØØØØØØØØØØØØØØØØØØØØØØØØØ"
240  FOR PA = 1 TO 2000: NEXT
250  NORMAL : PRINT : PRINT
260  PRINT "HAVE YOU ENTERED YOUR BOUNDARY LIMITS": PRINT : PRINT
     "IN LINES  40 TO  99 AS DATA LINES?": PRINT
270  PRINT "(SAVE AS GENMOD.PROG)": PRINT
280  PRINT "     E.G. 10 DATA L,H": PRINT "          20 DATA L
     ,H": PRINT
290  PRINT "(L=LOWER LIMIT, H=UPPER LIMIT)    Y/N?": PRINT
300  GET Q$: PRINT
310  IF Q$ = "Y" THEN 340
320  PRINT "PROGRAM HALTED TO ENABLE DATA LINE ENTRY": END
330  END
340     'NT : PRINT "SWITCH PRINTER ON TO OBTAIN HARDCOPY": PRINT
        .CORD OF OPTIMIZATION?  Y/N";: GET Q3$: PRINT
350  IF Q3$ = "N" THEN 380
360  IF Q3$ = "Y" THEN 380
370  GOTO 340
380  PRINT : PRINT "SELECT RESPONSE FUNCTION -": PRINT
390  PRINT "[ S ]  FOR NET SIGNAL TO BACKGRD RATIO": PRINT
395  PRINT "[ I ] FOR IONIZATION INTERFERENCE": PRINT
400  PRINT "[ P ]  FOR NET SIGNAL";: INPUT R$
410  IF R$ = "S" OR R$ = "P" OR R$ = "I" THEN 430
420  GOTO 380
430  HOME
440  IF R$ = "P" THEN  LET PR = 1: GOTO 460
450  GOSUB 3430
460  GOSUB 3530
470  HOME
480  IF Q3$ = "Y" THEN  PRINT  CHR$ (4);"PR#1"
```

```
490  PRINT "GENERAL MODIFIED SIMPLEX OPTIMIZATION": PRINT "***
     **********************************"
500  POKE 34,2
510  PRINT : IF R$ = "S" THEN  PRINT "RESPONSE = NET SBR"
520  IF R$ = "P" THEN  PRINT "RESPONSE = NET SIGNAL": PRINT
530  HOME
540  PRINT "NO. OF VARIABLES (MAX. 10) = ";: INPUT N
550  IF N > 10 THEN  CALL  - 1959: GOTO 540
560  PRINT : PRINT "ENTER NAMES OF VARIABLE PARAMETERS:": PRINT

570  FOR J = 1 TO N
580  PRINT "                    *****************"
590  PRINT "VARIABLE NO. ";J;" ";: INPUT V$(J)
600  IF  LEN (V$(J)) > 16 THEN 590
610  NEXT J
620  HOME
630  VTAB 3
640  FOR J = 1 TO N STEP 2
650  PRINT J;"=";: HTAB 4: PRINT V$(J);: HTAB 21: PRINT J + 1;
     "=";: HTAB 24: PRINT V$(J + 1)
660  NEXT J
670  POKE 34,2.5 ^ N / 2
680  PRINT
690  PRINT : PRINT "BOUNDARY LIMITS": PRINT "***************":
      PRINT
700  FOR J = 1 TO N
710  READ L,H
720  PRINT "VARIABLE NO. ";J;"  ";V$(J);: HTAB 34: PRINT L;"
     ";H
730  NEXT J
740  RESTORE
750  PRINT
760  PRINT "NO. OF ANALYTICAL LINES (MAX. 20) = ";: INPUT M
770  PRINT
780  PRINT "IN CALCULATING A COMPOSITE RESPONSE A": PRINT : PRINT
     "WEIGHTING FUNCTION IS USED THAT PLACES": PRINT : PRINT "
     MORE WEIGHT ON THE LOWER RESPONSES.": PRINT
790  PRINT "(ENTER ZERO FOR NO WEIGHTING)": PRINT
800  PRINT "WEIGHTING POWER TO BE USED = ";: INPUT PW
810  DIM L(10),H(10),P1(10),V(10),V2(10),V3(10),V4(10),V5(10),
     S2(20),B2(20),W(100),R0(20),V1(10,10),W1(100,10),Y(100),Y
     A(100),X(100)
820  REM  SET BOUNDARY LIMITS FOR N VARIABLES
830  FOR I = 1 TO N
840  READ L(I),H(I)
850  NEXT I
860 T = 0
870  REM  SET UP INITIAL SIMPLEX
880  HOME
890  PRINT : PRINT "******* STARTING SIMPLEX *******": PRINT
900  PRINT "VERTEX NO.   VARIABLE NO.  VALUE"
910  PRINT
```

```
920  FOR J = 1 TO N + 1
930  FOR I = 1 TO N
940  PRINT J;"              ";I;
950  PRINT "              ";
960  INPUT V1(J,I)
970  NEXT I
980  GOSUB 3410
990  IF Q$ =  CHR$ (32) THEN 1020
1000  IF Q$ = "R" THEN 930
1010  GOTO 980
1020  GOSUB 1560
1030 R1(J) = R
1040  NEXT J
1050  PRINT : PRINT "RANK INITIAL VERTICES"
1060  GOSUB 1630
1070  GOSUB 3050
1080  GOSUB 3340
1090 C = 1
1100  GOSUB 1950
1110  PRINT
1120  PRINT "NEW VERTEX, STANDARD SIMPLEX"
1130  FOR I = 1 TO N
1140 V2(I) = V(I)
1150  PRINT V2(I);" ";
1160  NEXT I
1170  GOSUB 1870
1180  IF R =  - 100 THEN 2480
1190  GOSUB 1560
1200 R2 = R
1210  IF R2 > R1(1) THEN 2840
1220  IF R2 > R1(N) THEN 2780
1230  IF R2 > R1(N + 1) THEN 1380
1240 C =  - 0.5
1250  GOSUB 1950
1260  PRINT "NEW VERTEX, NEGATIVE CONTRACTION"
1270  FOR I = 1 TO N
1280  PRINT V(I);" ";
1290 V5(I) = V(I)
1300  NEXT I
1310  GOSUB 1560
1320 R5 = R
1330  IF R5 > R1(N + 1) THEN 2620
1340  PRINT "NEGATIVE CONTRACTION FAILED"
1350  PRINT "REJECT SECOND WORST VERTEX"
1360 R1(N) =  - 100 - T
1370  GOTO 1060
1380 C = 0.5
1390  GOSUB 1950
1400  PRINT "NEW VERTEX, POSITIVE CONTRACTION"
1410  FOR I = 1 TO N
1420 V4(I) = V(I)
1430  PRINT V(I);" ";
1440  NEXT I
1450  GOSUB 1560
1460 R4 = R
```

```
1470  IF R4 > R2 THEN 2700
1480  PRINT "POSITIVE CONTRACTION FAILED"
1490  PRINT "REJECT SECOND WORST VERTEX"
1500 R1(N) =  - 100 - T
1510  FOR I = 1 TO N
1520 V1(N + 1,I) = V2(I)
1530  NEXT I
1540 R1(N + 1) = R2
1550  GOTO 1060
1560  REM  RESPONSE CALC SUB
1570  IF R$ = "P" THEN  GOSUB 2270
1580  IF R$ = "S" THEN  GOSUB 2060
1590  PRINT "WEIGHTED RESPONSE (POWER ";PW;") = ";R
1600 YA(T) = R
1610  PRINT
1620  RETURN
1630  REM  SUB TO RANK AND PRINT
1640  PRINT "----------------------------------------"
1650  FOR K = 1 TO N
1660  FOR Z = K + 1 TO N + 1
1670  IF R1(K) =  > R1(Z) THEN 1760
1680 B = R1(K)
1690 R1(K) = R1(Z)
1700 R1(Z) = B
1710  FOR I = 1 TO N
1720 B1 = V1(K,I)
1730 V1(K,I) = V1(Z,I)
1740 V1(Z,I) = B1
1750  NEXT I
1760  NEXT Z
1770  NEXT K
1780  FOR J = 1 TO N + 1
1790  PRINT R1(J);" ";
1800  FOR I = 1 TO N
1810  IF I = 1 THEN  HTAB 8
1820  PRINT V1(J,I);" ";
1830  NEXT I
1840  PRINT
1850  NEXT J
1860  RETURN
1870  REM  BOUNDARY LIMITS
1880  FOR I = 1 TO N
1890  IF V(I) < L(I) THEN 1930
1900  IF V(I) > H(I) THEN 1930
1910  NEXT I
1920  GOTO 1940
1930 R =  - 100
1940  RETURN
1950  REM   SUB TO CALC NEW VERTICES
1960  FOR I = 1 TO N
1970 S = 0
1980  FOR J = 1 TO N
1990 S = S + V1(J,I)
2000  NEXT J
```

```
2010 P = S / N
2020 V(I) = P + C * (P - V1(N + 1,I))
2030 V(I) = ( INT (V(I) * PP + 0.5)) / PP
2040  NEXT I
2050  RETURN
2060  REM  SUB TO CALC NET SBR
2070 R9 = 0:W9 = 0
2080  FOR I = 1 TO M
2090  PRINT
2100  PRINT "  LINE    ";I;"    BACKGROUND, SIGNAL";
2110  INPUT B2(I),S2(I)
2120  IF S2(I) > B2(I) THEN 2140
2130 S2(I) = B2(I) + 0.01
2140 R0(I) = (S2(I) - B2(I)) / B2(I)
2150  PRINT "SIGNAL TO BACKGROUND RATIO = ";R0(I)
2160 W8 = (1 / R0(I)) ^ PW
2170 R9 = R9 + R0(I) * W8
2180 W9 = W9 + W8
2190  NEXT I
2200 R = R9 / W9
2210 R = ( INT ((R * PR) + 0.5)) / PR
2220  GOSUB 5410
2230  IF Q$ =  CHR$ (32) THEN 2260
2240  IF Q$ = "R" THEN 2060
2250  GOTO 2220
2260  RETURN
2270  REM  SUB TO CALC NET SIGNAL
2280 R9 = 0:W9 = 0
2290  FOR I = 1 TO M
2300  PRINT
2310  PRINT "  LINE    ";I;"    BACKGROUND, SIGNAL";
2320  INPUT B2(I),S2(I)
2330  IF S2(I) > B2(I) THEN 2350
2340 S2(I) = B2(I) + 0.01
2350 R0(I) = S2(I) - B2(I)
2360  PRINT "NET SIGNAL = ";R0(I)
2370 W8 = (1 / R0(I)) ^ PW
2380 R9 = R9 + R0(I) * W8
2390 W9 = W9 + W8
2400  NEXT I
2410 R = R9 / W9
2420 R =  INT (R + 0.5)
2430 GOSUB13000
2440  IF Q$ =  CHR$ (32) THEN 2470
2450  IF Q$ = "R" THEN 2270
2460  GOTO 2430
2470  RETURN
2480  PRINT : PRINT "BOUNDARY VIOLATION, STANDARD SIMPLEX"
2490 C =  - 0.5
2500  GOSUB 1950
2510  PRINT "NEW VERTEX, NEGATIVE CONTRACTION"
2520  FOR I = 1 TO N
2530  PRINT V(I);" ";
2540 V1(N + 1,I) = V(I)
2550  NEXT I
```

```
2560  GOSUB 1560
2570 R1(N + 1) = R
2580  GOTO 1060
2590 R =  - 50
2600  PRINT : PRINT "BOUNDARY VIOLATION ON ATTEMPTED EXPANSION
"
2610  GOTO 2780
2620  PRINT : PRINT "NEGATIVE CONTRACTION SUCCESSFUL"
2630 R1(N + 1) = R5
2640  FOR I = 1 TO N
2650 V1(N + 1,I) = V5(I)
2660  NEXT I
2670  IF R5 > R1(N) THEN 2690
2680 R1(N) =  - 100 - T
2690  GOTO 1060
2700  PRINT "POSITIVE CONTRACTION SUCCESSFUL"
2710 R1(N + 1) = R4
2720  FOR I = 1 TO N
2730 V1(N + 1,I) = V4(I)
2740  NEXT I
2750  IF R4 > R1(N) THEN 2770
2760 R1(N) =  - 100 - T
2770  GOTO 1060
2780  REM   STANDARD SIMPLEX MOVE
2790 R1(N + 1) = R2
2800  FOR I = 1 TO N
2810 V1(N + 1,I) = V2(I)
2820  NEXT I
2830  GOTO 1060
2840  REM  EXPANSION
2850 C = 2
2860  GOSUB 1950
2870  PRINT "NEW VERTEX, EXPANDED SIMPLEX"
2880  FOR I = 1 TO N
2890  PRINT V(I);" ";
2900 V3(I) = V(I)
2910  NEXT I
2920  GOSUB 1370
2930  IF R =  - 100 THEN 2590
2940  GOSUB 1560
2950 R3 = R
2960  IF R3 > R2 THEN 2990
2970  PRINT "EXPANSION FAILED"
2980  GOTO 2780
2990  PRINT "EXPANSION SUCCESSFUL"
3000 R1(N + 1) = R3
3010  FOR I = 1 TO N
3020 V1(N + 1,I) = V3(I)
3030  NEXT I
3040  GOTO 1060
3050  REM  VERTEX RETAINED N+1 TIMES
3060 A1 = 0:A2 = 0
3070  PRINT
3080 T = T + 1
```

```
3090  PRINT "NUMBER OF SIMPLEX MOVES = ";T
3100 W(T) = R1(1)
3110  FOR I = 1 TO N
3120 W1(T,I) = V1(1,I)
3130  NEXT I
3140  FOR I = 1 TO N + 1
3150 A1 = A1 + R1(I)
3160 A2 = A2 + R1(I) ^ 2
3170  NEXT I
3180 A3 = A2 - A1 ^ 2 / (N + 1)
3190 A4 =  SQR (A3 / N)
3200  PRINT "STD DEVIATION OF RESPONSE": PRINT "     (N+1) VERT
    ICES        = ";A4
3210  IF T < N + 1 THEN 3330
3220  IF W(T) = W(T - N) THEN 3240
3230  GOTO 3330
3240  FOR I = 1 TO N
3250  IF W1(T,I) = W1(T - N,I) THEN 3270
3260  GOTO 3330
3270  NEXT I
3280  PRINT "VERTEX KEPT N+1 TIMES: RESPONSE AVERAGED"
3290  GOSUB 1560
3300 R1(1) = (R1(1) + R) / 2
3310 W(T) = R1(1)
3320  GOSUB 1630
3330  RETURN
3340  INVERSE : PRINT "SPACE-BAR";: NORMAL : PRINT " - CONT, G
    - GRAPH, 0 - END";
3350  GET Y$: PRINT
3360  IF Y$ =  CHR$ (32) THEN 3420
3370  IF Y$ = "G" THEN  GOTO 3760
3380  IF Y$ = "0" THEN 3400
3390  GOTO 3340
3400  GOSUB 3630
3410  PRINT  CHR$ (4);"PR#0": END
3420  RETURN
3430  REM  SET DEC PLACES IN RESP
3440  PRINT "HOW MANY DEC PLACES DO YOU WANT IN SBR";: INPUT P
    R
3450  IF PR < 0 OR PR > 5 THEN  PRINT "ONLY 0 -5 ALLOWED": GOTO
    3440
3460  IF PR = 0 THEN  LET PR = 1
3470  IF PR = 1 THEN  LET PR = 10
3480  IF PR = 2 THEN  LET PR = 100
3490  IF PR = 3 THEN  LET PR = 1000
3500  IF PR = 4 THEN  LET PR = 10000
3510  IF PR = 5 THEN  LET PR = 100000
3520  RETURN
3530  REM  SET DEC PLACES IN NEW PARAMS
3540  PRINT "HOW MANY DEC PLACES DO YOU WANT": PRINT : PRINT "
    IN NEW PARAMETERS";: INPUT PP
3550  IF PP < 0 OR PP > 5 THEN  PRINT "ONLY 0 -5 ALLOWED": GOTO
    3540
```

```
3560  IF PP = 0 THEN  LET PP = 1
3570  IF PP = 1 THEN  LET PP = 10
3580  IF PP = 2 THEN  LET PP = 100
3590  IF PP = 3 THEN  LET PP = 1000
3600  IF PP = 4 THEN  LET PP = 10000
3610  IF PP = 5 THEN  LET PP = 100000
3620  RETURN
3630  REM  E. SUBROUTINE SUB
3640  PRINT : PRINT "**** FINAL SIMPLEX *******": PRINT
3650  FOR I = 1 TO N
3660 S = 0
3670  FOR J = 1 TO N + 1
3680 S = S + V1(J,I)
3690  NEXT J
3700 S = S / (N + 1)
3710  PRINT "VARIABLE ";I;"  AVERAGE = ";S
3720  NEXT I
3730  GOSUB 1560
3740  PRINT : PRINT "*******  THE END  *******"
3750  RETURN
3760  REM  RESP SBR GRAPH SUBR
3770  LET X$ = "----SIMPLEX MOVES--->"
3780  IF R$ = "S" THEN  LET Y$ = "SIGNAL/BACKGROUND RATIO"
3785  IF R$ = "I" THEN  LET Y$ = "RECIPROCAL OF II"
3790  IF R$ = "P" THEN  LET Y$ = "NET SIGNAL"
3800  LET T$ = "GENERAL MODIFIED SIMPLEX OPT."
3810  GOTO 4070
3820  IF M8 = 10 THEN  LET XM$ = "10"
3830  IF M8 = 30 THEN  LET XM$ = "30"
3840  IF M8 = 20 THEN  LET XM$ = "20"
3850  IF M8 = 40 THEN  LET XM$ = "40"
3860  IF M8 = 35 THEN  LET XM$ = "35"
3870  IF M8 = 25 THEN  LET XM$ = "25"
3880  IF M8 = 15 THEN  LET XM$ = "15"
3890  IF M9 = 50 THEN  LET YM$ = "50"
3900  IF M9 = 1 THEN  LET YM$ = "1"
3910  IF M9 = 5 THEN  LET YM$ = "5"
3920  IF M9 = 10 THEN  LET YM$ = "10"
3930  IF M9 = 20 THEN  LET YM$ = "20"
3940  IF M9 = 30 THEN  LET YM$ = "30"
3950  IF M9 = 40 THEN  LET YM$ = "40"
3960  IF M9 = 100 THEN  LET YM$ = "100"
3970  IF M9 = 200 THEN  LET YM$ = "200"
3980  IF M9 = 300 THEN  LET YM$ = "300"
3990  IF M9 = 400 THEN  LET YM$ = "400"
4000  IF M9 = 500 THEN  LET YM$ = "500"
4010  IF M9 = 600 THEN  LET YM$ = "600"
4020  IF M9 = 1600 THEN  LET YM$ = "1000"
4030  IF M9 = 2000 THEN  LET YM$ = "2000"
4040  IF M9 = 3000 THEN  LET YM$ = "3000"
4050  IF M9 = 4000 THEN  LET YM$ = "4000"
4060  RETURN
4070  FOR J = 1 TO T
4080 Y(J) = YA(J)
4090  LET X(J) = J
4100  NEXT J
```

```
4110  GOSUB 5010: REM   FIND MAXIMA OF X AND Y
4120  IF L7 <  = 4000 THEN  LET M9 = 4000
4130  IF L7 <  = 3000 THEN  LET M9 = 3000
4140  IF L7 <  = 2000 THEN  LET M9 = 2000
4150  IF L7 <  = 1000 THEN  LET M9 = 1000
4160  IF L7 <  = 600 THEN  LET M9 = 600
4170  IF L7 <  = 500 THEN  LET M9 = 500
4180  IF L7 <  = 400 THEN  LET M9 = 400
4190  IF L7 <  = 300 THEN  LET M9 = 300
4200  IF L7 <  = 200 THEN  LET M9 = 200
4210  IF L7 <  = 100 THEN  LET M9 = 100
4220  IF L7 <  = 50 THEN  LET M9 = 50
4230  IF L7 <  = 40 THEN  LET M9 = 40
4240  IF L7 <  = 30 THEN  LET M9 = 30
4250  IF L7 <  = 20 THEN  LET M9 = 20
4260  IF L7 <  = 10 THEN  LET M9 = 10
4270  IF L7 <  = 5 THEN  LET M9 = 5
4280  IF L7 <  = 1 THEN  LET M9 = 1
 290 N8 = T:M8 = 10
  00  IF N8 > 10 THEN  LET M8 = 15
  10  IF N8 > 15 THEN  LET M8 = 20
      IF N8 > 20 THEN  LET M8 = 25
      IF N8 > 25 THEN  LET M8 = 30
 340  IF N8 > 30 THEN  LET M8 = 35
4350  IF N8 > 35 THEN  LET M8 = 40
4360  GOSUB 3820
4370  IF N8 > 100 THEN  PRINT "VERTEX NO >100 MAX!": STOP
4380  FOR J = 1 TO N8
4390  LET X(J) = (20 + (X(J) * 250) / M8)
4400  LET Y(J) = (139 - (Y(J) * 130) / M9)
4410  NEXT J
4420  REM  GRAPH PLOT
4430  HGR : HCOLOR= 3
4440  HPLOT 0,0 TO 0,159 TO 279,159 TO 279,0 TO 0,0
4450  LET TX = 20
4460  FOR J = 0 TO M8
4470  IF J = 10 THEN  HPLOT TX,139 TO TX,133
4480  IF J = 20 THEN  HPLOT TX,139 TO TX,133
4490  IF J = 30 OR J = 40 THEN  HPLOT TX,139 TO TX,133
4500  IF J = 5 THEN  HPLOT TX,139 TO TX,135
4510  IF J = 15 THEN  HPLOT TX,139 TO TX,135
4520  IF J = 25 THEN  HPLOT TX,139 TO TX,135
4530  IF J = 35 THEN  HPLOT TX,139 TO TX,135
4540  REM  DRAW TICS-MARKS ON Y AXIS
4550  HPLOT TX,139 TO TX,137
4560  LET TX = TX + (250 / M8)
4570  NEXT J
4580  LET MT9 = (M9 / 10)
4590  IF M9 > 200 THEN  LET MT9 = (M9 / 50)
4600  IF M9 < 50 THEN  LET MT9 = M9
4610  LET TY = 10
4620  FOR J = 0 TO MT9
4630  HPLOT 20,TY TO 22,TY
4640  IF M9 > 200 THEN 4730
```

```
4650  IF J = 10 THEN  HPLOT 20,TY TO 26,TY
4660  IF J = 5 THEN  HPLOT 20,TY TO 24,TY
4670  IF J = 15 THEN  HPLOT 20,TY TO 24,TY
4680  IF J = 0 THEN  HPLOT 20,TY TO 26,TY
4690  IF J = 20 THEN  HPLOT 20,TY TO 26,TY
4700  IF J = 30 THEN  HPLOT 20,TY TO 26,TY
4710  IF J = 25 THEN  HPLOT 20,TY TO 24,TY
4720  IF J = 35 THEN  HPLOT 20,TY TO 24,TY
4730  LET TY = TY + (130 / MT9)
4740  NEXT J
4750  REM   DRAW AXES 20,10 TO 20,139 TO 269,139
4760  HPLOT 20,10 TO 20,139 TO 269,139
4770  FOR J = 1 TO (N8 - 1)
4780  HPLOT X(J),Y(J)
4790  IF J = 1 THEN 4810
4800  HPLOT X(J),Y(J) TO X(J - 1),Y(J - 1)
4810  GOSUB 5110
4820  NEXT J
4830  GOSUB 5150
4840  VTAB 24
4850  PRINT "HAVE YOU A GRAPPLER? Y/N";: INPUT Z3$
4860  IF Z3$ = "N" THEN  TEXT : GOTO 3390
4870  IF Z3$ = "Y" GOTO 4890
4880  GOTO 4850
4890  TEXT : HOME : PRINT "SMALL GRAPH ------- [ S ]"
4900  PRINT "LARGE GRAPH ------- [ L ]"
4910  PRINT "CONT ------------- [ C ]"
4920  INPUT Z4$
4930  IF Z4$ = "S" THEN 4970
4940  IF Z4$ = "L" THEN 4980
4950  IF Z4$ = "C" THEN  GOTO 3390
4960  GOTO 4890
4970  PRINT  CHR$ (4);"PR#1": PRINT  CHR$ (9);"G": GOTO 4990
4980  PRINT  CHR$ (4);"PR#1": PRINT  CHR$ (9);"GD"
4990  IF Q3$ = "Y" THEN 4890
5000  IF Q3$ = "N" THEN  PRINT  CHR$ (4);"PR#0": GOTO 4890
5010  REM   FIND MAX OF X
5020  LET G7 = 1E - 38
5030 L7 = 1E - 38
5040  FOR J = 1 TO T
5050  IF X(J) > G7 THEN  LET G7 = X(J)
5060  REM    FIND MAX OF Y
5070  IF Y(J) > L7 THEN  LET L7 = Y(J)
5080  IF L7 > 4000 THEN  VTAB 24: PRINT "RESP>4000,PROG EXCEED
     ED": CALL  - 1059: GOTO 2220
5090  NEXT J
5100  RETURN
5110  REM  SUB TO PLOT SQUARES
5120  LET C = 3:D = 2
5130  HPLOT X(J) - C,Y(J) - D TO Y(J) + C,Y(J) - D TO X(J) + C
     ,Y(J) + D TO X(J) - C,Y(J) + D TO X(J) - C,Y(J) - D
5140  RETURN
```

```
5150  REM  SUB TO DRAW LABELS ON HGR
5160  POKE 232,0: POKE 233,64
5170  HCOLOR= 3: SCALE= 1
5180  FOR J = 1 TO 7
5190  IF J = 1 THEN  LET A$ = T$
5200  IF J = 2 THEN  LET A$ = X$
5210  IF J = 3 THEN  LET A$ = Y$
5220  IF J = 4 THEN  LET A$ = "0"
5230  IF J = 5 THEN  LET A$ = XM$
5240  IF J = 6 THEN  LET A$ = YM$
5250  IF J = 7 THEN  LET A$ = "0"
5260  FOR I = 1 TO  LEN (A$)
5270 A =  ASC ( MID$ (A$,I,1)) - 31
5280  IF J = 1 OR J = 2 THEN  LET R = 0
5290  IF J > 3 THEN  LET R = 0
5300  IF J = 3 THEN  LET R = 16
5310  ROT= R
5320  IF J = 1 THEN  DRAW A AT (I * 7) + 50,8
5330  IF J = 2 THEN  DRAW A AT (I * 10) + 20,157
5340  IF J = 3 THEN  DRAW A AT 5,I * 6
5350  IF J = 4 THEN  DRAW A AT (I * 8) + 10,150
5360  IF J = 5 THEN  DRAW A AT (I * 8) + 255,150: REM    X AXI
      S MAX
5370  IF J = 6 THEN  DRAW A AT (I * 8) + 20,15: REM    Y AXIS
      MAX
5380  NEXT I
5390  NEXT J
5400  RETURN
5410  PRINT "PROCEED - ";: INVERSE : PRINT "SPACE-BAR";: NORMAL
      : PRINT ", REPEAT - R";: GET Q$: PRINT
5420  RETURN
6000  REM  SUB TO CALC IONIZ.INTERF.
6010  REM
6280 R9 = 0:W9 = 0
6290  FOR I = 1 TO M
6300  PRINT
6310  PRINT " LINE  ";I;" SIGNAL (NO NA), SIGNAL (+NA)";
6320  INPUT B2(I),S2(I)
6330  IF B2(I) = S2(I) THEN  LET S2(I) = S2(I) + 0.01
6350 R0(I) = ((S2(I) - B2(I)) / B2(I)) * 100
6360  PRINT "IONIZ.INTERF.= ";R0(I)
6361 R0(I) = 100 / ( ABS (R0(I)))
6370 W8 = (1 / R0(I)) ^ PW
6380 R9 = R9 + R0(I) * W8
6390 W9 = W9 + W8
6400  NEXT I
6410 R = R9 / W9
6420 R =  INT ((R * PR + 0.5)) / PR
6430  GOSUB 5410
6440  IF Q$ =  CHR$ (32) THEN 6470
6450  IF Q$ = "R" THEN 6270
6460  GOTO 6430
6470  RETURN
```

Author Jones E A
Name of thesis Flow injection analysis in analytical Chemistry 1985

PUBLISHER:
University of the Witwatersrand, Johannesburg
©2013

LEGAL NOTICES:

Copyright Notice: All materials on the University of the Witwatersrand, Johannesburg Library website are protected by South African copyright law and may not be distributed, transmitted, displayed, or otherwise published in any format, without the prior written permission of the copyright owner.

Disclaimer and Terms of Use: Provided that you maintain all copyright and other notices contained therein, you may download material (one machine readable copy and one print copy per page) for your personal and/or educational non-commercial use only.

The University of the Witwatersrand, Johannesburg, is not responsible for any errors or omissions and excludes any and all liability for any errors in or omissions from the information on the Library website.